AN ABSTRACT OF THE DISSERTATION OF

Mohammad Ali Davarpanah for the degree of Doctor of Philosophy in Mechanical Engineering presented on November 21, 2018.

Title: Incremental Forming of Polymers at Room Temperature

Abstract approved:

_____

J. David Porter

Single Point Incremental Forming (SPIF) is a forming process in which a fully clamped sheet is formed by a hemispherical ended tool that moves along a predefined 3D toolpath. The sheet is formed in a series of local deformations to reach its desired shape. Double Sided Incremental Forming (DSIF) includes one tool on each side of the sheet so that the second tool can take the role of the local die or the forming tool to improve the part shape geometry and forming parts with higher geometric complexity. Significant advantages of incremental forming process include, (i) low tooling cost due to easy fabrication and geometry independence of the tools, (ii) absence of the heating energy cost due to room temperature nature of the process, and (iii) its capability of forming complex parts which make it suitable for low volume forming of the polymer sheets as well as prototype fabrication. This work investigates the effects of SPIF process parameters on formability and failure mode in polymer, metal-polymer laminates, mechanical and microstructural properties, and chain orientation of the formed polymers. Capability of DSIF process in forming polymers is also shown and discussed.

Investigation on the effect of SPIF process parameters on formability and mode of failure shows that increasing incremental depth increases formability; however, this advantage is limited to the occurrence of wrinkling. The results show that the mode of failure depends on incremental depth and shape of the part being formed. Additionally, tool rotation speed reduces forming forces. Investigation of the influence of SPIF on mechanical properties and chain orientation of the formed polymers shows that SPIF increases the strain at fracture and Ultimate Tensile Strength (UTS). Yield stress and Young's modulus in the formed polymers are reduced as compared to the unformed polymers. The effect of process parameters on formability and failure mode in SPIF of Metal-Polymer laminates is also examined and it is shown that polymer thickness has a significant effect on formability. Additionally, the feasibility of forming polymers with DSIF process is presented. Preliminary results show that DSIF increases the formability and geometric definition as compared to SPIF.

Incremental Forming of Polymers at Room Temperature

by
Mohammad Ali Davarpanah

A DISSERTATION

submitted to

Oregon State University

in partial fulfillment of
the requirements for the
degree of

Doctor of Philosophy

Presented November 21, 2018
Commencement June 2019

Doctor of Philosophy dissertation of Mohammad Ali Davarpanah presented on November 21, 2018

APPROVED:

Major Professor, representing Mechanical Engineering

Head of the School of Mechanical, Industrial, and Manufacturing Engineering

---

Dean of the Graduate School

I understand that my dissertation will become part of the permanent collection of Oregon State University libraries. My signature below authorizes release of my dissertation to any reader upon request.

Mohammad Ali Davarpanah, Author

ACKNOWLEDGEMENTS

I would like to thank my Ph.D. committee members, Dr. Brian Paul, Dr. Christopher Hoyle, Dr. Karl Haapala, Dr. Ali Tabei and Dr. Kathy Mullet as well as previous committee members Dr. Rajiv Malhotra and Dr. Roger Graham Jr for their great support and invaluable advice. Moreover, I am thankful to Dr. Jian Cao and Dr. Srikanth Pilla for their collaboration and contributions in projects related to this dissertation.

I would like to thank my lab mates and colleagues at ATAMI, especially Neill Thornton, for their continued support. I am thankful to Shalu Bansal, Dr. Amin Mirkouei, Xiaoyan Yu, and Zixuan Zhang for their collaboration and contributions in projects related to this dissertation. I would also like to thank my friends Hank Pratte, Patrick McNeff and Kamyar Raoufi for their endless support and making my experience in graduate school exciting and fun.

Thanks are also due to Walmart Manufacturing Innovation Fund and U.S. Department of Energy (Award No. DE-EE0005764) for their financial support that I otherwise would not have been able to develop my scientific discoveries.

Last but not least, I would like to express my deepest gratitude to my lovely spouse, Hoda, for her endless love and support. I would like to thank my family and friends. This dissertation would not have been possible without their warm love, continued patience, and endless support.

CONTRIBUTION OF AUTHORS

Chapter 2: Manuscript 1

Mohammad Ali Davarpanah led the design of experiments, design of final shapes, performing the experiments, data collection, analysis of results, toolpath generation for the CNC machine, and authoring of the manuscript. Graduate research assistant, Amin Mirkouei, assisted with conducting experiments, force data collection, toolpath generation for the CNC machine, and manuscript review. Dr. Sirkhan Pilla and his student Xiaoyan Yu assisted with conducting SEM (Scanning Electron Microscopy) and DSC (Differential Scanning Calorimetry) tests, data collection, analysis of results, authoring of the material analysis section of the manuscript, and manuscript review. Dr. Rajiv Malhotra provided guidance throughout the work including the project concept, process development, design of experiments, experimental procedures, data analysis, manuscript review, and feedback.

Chapter 3: Manuscript 2

Mohammad Ali Davarpanah led the design of experiments, design and fabrication of the fixture, design of final shapes, toolpath generation for the CNC machine, conducting experiments and tensile tests, data collection, analysis of results, and authoring of the manuscript. Graduate research assistant, Shalu Bansal, assisted with running XRD (X-ray diffraction) and DSC tests, data collection, analysis of results, and manuscript review. Graduate research assistant, Roshan Bhandari, assisted with fabrication of the fixture. Dr. Rajiv Malhotra provided guidance throughout the work including the project concept, process development, design of experiments, experimental procedures, data analysis, manuscript review, and feedback.

Chapter 4: Manuscript 3

Mohammad Ali Davarpanah led the design of experiments, conducting experiments, data collection, analysis of results, toolpath generation for the CNC machine, design of the final shapes, and authoring of the manuscript. Dr. Rajiv Malhotra provided guidance throughout the work including the project concept, process development, design of experiments, experimental procedures, data analysis, and manuscript review and feedback.

Chapter 5: Manuscript 4

Mohammad Ali Davarpanah led the design of experiments, design of final shapes, conducting experiments, data collection, analysis of results, and authoring of the

manuscript. Graduate student, Zixuan Zhang, assisted with conducting experiments, data collection, force measurement, toolpath generation, manuscript review, and feedback. Dr. Jian Cao allowed the use of her lab facilities for performing experiments and provided manuscript review and feedback. Dr. Rajiv Malhotra provided guidance throughout the work, including the project concept, process development, design of experiments, experimental procedures, data analysis, manuscript review, and feedback.

TABLE OF CONTENTS

Page

TABLE OF CONTENTS (Continued)

Page

TABLE OF CONTENTS (Continued)

LIST OF FIGURES

Figure Page

LIST OF FIGURES (Continued)

Figure Page

LIST OF FIGURES (Continued)

Figure Page

LIST OF FIGURES (Continued)

Figure Page

LIST OF FIGURES (Continued)

Figure Page

LIST OF FIGURES (Continued)

Figure Page

LIST OF FIGURES (Continued)

Figure Page

LIST OF TABLES

Table Page

1 INTRODUCTION

1.1 Applications of Thermoplastic Surfaces

Thermoplastic surfaces are widely used in various applications including aerospace (Figure 1-1a), automotive [1] (Figure 1-1b), medicine [2, 3] (Figure 1-1c) and packaging (Figure 1-1d). This is because thermoplastics are characterized by greater toughness than thermosets and recyclability (thermoplastics can be remolded by heating above their glass transition temperature). Further, their use in the interiors of airplanes and automobiles is due to the fact that they comply more easily with safety regulations by minimizing release of toxic smoke when heated or burnt during an accident [4].

(a) (b) (c) (d)

Figure 1-1: Applications of formed thermoplastic surfaces (a) aerospace (b) automotive industry (c) medicine (d) packaging

Such thermoplastic surfaces can be conventionally manufactured via a variety of polymer forming processes, which are described in greater detail below.

Polymer extrusion is one of the oldest processes for shaping thermoplastic polymers. The development of the single screw extrusion based polymer extrusion started in 1880s, in which Rubbers and polymers were shaped with this process. Single screw extrusion is primarily used to make finished or semi-finished products (e.g. polymer sheets will be formed with thermoforming process). The key steps of the process are (i) melting

the thermoplastic polymer pellets, (ii) homogenization of the raw material, and then (iii) pumping the molten thermoplastic polymer through a die.

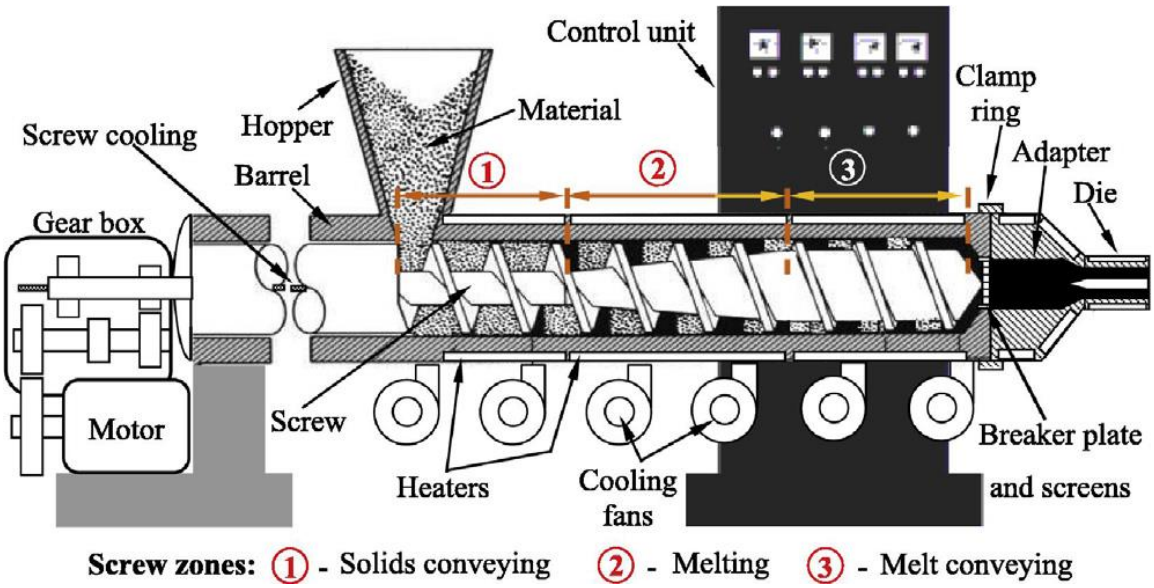

Figure 1-2: Components of a single-screw extruder and the functional zones [5].

Figure 1-2 shows the components and zones in a single-screw extruder. The polymer pellets are fed via hopper. The screw moves the pellets forward and the band heaters increase the temperature in the way that at the end of the barrel a homogeneous molting material is pumped out of the channel. Based on the cross section of the channel, the polymer is produced in the shape of sheet, plate, bar, wire or pellets.

Twin-screw extrusion machines are similar to single-screw extrusion machines, except as the name suggests, two screws rotate inside a barrel with figure-eight cross section. With respect to the cross section of the existing channel tubes, pipes, window frames, exterior cladding, wire, sheet and pellets (with a chopping process) can be shaped

with the polymer extrusion process. The polymer extrusion process is capable of mass production of the aforementioned parts [6].

Injection molding is a process in which molted polymer is injected into a die, kept under pressure, and cooled until it goes back to its solid state. The solid shaped polymer duplicates the shape of the die (cavity of the mold) into which the polymer is extruded. Figure 1-3 shows a schematic of the injection molding process and machine.

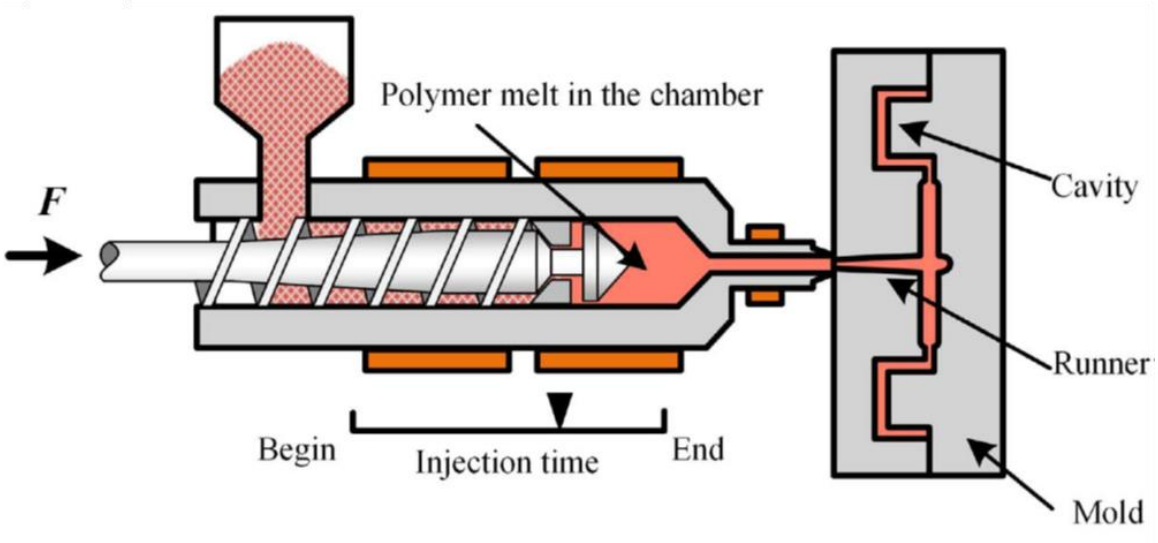

Figure 1-3: Diagram of injection molding process [7]

This process contains three basic operations: (1) heating the polymer in the injection unit to melt the polymer and flow under pressure, (ii) making molten polymer to fill and then solidify in the cavity, and at the end (iii) opening the mold and ejecting the shaped polymer. The injection molding process can produce complex molded parts accurately and repeatedly. It is suitable for mass production of high variety and geometry complexity of shapes [8].

The thermoforming process is considered as a secondary process, as its input materials, polymer sheets and film, first must be produced via processes such as polymer extrusion. The thermoforming process needs the following operations: (i) sheet preparation, (ii) loading the sheet into the thermoforming machine, (iii) heating the sheet until it reaches its forming temperature, (iv) applying force to stretch the sheet into the desired shape, (v) cooling the sheet until it reaches the temperature where it can hold its new shape, (vi) unloading the shaped part, and at the end (vii) trimming the sheet to the desired final shape.

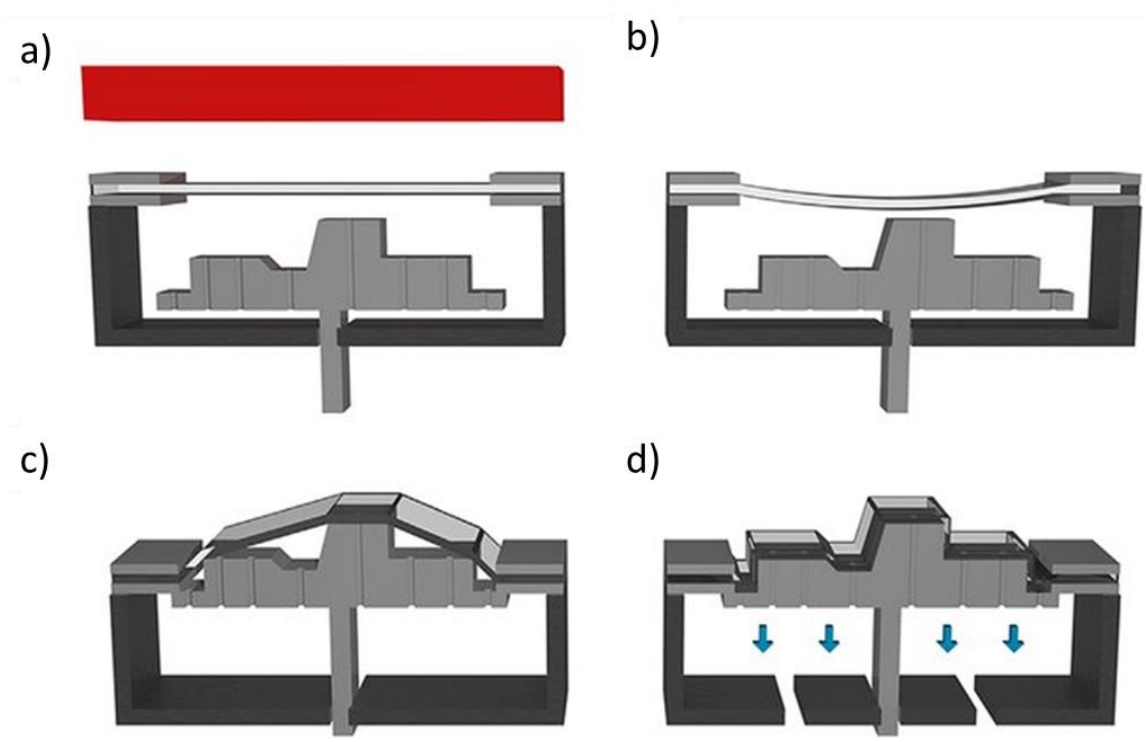

Figure 1-4: Vacuum forming process flow; (a) Thermoplastic sheet is clamped in a frame and heated; (b) The heater is removed once the sheet reached forming temperature, at this point the sheet sags; (c) The mold is pressed up against the sheet by a hydraulic cylinder;. (d) A vacuum applied from below forces the sheet against the surface of the mold until it is sufficiently cooled down and rigid again for removal after the metal mold moves away [9].

For the stretching step, there are typically four options available, as follows:

1. Mechanical force: This type of force might be very simple like a strip heater softening a limited area of the sheet and the operator may bend the sheet manually to shape the news geometry. The mechanical force required can be very high.

2. Vacuum: This is the most common forming force in the thermoforming process. A vacuum is drawn between the sheet and the die/mold, consequently the sheet is formed into the new shape by atmospheric pressure (Figure 1-4).

3. Pressure forming: This method is used when the atmospheric pressure is inadequate. Compressed air, which is up to 10 times greater than the force of vacuum forming, is used to form the heated sheet.

4. Combination of the forces: This method is used to form the sheet into large and detailed parts. For example, mechanical force may stretch the sheet and a vacuum draws the sheet into the die/mold.

Thermoforming is used to produce many product from blister packaging to aircraft interior panels. It is capable of mass production to produce industrial, disposable, and packaging products [10].

Additive Manufacturing, or AM processes, were originally developed in the late 1980s to early 1990s. Following AM processes are specifically related to polymers and composites [11]:

1. Binder jetting: In this process, a liquid binding agent is selectively deposited to bind powder materials.

2. Material extrusion: In this process, a material is selectively dispensed through a nozzle or orifice.

3. Material jetting: In this process, droplets of build material are selectively deposited and form/build the desired shape.

4. VAT photopolymerization: In this process, a liquid photopolymer is selectively cured by light-activated polymerization.

Polymers are one of the most advanced materials for AM techniques. Extrusion-based processes are mainly used for polymers and composites (Figure 1-5).

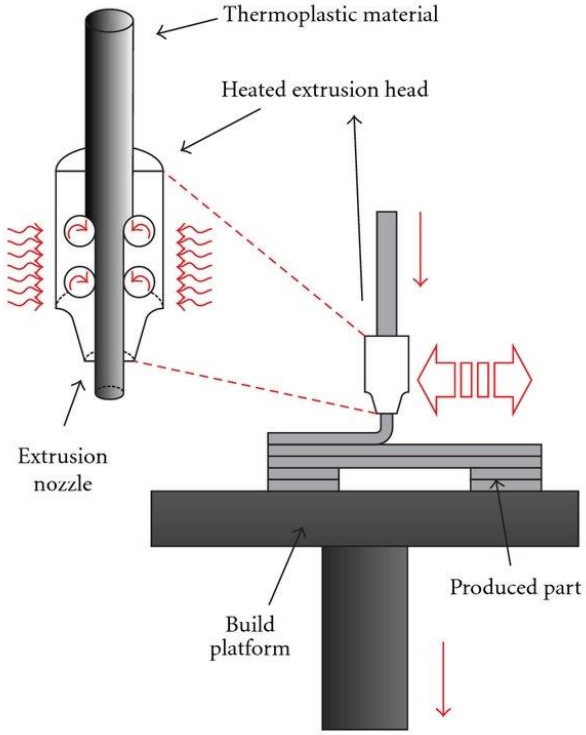

Figure 1-5: Schematic of the fused deposition modeling process [12]

The extrusion-based processes have their own limitations, which is mainly due two reasons [11]:

1. Temperature limit of the extruder in the equipment limits the variety of polymers that can be used
2. Temperature limit of the support material for fabricating the support structure

Removing the support material could be challenging. Especially for the shapes with thin wall sections, there is a risk of fracture or deformation while support material is removing [11].

Many thermoplastic polymers can undergo plastic deformation to significant magnitudes when strained below their glass transition temperature; This phenomenon is called “cold flow”. The cold flow phenomenon shows polymers’ potential to shape by means of fast sheet metal forming techniques such as cold drawing, deep drawing, and cold matched die stamping [13]. Cold forming can form material sheets to complex geometries (Figure 1-6).

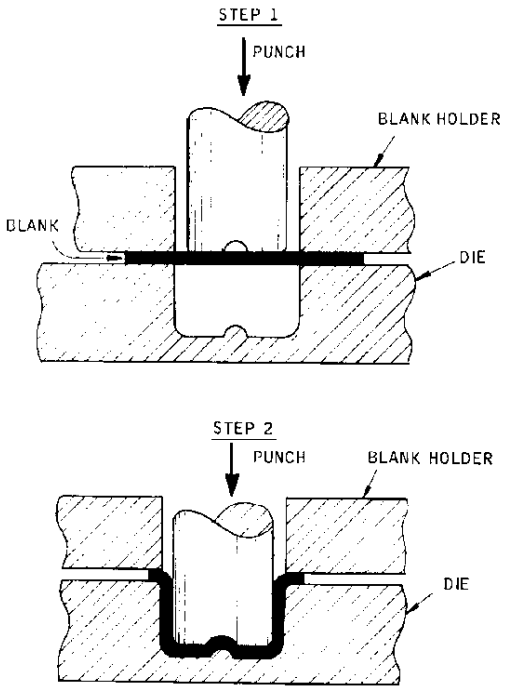

Figure 1-6: Illustration of a cold stamping process [14]

Cold forming of thermoplastics shares similarities with the drawing process of thermoplastics, with the major difference being in tooling (both stamp and die are needed) and the rapid application of pressure [15]. The forming forces in this process are relatively high, therefore large and expensive machines are needed to provide the essential forces for blank holding, and forming force [14, 15].

1.2 Motivation for This Work

1.2.1 Tooling Cost

Examining the above conventional processes for fabrication thermoplastic surfaces, it is recognizable that the tooling is part-shape dependent in all cases except for the additive manufacturing and the extrusion. The additive manufacturing is capable of producing different surface shapes without any modification in tooling. The capability of the extrusion process in producing surfaces is limited to sheets and plates.

In the rest of conventional processes for each surface geometry or each modification in final part shape, the tooling needs to be modified or completely new tool(s) should be fabricated. Fabrication of these tools is time consuming and costly due to the machines, which needs to be used and trained operators to fabricate the tools with high complexity.

1.2.2 Thermal Energy Cost

All conventional processes for forming thermoplastic surfaces other than cold stamping, which is a room temperature process, require externally supplied thermal energy to soften the polymer. This heat energy is lost upon cooling down the part. The heating and cooling cycle will increase the energy cost of the process. Furthermore, for biopolymer thermoplastics like Polylactic Acid (PLA), this heat cycle can degrade the mechanical properties of the part as well [16].

1.2.3 Complex Geometry Fabrication

Among all discussed processes, it is only extrusion that is not capable of forming complex surfaces. Extrusion is mostly used for manufacturing polymer sheets (used in cold

stamping and hydroforming), polymer wire, and polymer pellets. To make complex shaped parts other processes should be considered and used. Thus, there is a need for a manufacturing process, with the following qualities, for manufacturing of thermoplastic surfaces:

- Part-shape-independent tooling to reduce tooling costs and increase the process flexibility.
- Minimal or no supply of external thermal energy during the process, to reduce thermal energy cost and potential alteration in mechanical properties of the polymer.
- Capability to manufacture simple and complex thermoplastic surfaces, as needed.

The following section introduces the polymer incremental forming process, which has the potential to fulfill the above needs.

1.3 Incremental Forming

Incremental Forming (IF) is a deformation-based sheet forming method in which a fully peripherally clamped sheet is locally formed by one/two small hemispherical ended tool/s moving along pre-defined 3D toolpath/s [17]. The process is categorized into Single Point Incremental Forming (SPIF) and Double Sided Incremental Forming (DSIF). SPIF (Figure 1-7a) uses only one forming tool on one side of the sheet [18-20]. DSIF (Figure 1-7b) uses a forming tool on each side of the sheet [17]. In DSIF, each tool can be the forming or supporting tool during the forming process as needed, and the supporting

tool can also squeeze the sheet material at the local tool-sheet contact zone [21-24]. Note that in both SPIF and DSIF the tool used is part-shape-independent. For metals, it has been shown that the presence of the second supporting, or squeezing tool, in DSIF significantly improves the formability and the geometric accuracy of the formed part as compared to SPIF [24, 25].

There are five main process parameters in incremental forming:

1. Incremental depth (Δz), as shown in Figure 1-7a and Figure 1-7b for SPIF, and DSIF respectively.

2. Tool diameter (d_{tool}), i.e., the diameter of the hemispherical part of the tool used to form the sheet.

3. Tool rotation speed (ω), defined as the number of rotations around the tool's axis per minute (rpm).

4. Sheet thickness (t_0), i.e., thickness of unformed sheet

5. Squeeze factor *s*, in DSIF, as defined later in Eq. 1-1.

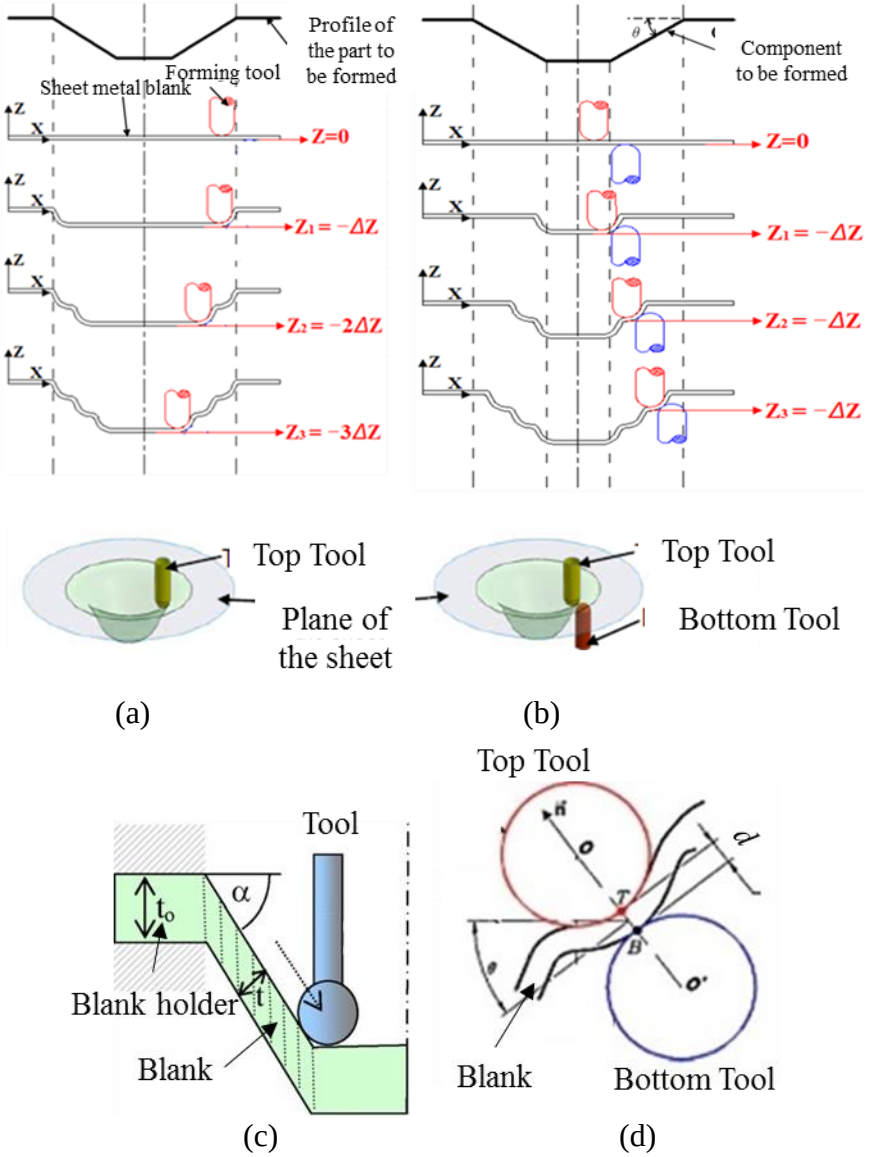

Figure 1-7: Schematic of (a) Single Point Incremental Forming for an axisymmetric cone profile and (b) Double Sided Incremental Forming for an axisymmetric cone profile (c) schematic of the Sine Law in SPIF [20] (d) positioning of the two tools in DSIF and squeeze factor *s* [25]

The above parameters control the failure of the sheet during forming, geometric accuracy of the formed part, as well as the mechanical properties and microstructural characteristics of the formed material. The sine law [20], which is commonly used in SPIF

and DSIF, is based on conservation of volume and the assumption of plane-strain deformation (Figure 1-7c). The wall thickness of the formed part (t) is related to the local wall angle of the part (α) and initial thickness of the sheet (t_0) as it is shown in Eq. 1-1 and Figure 1-7c**.**

$$t = t_0 \sin(90 - \alpha) \tag{1-1}$$

In DSIF, the squeeze factor (s) dictates the degree by which the sheet at the local tool-sheet contact region is squeezed between the tools [24]. If d is the normal distance between the contact points of DSIF tools with each side of the blank (points T and B in Figure 1-7d) and t is the formed sheet thickness (calculated based on sine law) then the squeeze factor s is defined as:

$$\boldsymbol{s = \frac{d}{t}} \tag{1-2}$$

Where $s = 1$ represents no squeezing of the sheet and $s < 1$ represents squeezing of the sheet to a thickness that is below the sine law predicted thickness. During toolpath generation the s is supplied by the user and the d, which is calculated from Eq. 1-2, is used to position the supporting tool. User also supplies the process parameters like incremental depth, toolpath, initial sheet thickness, tool diameter, frictional condition between tool-sheet, and tool rotation speed.

1.4 Literature Review

A significant amount of work has been performed on SPIF of metals. Kim et al. [26] investigated the effect of tool type, tool diameter, incremental depth, and friction on formability of metal SPIF. The results showed that that the ball tool shows better formability than the hemispherical end tool, due to increasing the tool pressure and reducing the state of stress, which results in delaying in crack occurrence. A small amount of friction at the tool-sheet contact area improves the formability, lower incremental depth increases the formability. The authors used Forming Limit Curve (FLC) to show the effect of process parameters (Figure **1-8**). Fracture was the only failure which was observed.

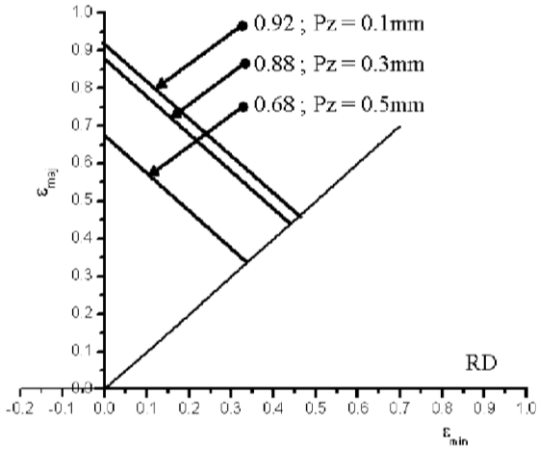

Figure 1-8: FLC with different incremental depths with 5 *mm* tool [26]

The effect of part shape on formability has been investigated by Hussain et al. [27]. They showed that for a funnel part shape the maximum reachable wall angle is higher than a cone or pyramid shape for a metal SPIF process (Figure **1-9**). Measuring the sheet thickness at fracture point showed that the Sine Law predicted higher sheet thickness compared to the experimental results, which is similar to the observations in previous studies [28, 29] (Figure 1-10).

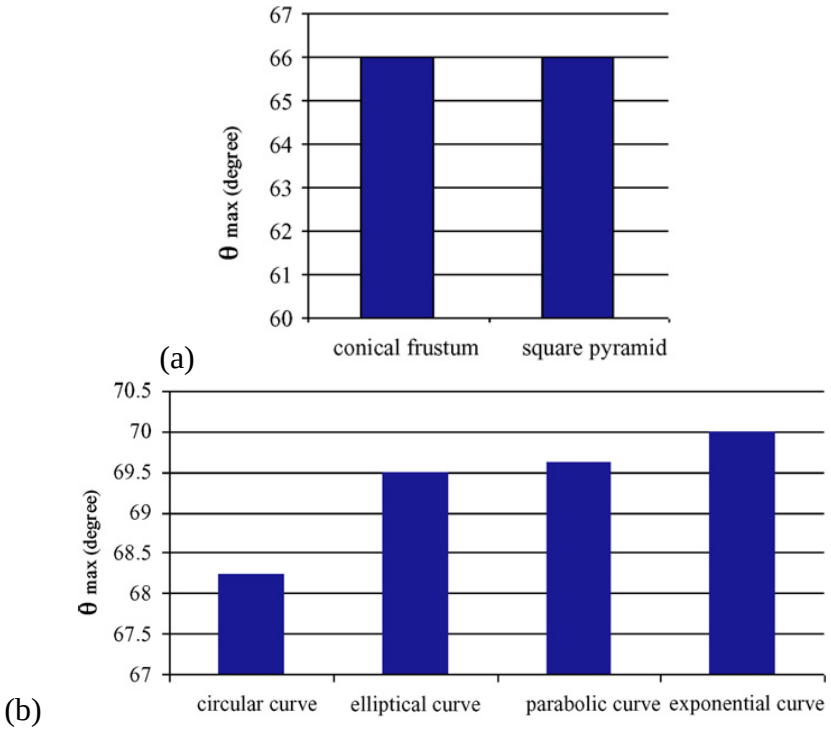

Figure 1-9: Formability values of the sheet: (a) by the cone or pyramid shape and (b) by funnel shape with various curvature [27]

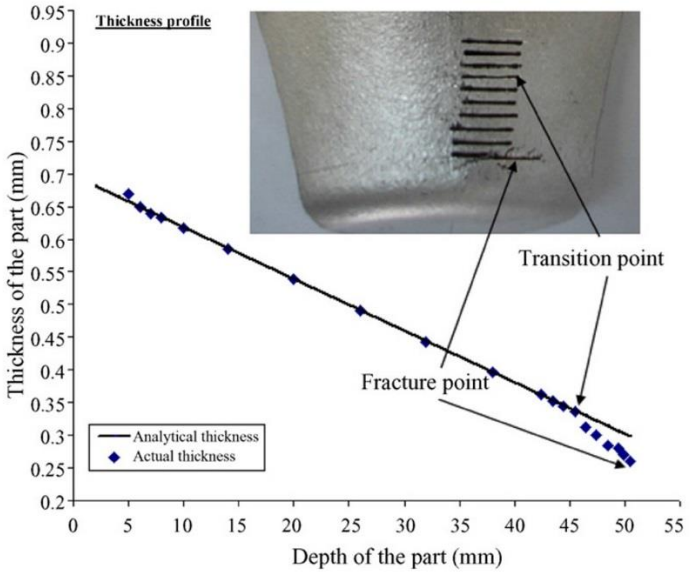

Figure 1-10: Illustration of the thickness profile of a funnel shape [27]

The mechanism of incremental forming process was investigated in previous works. Jackson et al. [20] stated that the deformation mechanism in SPIF is increasing stretching and shear in the plane perpendicular to tool direction as well as shear in the tool direction. The results showed that shear in the tool direction, which is due to friction between the tool and the sheet, has the most significant shear strain component. The authors concluded that the shear parallel and perpendicular to the forming tool is the most significant difference between deformation mechanism in SPIF and conventional stamping.

Malhotra et al. [30] analyzed the deformation mechanism in SPIF of metals. This work showed that higher shear in SPIF is only a partial explanation of the higher formability in SPIF as compared to conventional forming. A new theory ("noodle" theory) was proposed to explain the higher formability in SPIF as compared to conventional forming. This theory proposed that local deformation in SPIF increases plastic strain and damage very early on during the deformation and results in earlier onset of material instability, as compared to conventional forming. However, this region is not formed till fracture, due to the local deformation in SPIF (Figure 1-11). It was concluded that the effect of process parameters on shear and local bending can explain their effect of fracture in SPIF.

DSIF of metals has been introduced in previous works and its capability of forming complex metal parts has been shown [31, 32]. Malhotra et al. [24] introduced a novel toolpath strategy to improve the geometry accuracy of the formed part in metal DSIF

(Figure 1-12). The supporting tool is positioned in a way that the sheet is squeezed between forming and supporting tool to increase the geometry accuracy of the formed part as well as increasing the formability.

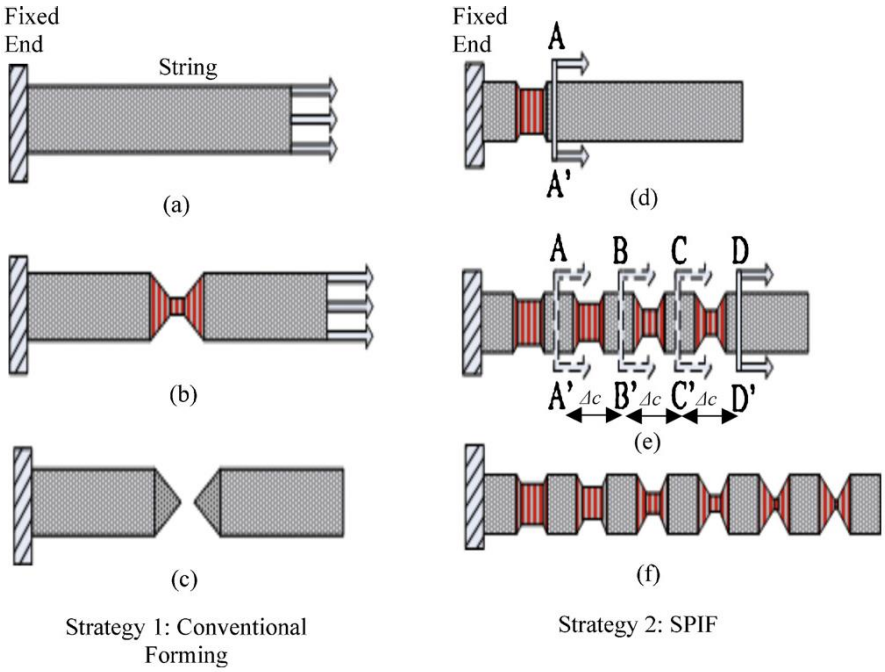

Figure 1-11: (a) Stretching the string at the free end (b) material localization at a single location on the string. (c) fracture at location of material localization. (d) Stretching the string by Δs at location Δc from the free end (e) continuous material localization along length of the string (f) elongation to a greater length without fracture [30]

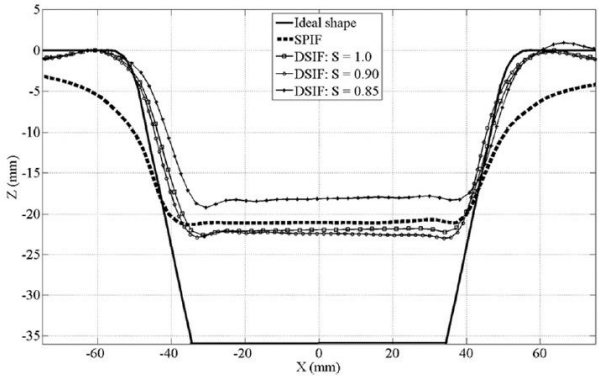

Figure 1-12: Comparison of profile geometries from SPIF and DSIF with the designed geometry [24]

Malhotra et al. [25] introduced the Accumulative-DSIF (ADSIF) toolpath strategy to prevent loss of contact between tools and the metal sheet. For example, for a cone part shape in conventional DSIF toolpath, the forming starts from out-to-in (from the largest diameter to the smallest). In the ADSIF the process starts from in to out (from the smallest diameter to the largest (Figure 1-13b). The results showed that ADSIF increased the geometric accuracy significantly as compared to out-to-in DSIF and SPIF process. A constant desirable wall thickness is achievable by ADSIF in comparison with SPIF. The drawback is that to maintain the high geometry accuracy low incremental depth needs to be used for toolpath, which increases the forming process time.

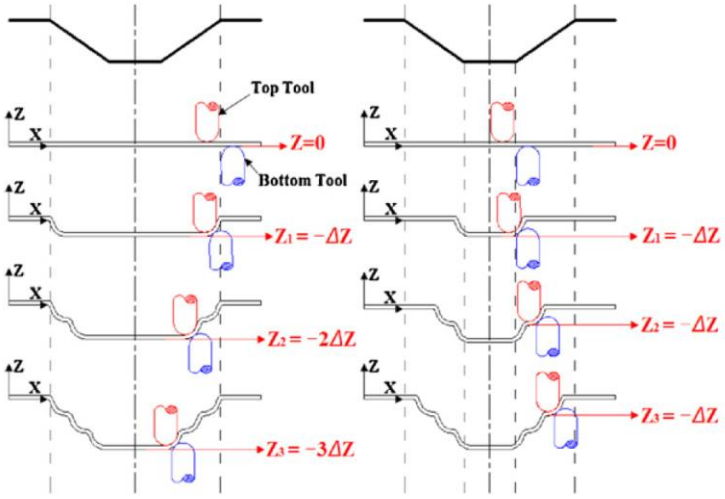

(a) (b)

Figure 1-13: Illustrations of (a) conventional DSIF toolpath strategy and (b) ADSIF strategy [25]

A series of works have been done on simulation of metal incremental forming. Cerro et al. [33] modeled the SPIF of Al 1050-0. The material behavior beyond yield point was modeled as an exponential material hardening. The effect of material and strain rate

were neglected. The FE-Model showed good agreement for forming force along the tool axis (Figure 1-14).

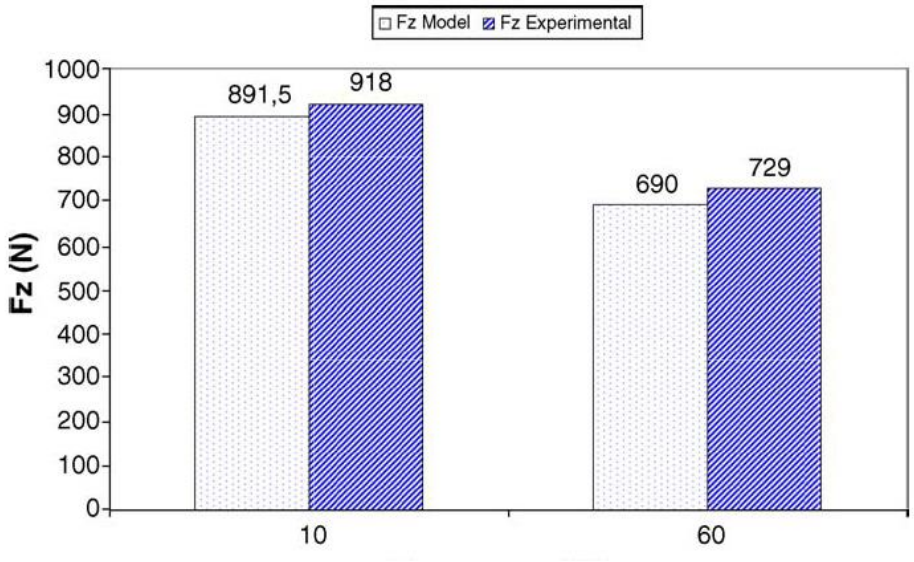

Figure 1-14: Force measurements predicted by the model in comparison with the experimental results [33]

Smith et al. [17] Finite Element-Simulated the SPIF and ADSIF process of metal sheet. The results showed that plastic strains, through-the-thickness shear strains, and hydrostatic pressure are higher in ADSIF than SPIF. The authors reported that the higher formability of ADSIF than SPIF is probably due to the higher hydrostatic pressure and through-the-thickness shear strain in ADSIF as compared to SPIF.

Prior research on polymer SPIF has been performed both using experimental and computational investigations. Franzen et al. [34] experimentally examined the feasibility of forming Polyvinyl Chloride (PVC) sheets into axisymmetric shapes using SPIF. The following three modes of sheet failure were observed:

Mode 1: Sheet fracture by ductile tearing along the circumferential direction, at the transition between the wall and the corner radius of formed parts (Figure 1-15a).

Mode 2: Wrinkling of the sheet along the wall of the part (Figure 1-15b).

Mode 3: Tearing of the sheet in the radial direction, along the wall of the part (Figure 1-15c).

The authors noted that only Mode 1 failure is typically seen in SPIF of metals and that Mode 3 failure is probably due to the occurrence of defects in the as-received sheet. The Mode 2 failure is seen at area near the corner radius and in the direction of rotation of the forming tool, where thinning is more pronounced. The authors also showed stress whitening in the formed PVC material and noted that this was probably due to deformation induced crazing in PVC. Crazing in polymers is the creation of submicron voids as an effect of a tensile hydrostatic stress on the material, and leads to creation of micro voids. The growth and coalescence of these micro voids eventually results in a macroscopic crack in the material.

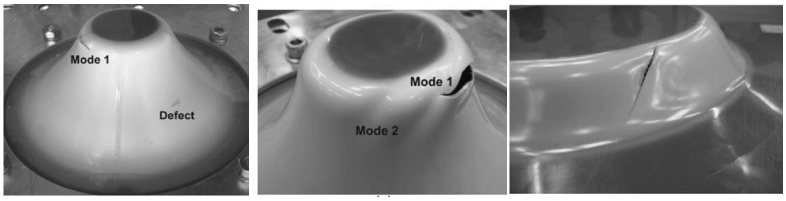

(a) (b) (c)

Figure 1-15: Failure modes in polymer SPIF (a) Mode 1 and Defect (b) Mode 2 and Mode1 (c) Mode 3 [34]

Franzen et al. [35] performed SPIF of five different polymers with varying degrees of crystallinity. It was shown that the reduction in density of the formed PVC material was larger than that of materials like Polycarbonate (PC) and Polyamide (PA). The authors also experimentally demonstrated that the change in formed material density depends on the wall angle of the part being formed, and therefore on the strain induced in the material during SPIF. Furthermore, the dependence of springback on the sheet material properties was qualitatively examined in terms of the ratio of the yield stress of the material to the product between the thickness and elasticity modulus of the sheet material.

Past works showed the effect of forming tool diameter on polymer SPIF. Le et al. [36] showed that increasing tool diameter increased the formability of Polypropylene (PP) sheet incremental forming (Figure 1-16a). However, other works exhibited that a reduction in tool radius increases the formability in polymer SPIF, much like in metals SPIF [37-39](Figure 1-16b).

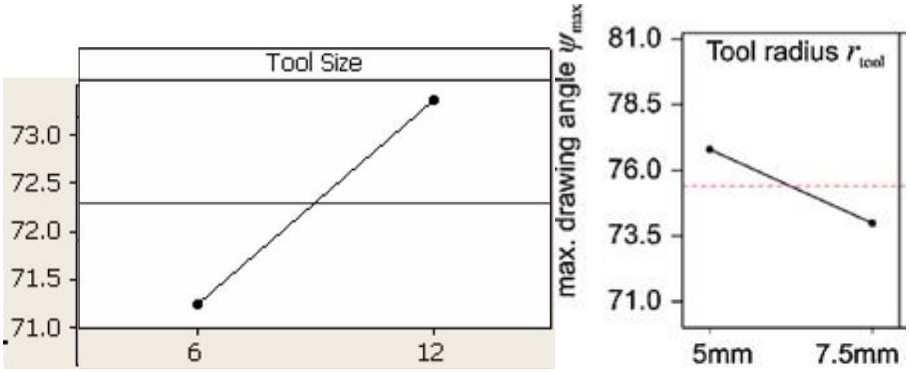

(a) (b)

Figure 1-16: Main effect of tool size on formability (a) Le et al. [36] results, Y-axis represents wall angle at failure in degree, X-axis represents tool diameter in *mm* (b) Martins et al. [39] results, Y-axis represents wall angle at failure in degree, X-axis represents tool radius in *mm*

Past works on effect of feedrate in polymer incremental forming showed that increasing feedrate increases formability for SPIF of PVC [37] and reduces formability for PP single point incremental forming [36] (Figure 1-17). It was shown that increasing feedrate reduces forming force along forming tool axis during the forming process and increases the surface roughness [37].

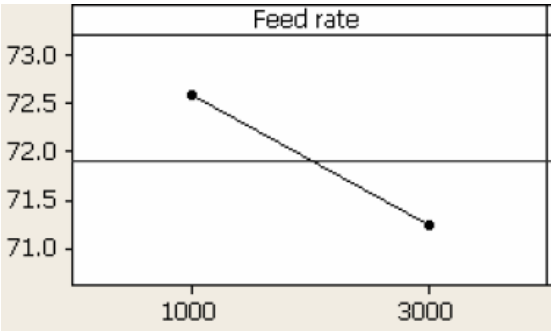

Figure 1-17: Main effect of federate on formability (Y-axis shows wall angle at failure in degree, X-axis represents feedrate in *mm/min*) [36]

Past works on effect of sheet thickness showed that increasing sheet thickness increases formability [37-39] (Figure 1-18). Bagudanch et al. [37] shows that increasing sheet thickness increases the forming force along tool axis. Maaβ et al. [40] demonstrated that increasing sheet thickness increases geometry accuracy of the formed part.

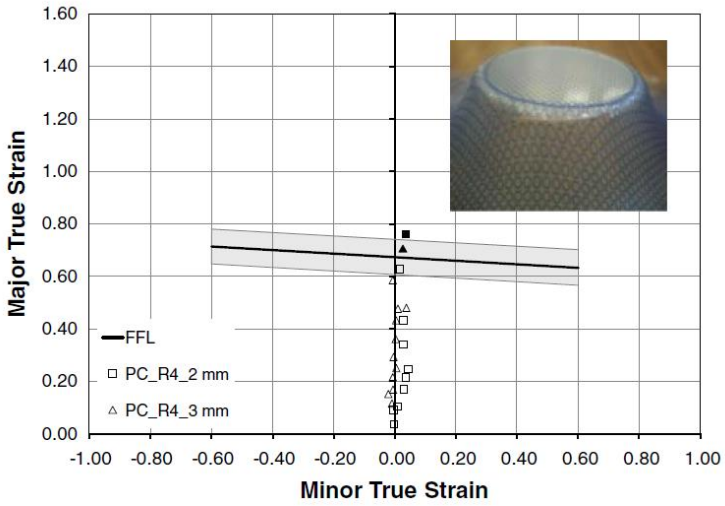

Figure 1-18: Increasing sheet thickness reduces experimental strain and consequently increases the formability [38]

The effect of tool rotation speed has been investigated in previous works on Polymer SPIF. Series of previous research showed that increasing the tool rotation speed increases the formability [36, 41, 42]. It was shown that increasing tool rotation speed increases the temperature near the local forming area [37, 41, 43] (Figure 1-19), reduces the maximum forming forces [37, 43] and generally increases formability [41, 42].

Bagudanch et al. [41] investigated the effect of the tool rotation speed on formability and mode of failure in polymer SPIF. Polycaprolactone (PLC), Ultra-High-Molecular-Weight Polyethylene (UHMWPE), PP, PVC, and PC were used for the experimental works. The results showed that with the tool rotation speed, for the polymers with glass transition temperature above the forming zone temperature, increasing tool rotation speed results in tearing. If the temperature near the forming zone reaches glass transition temperature or goes beyond it, the part could fail by twisting at the corner of the pyramid shape. For polymers with glass transition temperatures below room temperature

(PP and UHMWPE in this work), increasing tool rotation speed showed no significant effect on formability. The PLC results showed that if the temperature near the forming zone reached close to melting point of the polymer, the forming process could initiate localized melting process and compromise the formability.

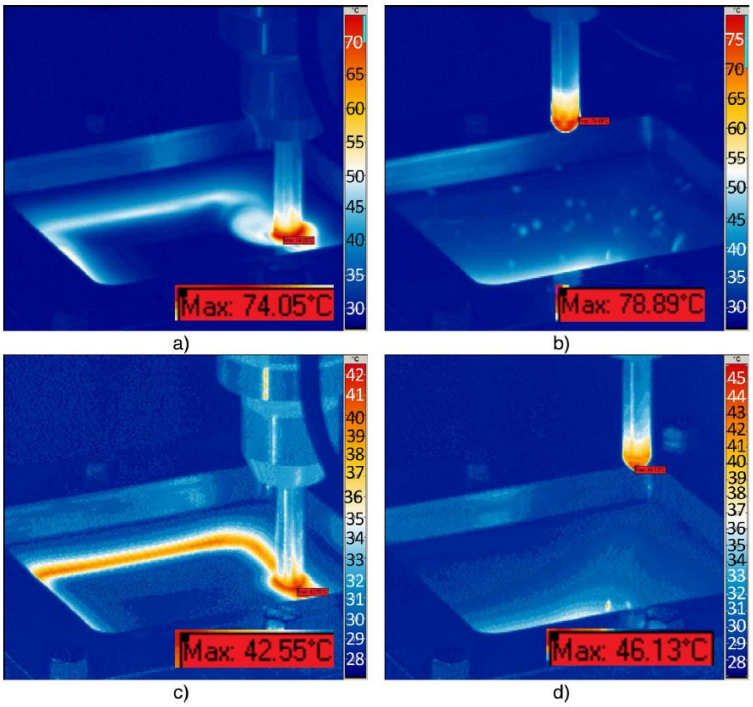

Figure 1-19: Tool tip and polymeric part temperature distribution recorded at the spindle speed of: (a) 2000 *rpm* during the SPIF process, (b) 2000 *rpm* at the end of the SPIF process, (c) "free" during the SPIF process and (d) "free" at the end of the SPIF process [37]

Effect of tool–sheet friction conditions has been investigated in past research. Medina-Sánchez et al. [43] investigated the effect of forming tool material on sheet temperature during the forming process and surface roughness by using steel and aluminum tools for PVC SPIF. The results showed the steel forming tool generates higher temperature

during the forming process than aluminum forming tool (Figure 1-20). The aluminum forming tool resulted in higher forming forces due to lower generated temperature during the forming process. The aluminum forming tool fabricated parts with lower surface roughness. Very high tool rotation speed increases the risk of surface wear.

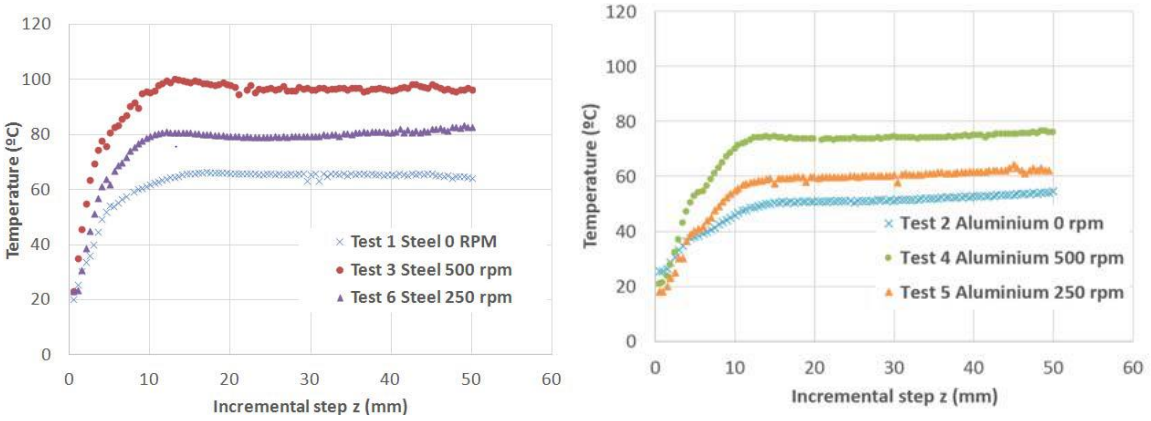

(a) (b)

Figure 1-20: Maximum temperature versus incremental step, (a) steel punch and (b) aluminum punch [43]

Durante et al. [44] investigated the effect of tool-sheet friction conditions on the formability of the PC sheets formed by SPIF. Two forming tools with a fixed and with a rotating end were applied for the forming process. The results showed that the tool-sheet friction conditions has no significant effect on formability. The rotating end tool shows slightly higher forming force along the tool axis (Figure 1-21). The rotating end tool results in higher spring back, due to lower shear stress production on the sheet, which leads to a higher elastic strain.

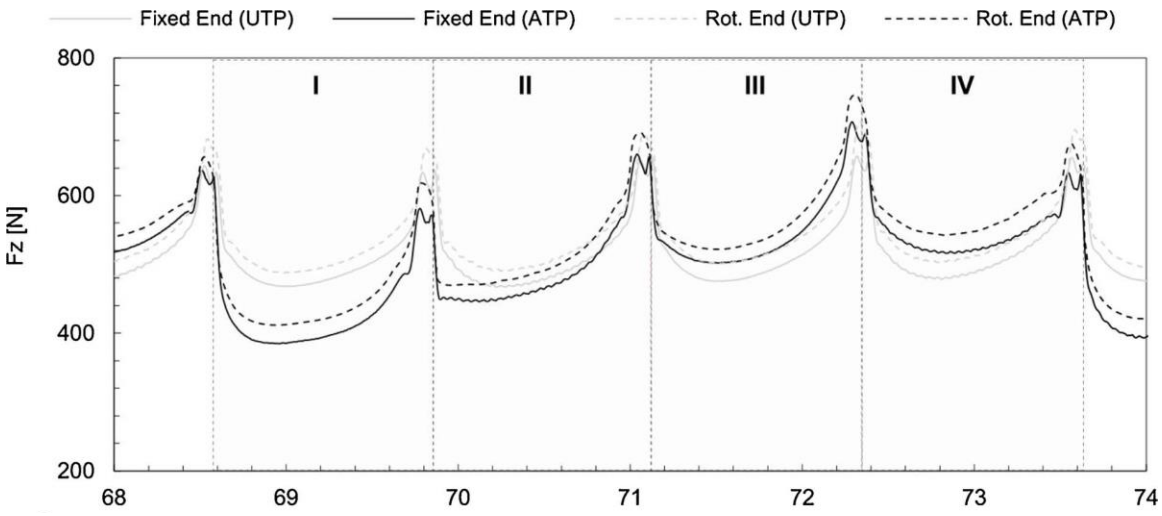

Figure 1-21: Trend of F_Z [44]

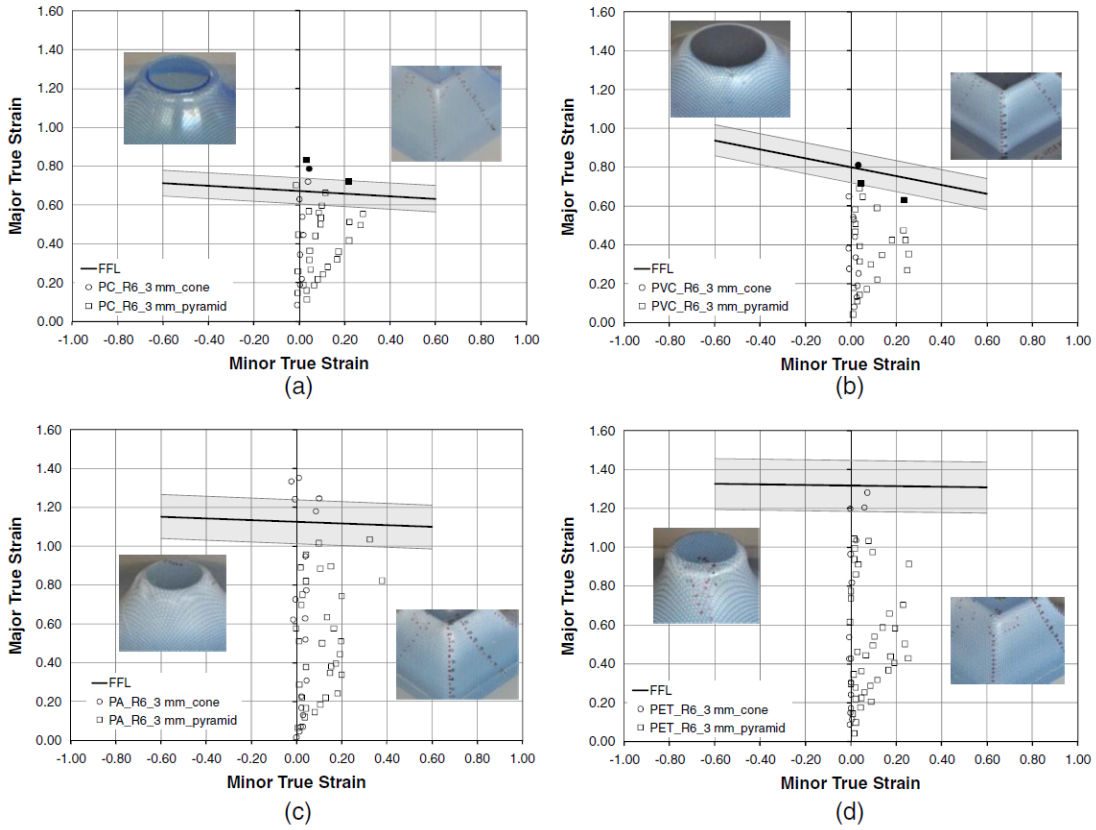

Figure 1-22: Experimental strains in truncated conical and pyramidal benchmark SPIF parts with 3 mm thickness with 30˚ initial drawing angles (note: solid markers refer to strains at failure). (a) PC, (b) PVC, (c) PA. d PET [38]

Marques et al. [38] studied the effect of part formability of Polyethylene terephthalate (PET), PA, PC, and PVC. The polymers were formed to conical and pyramidal shape with the various initial drawing angle. Fracture forming limit lines (FFLs) were plotted and applied to predict the fracture failure in polymer SPIF. The FFL showed a good agreement between experimental strains at failure and the FFL for PVC and PC. For PA, the experimental strains at failure were higher than the corresponding FFL, due to the wrinkling failure in formed part. The PET formed parts showed a very high formability and observations showed good agreement with FFL prediction (Figure 1-22).

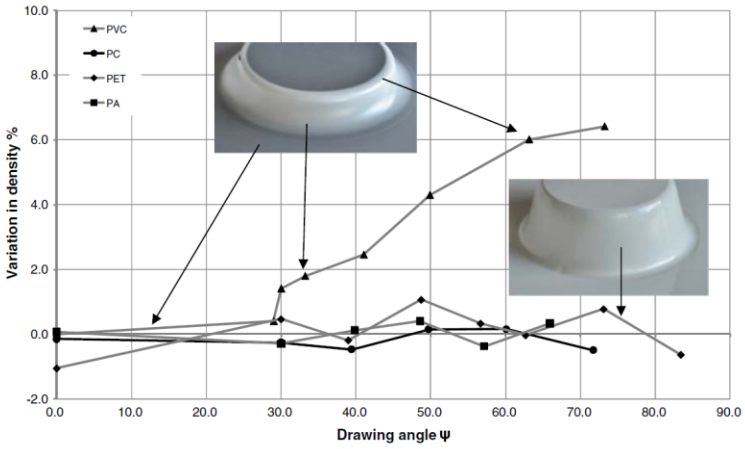

Figure 1-23: Variation in density as a function of the drawing angle along the conical wall of SPIF parts made from PA, PC, PET and PVC (r_{tool} = 8 *mm*, ψ_0 = 30˚, t_0 = 2 *mm*). Inset shows photographs of SPIF parts made from PVC and PET [38]

The results showed that variation in density is not significant in PA, PET and PC formed part, however, the PVC formed part showed a significant and progressive reduction in density for the conical shape formed part due to crazing in formed PVC parts (Figure 1-23).

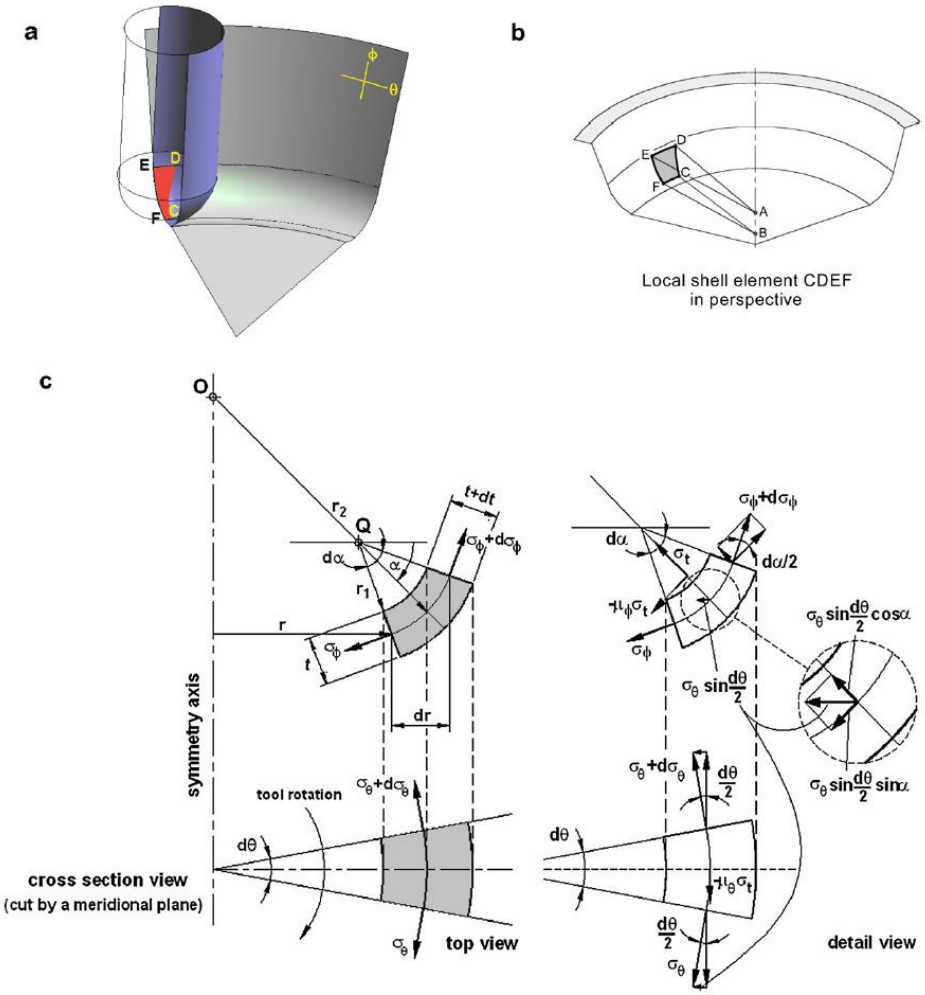

Figure 1-24: Membrane analysis of SPIF. (a) schematic representation of the local contact area between the tool and sheet placed immediately ahead. (b) approximation of the local contact area by a shell element. (c) cross section view showing the acting stresses in meridional, circumferential and thickness directions [45]

Silva et al. [45] focused on computationally examining the deformation mechanics in polymer SPIF by extending the membrane-based analysis (Figure 1-24) developed by Martins et al. [46] via a pressure modified Tresca yield criterion. This single-step analysis models only Mode 1 failure by tearing and considered the influence of part shape, tool

diameter, sheet thickness, and mechanical properties of the polymer sheet on tearing in polymer SPIF.

The authors successfully predicted experimental observations that reducing the tool radius can increase the formability of the material, more so for thicker sheets than for thinner sheets. However, the effect of through-the-thickness shear which is significant in incremental forming process [20] was not covered in the membrane model. In addition, due to the single-step nature of analysis this technique did not account for the effects of incremental depth on Mode 1 and Mode 2 failure.

$$\sigma_\varphi = \sigma_1 = \left(\frac{\sigma_Y\sqrt{(1-\beta\sigma_{kk})}}{(1+t/r_{tool})}\right) \quad (1\text{-}3)$$

$$\sigma_\theta = \sigma_2 = \frac{1}{2}\left(\sigma_1 + \sigma_3 - \beta\sigma_Y\right) \quad (1\text{-}4)$$

$$\sigma_t = \sigma_3 = -\left(\frac{\sigma_Y\sqrt{(1-\beta\sigma_{kk})}}{(1+r_{tool}/t)}\right) \quad (1\text{-}5)$$

$$\sigma_Y = \sqrt{\sigma_{YC}\sigma_{YT}} \quad (1\text{-}6)$$

$$\beta = (\sigma_{YC} - \sigma_{YT})/{\sigma_Y}^2 \quad (1\text{-}7)$$

Where, σ_θ, σ_φ, σ_t ,σ_{YC}, σ_{YT}, t and r_{tool} represent circumferential stress, meridional stress, thickness stress, yield stress in tension, yield stress in compression, sheet thickness and tool radius respectively.

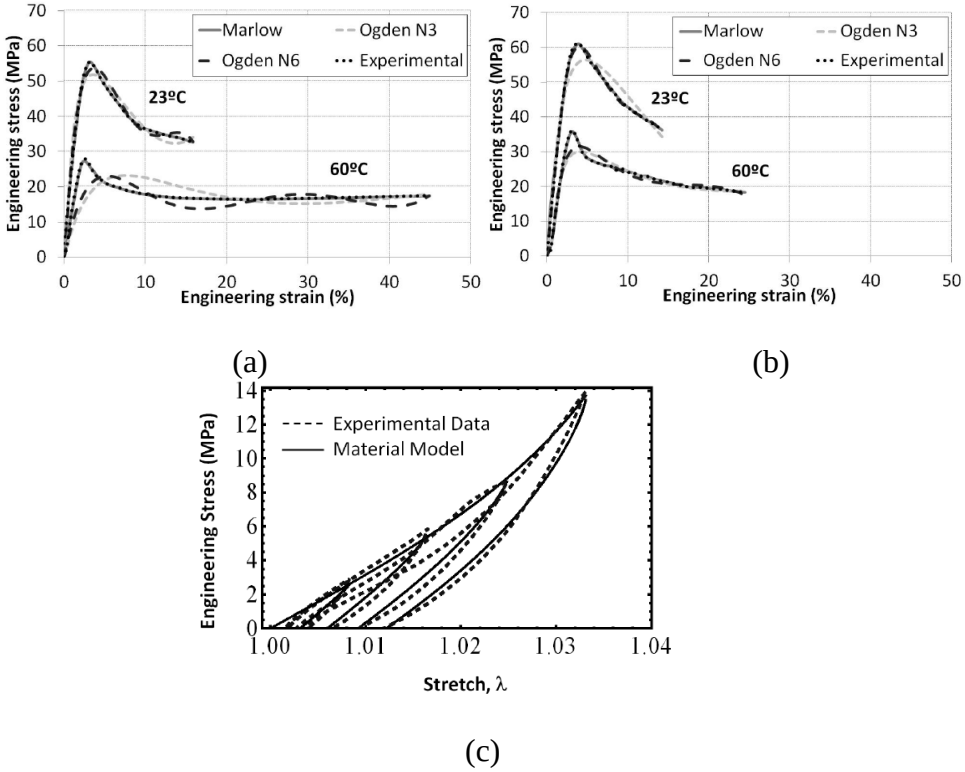

Figure 1-25: Experimental results of uniaxial tensile tests and material model evaluation for: (a) PVC at 50 mm/min, (b) PVC at 500 mm/min and (c) experimental and material model adjustment results of cyclic loading-unloading test for PVC [47].

Bagudanch et al. [47] investigated various material models which are capable in predicting the polymer behavior during the incremental forming process (qualitatively and quantitatively). PC and PVC were chosen for experimental tests and simulation. Five different material models were implemented in ABAQUS to simulate a uniaxial tensile test. The Marlow model showed the best match between experimental and simulation results for the uniaxial tensile test for both PC and PVC. A material model, based on the rule of mixtures, was implemented in the ABAQUS commercial package in order to capture the anisotropic effects. The cyclic loading and unloading tests showed a good agreement between experimental and modeling results. However, the suggested model was

not applied in a polymer incremental simulation to examine the capability of the model for simulating the process. Furthermore, the results did not show the capability of the chosen model to simulate the effect of hydrostatic pressure, which is involved in incremental forming process, on polymers.

Yonan et al. [48] presented a material model for modeling polymer incremental forming. The aim of the work was to introduce a model, which can cover the special effects of thermoplastics during the incremental forming process with low number of parameters to make the parameter identification easier and with fewer experiments. The constitutive model breaks down the total stress into equilibrium stress and over stress. The stress and strain tensors (Eq. 1-8) are divided into a deviatoric (Eq. 1-9) and a volumetric tensor (Eq. 1-10):

$$\mathbf{S} = \mathbf{S}^{\mathrm{D}} + \frac{1}{3}(\mathrm{tr}\mathbf{S}) \tag{1-8}$$

$$\mathbf{E} = \mathbf{E}^{\mathrm{D}} + \frac{1}{3}(\mathrm{tr}\mathbf{E}) \tag{1-9}$$

$$\frac{1}{3}(\mathrm{tr}\mathbf{S}) = K(\mathrm{tr}\mathbf{E}) \tag{1-10}$$

Where, **S**, **E,** and *K* represent total stress tensor, total strain tensor, and bulk module respectively. The superscription D represents the deviatoric part of the tensor.

$$\mathbf{S}^{\mathrm{D}} = \mathbf{S}_1^{\mathrm{D}} + \mathbf{S}_2^{\mathrm{D}} + \mathbf{S}_{\mathrm{ov}}^{\mathrm{D}} \tag{1-11}$$

$$\dot{\mathbf{S}}_1^{\mathrm{D}} = \frac{2G_1}{1+a\sqrt{\frac{2}{3}\mathbf{E}^{\mathrm{D}}.\,\mathbf{E}^{\mathrm{D}}}}\,\dot{\mathbf{E}}^{\mathrm{D}} - \frac{2G_1\frac{2}{3}a\,\mathbf{E}^{\mathrm{D}}.\,\dot{\mathbf{E}}^{\mathrm{D}}}{\sqrt{\frac{2}{3}\mathbf{E}^{\mathrm{D}}.\,\mathbf{E}^{\mathrm{D}}}\left(1+a\sqrt{\frac{2}{3}\mathbf{E}^{\mathrm{D}}.\,\mathbf{E}^{\mathrm{D}}}\right)^2}\,\mathbf{E}^{\mathrm{D}} \tag{1-12}$$

$$\dot{\mathbf{S}}_2^{\mathrm{D}} = 2G_2\dot{\mathbf{E}}^{\mathrm{D}} - b\sqrt{\frac{2}{3}\mathbf{E}^{\mathrm{D}}.\,\mathbf{E}^{\mathrm{D}}}\,\mathbf{S}_2^{\mathrm{D}} \tag{1-13}$$

$$\dot{\mathbf{S}}_{\mathrm{ov}}^{\mathrm{D}} = 2G_{ov}\dot{\mathbf{E}}^{\mathrm{D}} - \frac{2G_{ov}}{\eta}\left[\sqrt{\frac{2}{3}\mathbf{S}_{\mathrm{ov}}^{\mathrm{D}}.\mathbf{S}_{\mathrm{ov}}^{\mathrm{D}}}\right]^{m-1}\mathbf{S}_{\mathrm{ov}}^{\mathrm{D}} \tag{1-14}$$

Where G_1, G_2, G_{ov}, a, b, η and m are the material parameters and need to be identified. The material model showed the capability of prediction of a specified tensile test with intermediate holding times for High-Density Polyethylene (HDPE), Polycarbonate (PC) and PVC (Figure 1-26). The presented model was validated for low plastic strains (below 0.04) [48, 49], whereas past work showed that true major strain could be higher for PVC [38]. In addition, the model did not show its capability to predict softening and re-hardening of the polymer, which is observed in semi-crystalline polymers.

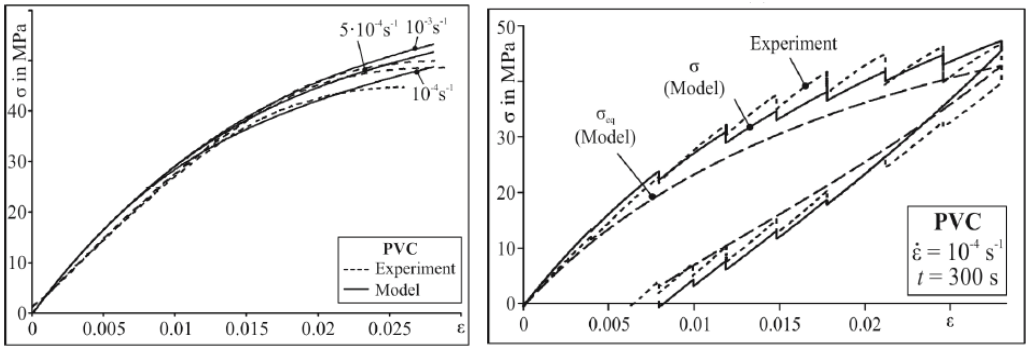

(a) (b)

Figure 1-26: Prediction of the model to (a) strain-controlled tensile tests at three different strain-rates with intermediate holding times, (b) specific tensile tests for PVC [48]

Yonan et al. [50] implemented the non-linear visco-plastic material model, which was presented in their previous work [48], in ABAQUS software to simulate the PVC sheet single point incremental forming. A cone shape with 60˚ and 80˚ wall angle was chosen as the part shape. The FE-Model was evaluated by forming tool forces. The simulation results showed the reasonable prediction of tool force (Figure 1-27), as well as geometry and wall thickness, especially for thin PVC sheets. Also, the presented model, as previously mentioned, was validated for low plastic strains (below 0.04) [48, 49], while the true major strain could be higher for PVC [38]. It was not shown that the model can predict softening and re-hardening in polymers, therefore this model may not be suitable for semi-crystalline polymers.

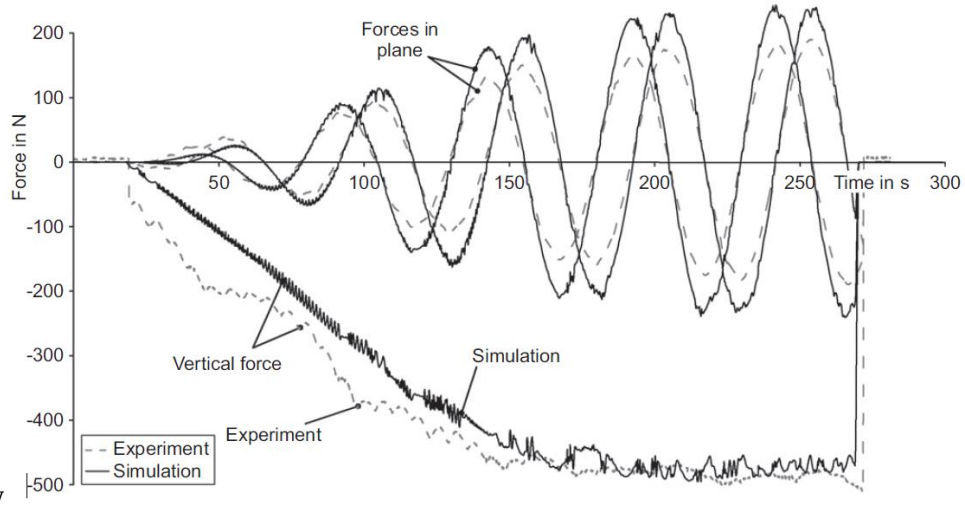

W

Figure 1-27: Forces in incremental forming experiment and simulation [50]

Yonan et al. [49] used a pressure modified version of the Von Mises yield criterion with the Ludwik-Hollman law and three non-coupled ductile damage criteria (Cockcroft and Latham, Rice and Tracey and Ayada et al. [49]) to capture the tearing mode of failure

in forming of axisymmetric PVC parts. Their derived Fracture Forming Limit (FFL) was able to capture tearing in polymer SPIF (Figure 1-28).

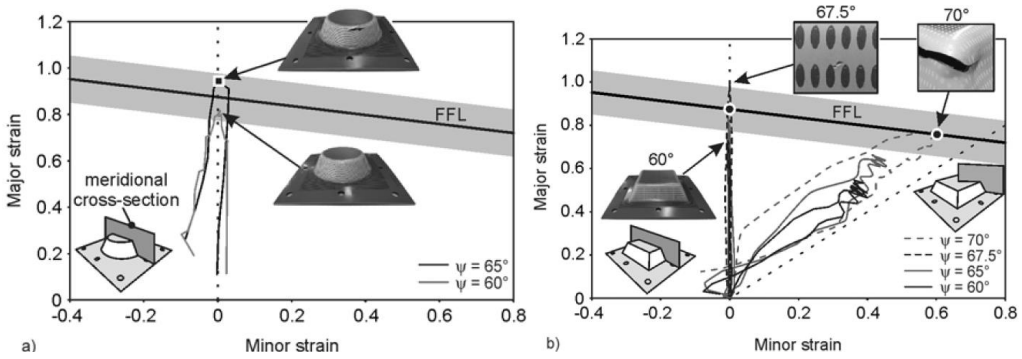

Figure 1-28: Experimental in-plane true strains in (a) conical and (b) pyramidal PVC parts produced by SPIF with different drawing angles [49]

They also showed that significant anisotropy was induced in the formed material after SPIF of PVC, so that yield stress of the formed material along the meridional direction is higher than yield stress along the circumferential direction (Figure 1-29). It was also indicated that non-coupled damage models, which are currently utilized in sheet metal forming, should not be applied to characterize formability in the SPIF of PVC sheets. The utilization of the FFL described formability in single-stage SPIF and multistage SPIF with complex strain paths successfully.

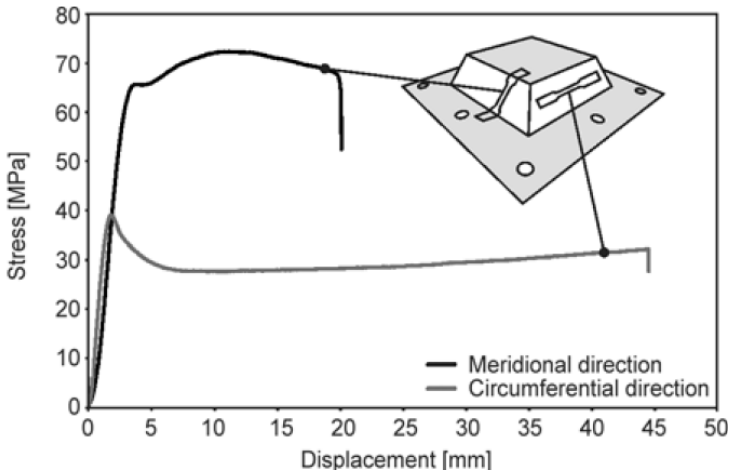

Figure 1-29: Stress-displacement curves obtained from tensile tests performed on specimens taken from the longitudinal and meridional directions along the mid-side of a pyramidal part produced by SPIF [49]

Lozano-Sánchez et al. [42] investigated the effect of SPIF process on structural properties of the formed PCL and UHMWPE parts. The X-ray Diffraction (XRD) results showed the chain reorientation in the formed polymer in comparison to the unformed polymer (Figure 1-30). The formed UHMWPE showed the unit cell distortion and converting from orthorhombic to monoclinic.

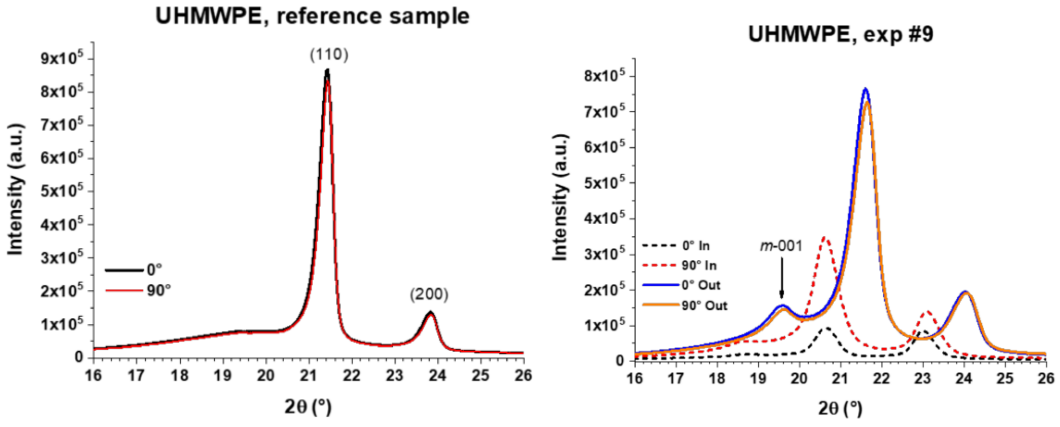

(a) (b)

Figure 1-30: XRD patterns of UHMWPE (a) unformed sheets and (b) sheets formed by SPIF [42]

Durante et al. [44] investigated the effect of toolpath strategy on the formability and main quality issues of the PC sheets formed by SPIF. An Unidirectional Toolpath (UTP) and an Alternative Toolpath (ATP) were adopted for experiments (Figure 1-31). The results showed that the ATP improves formability and reduces the risk of twisting in the formed part significantly as compared to the UTP (Figure 1-32).

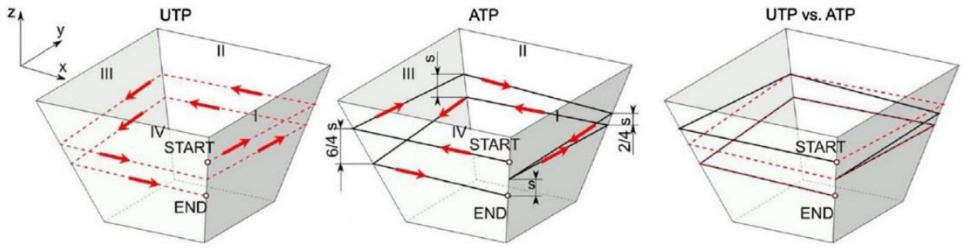

(a) (b) (c)

Figure 1-31: Schematic of the toolpath strategies: (a) UTP, (b) ATP and (c) UTP vs. ATP [44]

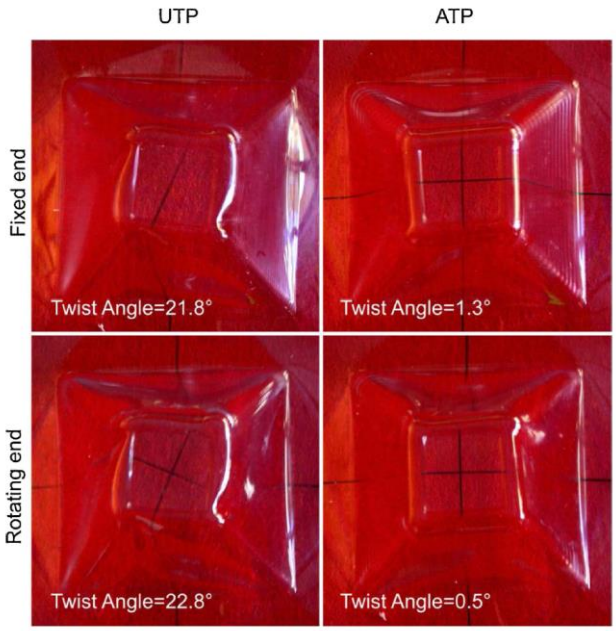

Figure 1-32: Effect of toolpath strategy on twisting of the formed part and twisting angle [44]

Bagudanch et al. [51] formed PLC, which is a biocompatible polymer, to examine the possibility to obtain a cranial implant by SPIF (Figure 1-33). Their findings showed that to improve the part geometry accuracy, a full negative die or the DSIF process is necessary.

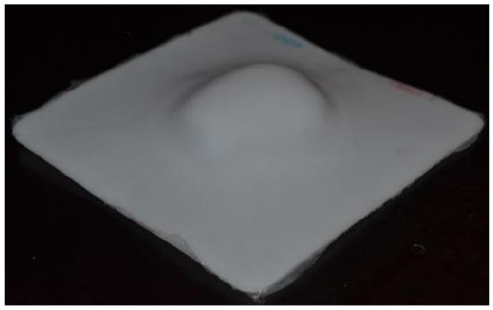

Figure 1-33: Manufactured cranial implant SPIF [51]

Jackson et al. [52] demonstrated the feasibility of forming laminated sandwich panels consisting of Polypropylene (PP) core material with mild steel and aluminum (AA5182) faceplate materials. Faceplate fracture, core shear failure, local indentation and delamination are identified as the modes of failure, which may occur in sandwich incremental forming (Figure 1-34).

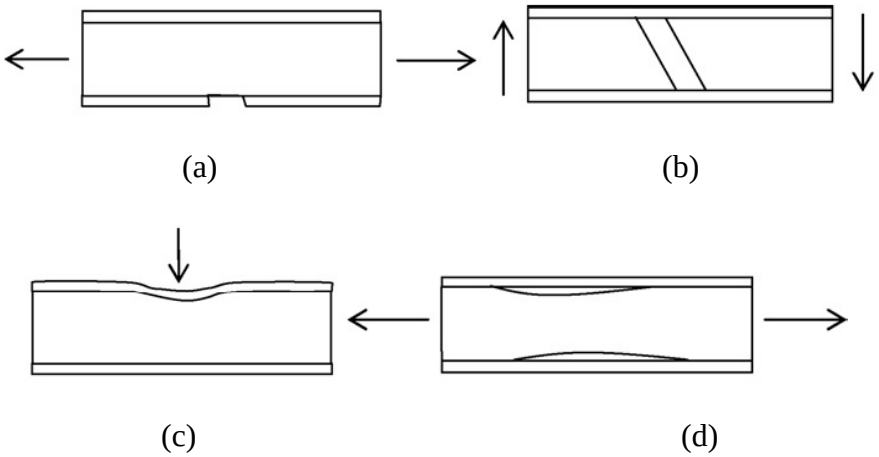

Figure 1-34: Four failure modes of sandwich panels which may occur in ISF and required loading: (a) faceplate fracture, (b) core shear failure, (c) local indentation and (d) delamination [52]

It was also shown that the effect of incremental depth and tool radius in sandwich panel SPIF is similar to metal sheet SPIF. However, the effect of the sheet thickness was not examined and only a tearing mode of failure was observed.

1.5 Goals and Approach of This Research

The goal of this research is to extend the state of knowledge and expand the process capabilities of incremental forming of thermoplastic polymers (amorphous and semi-crystalline). To achieve this objective, this project will tackle the following challenges in SPIF and DSIF of thermoplastic polymers.

1. *Limited knowledge on the effect of SPIF process parameters on failure modes and formability in polymer SPIF:* This results in a lack of a priori control of the SPIF process parameters to prevent failure of the sheet during forming.

2. *Limited knowledge of the effect of process parameters on the mechanical properties of polymers*: This results in lack of control on the process parameters, which affect the mechanical properties of the formed part.

3. *Limited knowledge on the effect of SPIF process parameters on failure modes and formability of metal-polymer laminate*: This results in lack of a priori control of the SPIF process parameters to prevent failure of the metal-polymer laminates during forming.

4. *Absence of knowledge on feasibility of DSIF process parameters on failure modes and formability of polymer DSIF*: This results in lack of a priori control of the DSIF process parameters to prevent failure of the sheet during forming.

Past works investigated the effect of SPIF process parameters and showed the capability of SPIF process for forming polymers. However, the effect of process parameters, specifically incremental depth and part shape on modes of failure and formability has rarely been investigated. In chapter 2, effects of incremental depth, tool rotation speed and part shape are investigated on formability, failure mode, forming forces and microstructural property of the formed material, and the results are discussed and analyzed. Past work showed anisotropy in formed polymer, however more research on the effect of SPIF process parameters on mechanical microstructural properties of the formed polymer is needed. In chapter 3, effect of SPIF process on mechanical properties and chain orientation of formed polymers is explained and discussed. Chapter 4 shows the results of incremental forming of metal-polymer laminates. The effect of incremental depth, polymer and metal sheet thickness on formability and mode of failure in polymer-metal SPIF is explored and discussed. Chapter 5 investigates the effect of DSIF process parameters on formability of polymers that fulfills the lack of research in polymer DSIF. The results show significant advantages of DSIF over SPIF in polymer incremental forming.

Effects of Incremental Depth and Tool Rotation on Failure Modes and Microstructural Properties in Single Point Incremental Forming of Polymers

Mohammad Ali Davarpanah, Amin Mirkouei, Xiaoyan Yu, Rajiv Malhotra and Srikanth Pilla

Journal of materials processing technology

DOI: https://doi.org/10.1016/j.jmatprotec.2015.03.014

Volume 222, August 2015, Pages 287-300

2 CHAPTER 2: EFFECTS OF INCREMENTAL DEPTH AND TOOL ROTATION ON FAILURE MODES AND MICROSTRUCTURAL PROPERTIES IN SINGLE POINT INCREMENTAL FORMING OF POLYMERS

2.1 Abstract

Single Point Incremental Forming (SPIF) is a sheet forming process characterized by advantages that include low-cost and part-shape-independent tooling, higher formability and greater process flexibility as compared to conventional sheet forming. While recent work has demonstrated the possibility of SPIF of polymers the effects of incremental depth and tool rotation speed, key process parameters in SPIF, have rarely been examined. This work experimentally examines how incremental depth and tool rotation speed affect the failure mode during forming, forming forces as well as the void structure and crystallinity of the formed material in polymer SPIF. The dependence of both tearing and wrinkling on the incremental depth and tool rotation speed is uncovered. It is shown that contrary to SPIF of metals, greater incremental depths result in increased formability in polymer SPIF, but this advantage is limited by the occurrence of sheet wrinkling at excessively high incremental depths. Further, the occurrence of sheet wrinkling depends not just on the incremental depth but also on the part shape being formed. Microstructural examination of the formed material shows that greater incremental depth results in greater void densities and that the material formed with SPIF has greater crystallinity than the unformed material. Additionally, it is shown that higher tool rotation speed can cause earlier onset of wrinkling. The implications of these observations on SPIF of polymers are discussed.

2.2 Introduction

Single Point Incremental Forming (SPIF) is a process in which a completely peripherally clamped sheet of material is locally deformed by a small hemispherical ended tool moving along a predefined toolpath. These local deformations accumulate to give the sheet its final desired shape. A significant amount of research has been performed on SPIF of metals in terms of deformation and fracture mechanics, forming forces, toolpath planning, geometric accuracy and surface finish in the process. Recent work on SPIF of polymers has also uncovered the possibility of expanding the materials capability window of SPIF beyond metals, by demonstrating SPIF of thermoplastic polymers at room temperature. This creates the possibility of saving on both tooling costs as well as on the thermal energy costs, which are inherent in injection molding or thermoforming processes that are typically used to fabricate freeform thermoplastic surfaces. Further, cold-state SPIF results in reduced heating of the sheet which is highly desirable for temperature sensitive biopolymers such as polylactic acid (PLA) and polyhydroxyalkanoates (PHAs). This lowered heating can alleviate thermal degradation and retain the virgin material properties that would have been lost in conventional fabrication processes. Past work on polymer SPIF has performed both experimental and computational investigations.. Franzen et al. (2009) [34] experimentally examined the feasibility of forming Polyvinyl Chloride (PVC) sheets into axi-symmetric shapes using SPIF. The following three modes of sheet failure were observed:

Mode 1: Sheet fracture by ductile tearing along the circumferential direction, at the transition between the wall and the corner radius of formed parts.

Mode 2: Wrinkling of the sheet along the wall of the part.

Mode 3: Tearing of the sheet in the radial direction, along the wall of the part.

The authors noted that only Mode 1 failure is typically seen in SPIF of metals and that Mode 3 failure is probably due to the occurrence of defects in the as-received sheet. The authors also showed stress whitening in the formed PVC material, and noted that this was probably due to deformation induced crazing in PVC. Martins et al. (2009) [39] further extended the above work to show that a reduction in tool radius and an increase in the sheet thickness result in increased formability in polymer SPIF, much like in metals SPIF. Franzen et al. (2008) [35] performed SPIF of five different polymers with varying degrees of crystallinity. It was shown that the reduction in density of the formed PVC material was larger than that of materials like Polycarbonate and Polyamide. The authors also experimentally demonstrated that the change in formed material density depends on the wall angle of the part being formed, and therefore on the strain induced in the material during SPIF. Furthermore, the dependence of springback on the sheet material properties was qualitatively examined in terms of the ratio of the yield stress of the material to the product between the thickness and elasticity modulus of the sheet material. Silva et al. (2010) [45] focused on computationally examining the deformation mechanics in polymer SPIF by extending the membrane-based analysis developed by Martins et al. (2008) [46]

via a pressure modified Tresca yield criterion. This single-step analysis models only Mode 1 failure by tearing and considers the influence of part shape, tool diameter, sheet thickness and mechanical properties of the polymer sheet on tearing in polymer SPIF. The authors successfully predicted experimental observations that reducing the tool radius can increase the formability of the material, more so for thicker sheets than for thinner sheets. However, due to the single-step nature of analysis this technique did not account for the effects of incremental depth (Δz) on mode 1 and mode 2 failure. The above literature review shows that the effects of incremental depth Δz and tool rotation ω on polymer SPIF have rarely been explored till date. The basis for expecting an effect of Δz, especially on the sheet failure modes, arises from the fundamental nature of deformation in SPIF in which a change in Δz can create a change in the stress history imposed on the sheet material. Past work on metal SPIF Xu et al. (2013) [53] has shown that tool rotation, and the resulting frictionally generated heat, can significantly increase formability and reduce the forming forces. A similar effect can be expected in polymer SPIF as thermoplastics exhibit softening and increase in ductility when heated.

This paper characterizes the effects of Δz and ω on failure, forming forces, as well as void content and crystallinity of the formed material in polymer SPIF. The experiments performed are described in Section 2.2. Section 2.3 describes the observed effects of Δz and ω on failure modes. We go beyond just Mode 1 failure and uncover a distinct transition between Mode 1 and Mode 2 failure that is dependent on the above process parameters as well as on the part shape being formed. Furthermore, the effects of Δz and ω on void density

and crystallinity of the formed material are obtained via Scanning Electron Microscopy and Differential Scanning Calorimetry. Section 2.4 discusses the implications of these observations in terms of failure modes during polymer SPIF, process throughput and formed material properties, along with a discussion on possible directions for future work.

2.3 Experimentation

An SPIF setup with a circular forming area of 40 *mm* diameter was assembled on a HAAS CNC machine platform (Fig. 2-1a). This setup consisted of the following components: (i) the clamped polymer sheet (ii) the blankholder mounted onto a Kistler 9257B plate type dynamometer (iii) the forming tool mounted on the CNC spindle. The dynamometer was mounted onto the bed of the CNC and was used to monitor the forming forces during SPIF. No backing die was used and a PTFE-based grease was used as the lubricant at the tool sheet interface during all experiments.

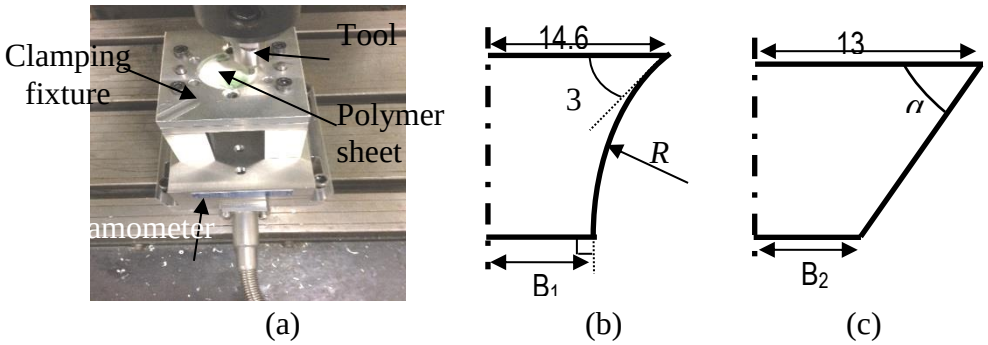

Figure 2-1: (a) SPIF setup (b) profile of funnel shape formed (c) profile of cone shape formed

To examine the effect of Δz and ω on failure modes two kinds of part shapes were formed namely, funnel shapes (Fig. 2-1b) with continuously varying wall angle from 30° to 90° and a variable radius of curvature R_f and cone shapes (Fig. 2-1c) with variable wall angle α. For the funnel shape the base diameter (B_1) varied from a minimum of 8.1 *mm* to

16 *mm* whereas for the cone shape the base diameter (B_2) varied from a minimum of 8.6 *mm* to 17 *mm*. Since a tool of diameter 5 *mm* was used in all the SPIF experiments shown in this paper there was no interference of the tool with the already formed region of the sheet during forming.

The funnel shape has been frequently used to examine formability in metal SPIF (Hussain et al. [54]) since its geometry provides a continuously increasing strain to be imposed on the sheet during deformation. On the other hand the constant wall angle of the cone shape results in a more uniform strain being imposed along the wall of the formed part. SPIF experiments were performed with contour toolpaths generated from the CAD geometry of the part using automated toolpath generation methods after Malhotra et al. (2010) [19]. Two polymer sheets, i.e., a 1.5 *mm* thick petroleum-based PVC material and 0.7 *mm* thick bio-based Polylactic Acid (PLA) material, were used as blank materials. The blank material was confined to these polymers because our goal was not to compare the ability of SPIF to form different thermoplastic materials but to examine the effects of Δz and ω on polymer SPIF in general.

A range of incremental depths from 0.2 *mm* upto a value greater than the sheet thickness were used to generate the toolpaths. The tool feed rate and tool diameter were kept constant at 300 *mm/min* and 5 *mm* respectively. The sheet thickness, tool feed rate and tool diameter were kept constant since the effect of these parameters has been shown in past literature. Table 2-1 summarizes the values of experimental parameters Δz and ω as well as the values of the shape parameters R_f and α used in the experiments. Only Mode 1

and Mode 2 failure were seen in this work and so only these failure modes are reported. The tool tip depth at failure during SPIF was recorded during forming experiments and was converted into the corresponding wall angle by using the CAD model of the desired part, the forming tool diameter and the designed toolpath. Each experiment was performed at least four times.

Table 2-1: Summary of experimental parameters used

Material	Incremental depth Δz (*mm*)	Tool rotation speed ω (*rpm*)	R_f (*mm*)	α (degrees)
PLA	0.2,0.4,0.6,0.8,1.0	0,1250,5000,7000	10,12,14,16	55,65,75
PVC	0.2,0.6,1.0,1.4,1.8	0,1250,5000,7000		

2.4 Experimental Observations and Discussion

This section discusses the results of the above experiments in terms of the sheet failure modes, forming forces as well as the measured void structure and crystallinity of the formed material.

2.4.1 Failure Modes

Figure 2-2 shows the effect of Δz, at ω = 0 rpm, on the maximum formable wall angle in SPIF of the PLA funnel shapes. In these plots the data points are supplemented with a description of whether tearing (i.e. mode 1 failure, denoted as T), wrinkling (i.e., mode 2 failure, denoted as W) or no failure (denoted as N) was observed. This kind of description is used throughout this paper. Figure 2-2a shows that for R_f = 10 *mm*, as Δz increases there is an increase in the maximum formable wall angle and therefore in the formability. Furthermore, failure occurs by tearing and not by wrinkling.

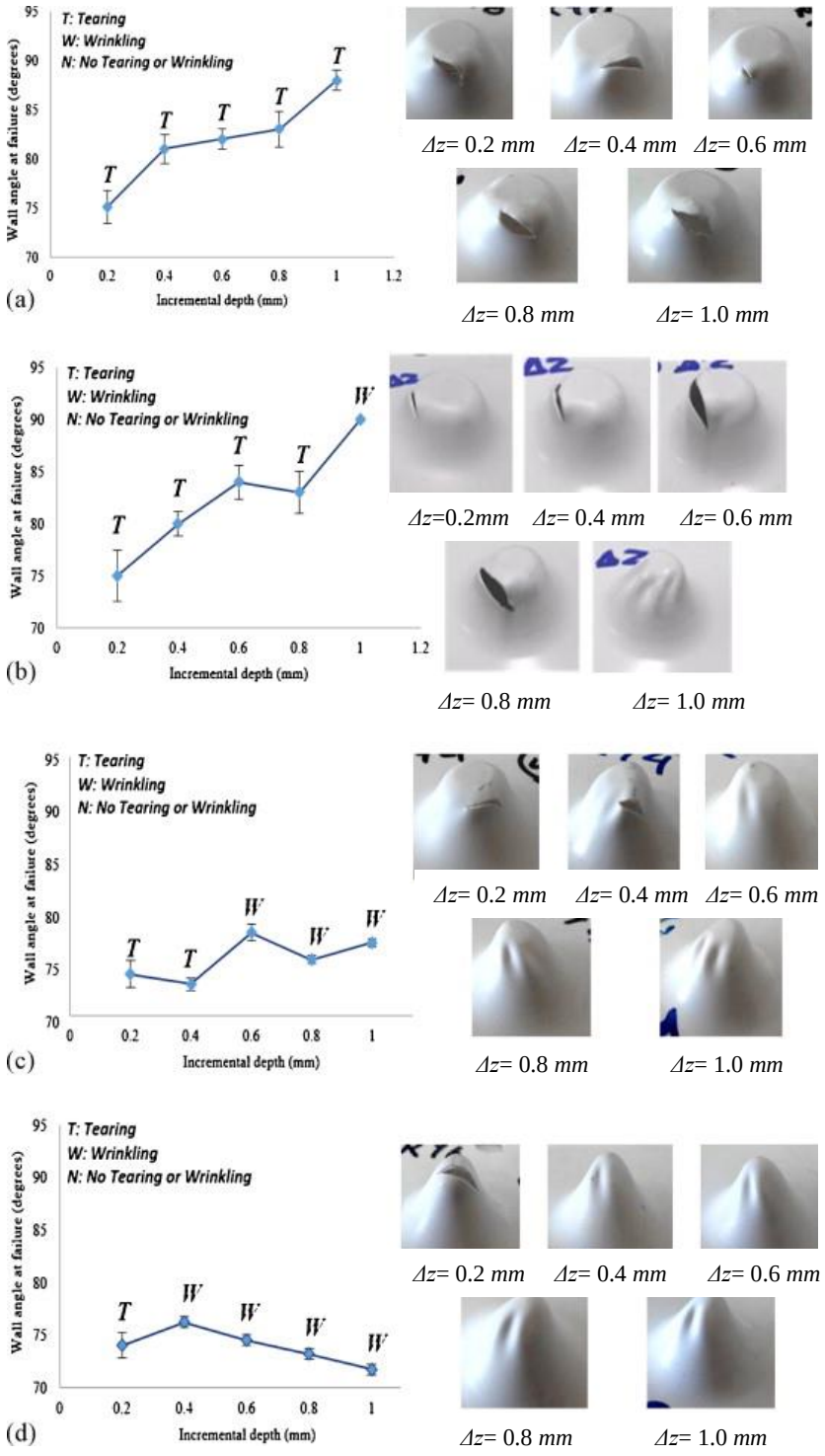

Figure 2-2: Effect of Δz on failure modes and formed parts for funnel shaped PLA parts with R_f = (a) 10 *mm* (b) 12 *mm* (c) 14 *mm* (d) 16 *mm*

At the same time, Figure 2-2b shows that for $R_f = 12\ mm$ at $\Delta z = 1.0\ mm$ wrinkling appears as the mode of failure. Furthermore, as the value of R_f increases there is a reduction in the Δz value at which this transition between mode 1 failure by tearing and mode 2 failure by wrinkling occurs. A possible conclusion to draw from these observations, is that in polymer SPIF the formability increases with the Δz, but if the Δz is too high then unwanted sheet wrinkling might occur. Therefore, the mode of failure transitions from Mode 1 failure by tearing to Mode 2 failure by wrinkling at a transitional Δz.

However, one must first consider past work in metals SPIF as well before accepting wrinkling as a universal phenomena in polymer SPIF. In past work on metals SPIF Jackson et al. (2009) [20] have shown that SPIF is characterized by much larger shear stresses than are typically present in conventional forming. Computational analysis by Malhotra et al. (2012) [30] showed that this shear plays a key role in formability in metals SPIF and that the magnitude of this shear depends on the shape of the part being formed.

Hussain et al. (2007a) [54] further observed that the formability in metals SPIF depends significantly on the part shape being formed. They formed funnel shapes with different radii of curvature of the wall to show that the formability changes with the radius of curvature.

Since different part shapes (e.g., varying R_f for the funnel shape) result in different stress states and stress histories being imposed on the sheet the conclusion was that the formability and deformation mechanics in SPIF depend significantly on the stress state and

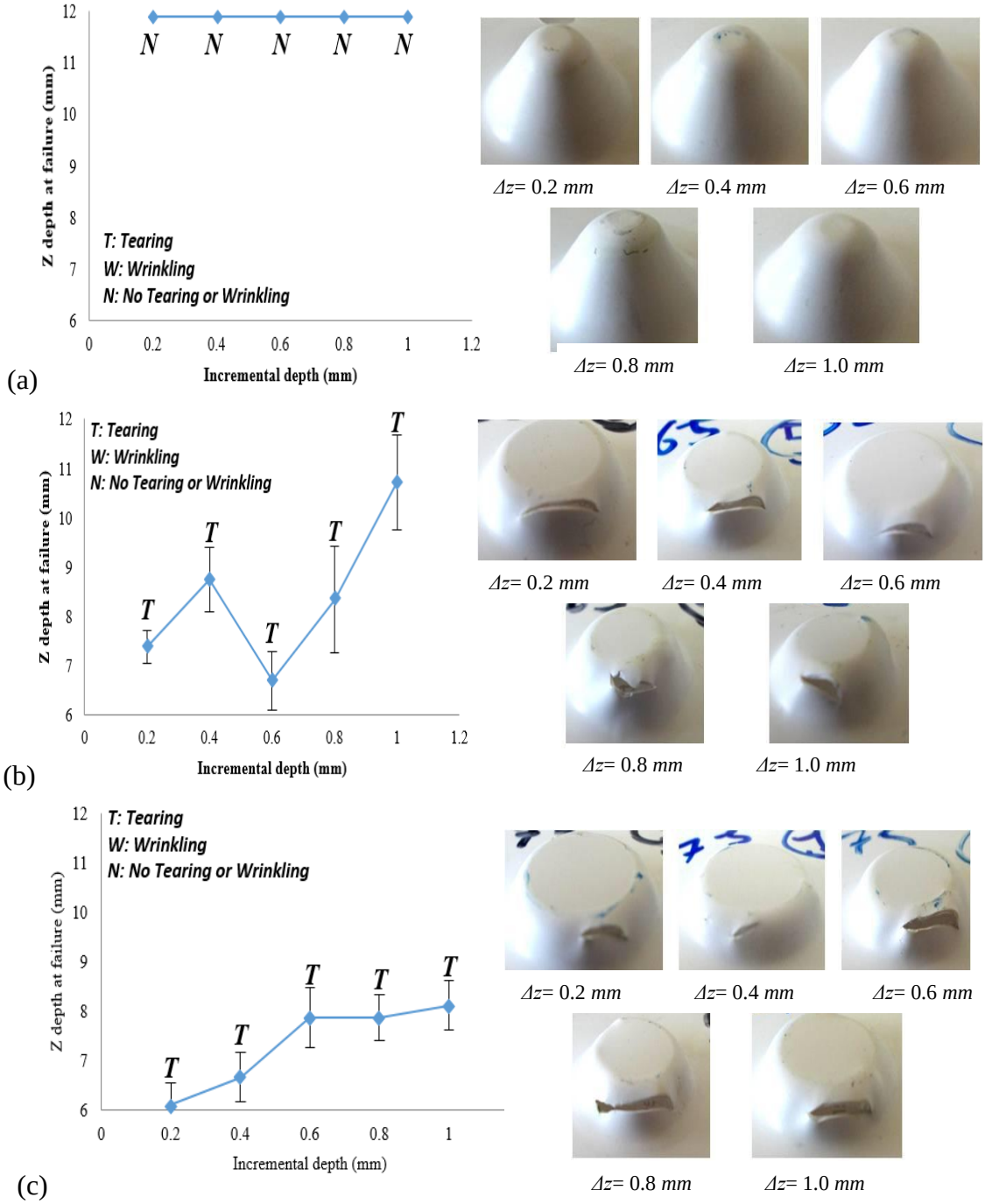

Figure 2-3: Effect of Δz on failure modes and formed parts for PLA cone parts with α = (a) 55° (b) 65° (c) 75°

stress history imposed on the material. In light of these observations it is useful to examine the effect of Δz on tearing and wrinkling for a part shape that is different than the funnel shape.

Figure 2-3 shows the effect of Δz at $\omega = 0$ *rpm* on the failure modes in SPIF of PLA cone shapes. Note that wrinkling does not occur at any Δz for the cone shape, irrespective of the wall angle. At the same time there is an increase in the formability with increasing Δz, shown by the increase in the formable depth at a constant wall angle. The lack of wrinkling in the cone shapes and its presence in the funnel shapes indicates that the occurrence of wrinkling also depends on the overall part shape being formed. Therefore, the constraint placed on maximum Δz usable due to the occurrence of wrinkling depends significantly on the part shape being formed.

In fact, Figure 2-2 shows a similar phenomena since a change in R_f causes a change in the mode of failure from tearing to wrinkling at the same incremental depth. For example at $\Delta z = 1.0$ *mm* tearing is observed in the case of $R_f = 10$ *mm* (Fig. 2-2a) whereas wrinkling is observed for $R_f = 12$ *mm* and above (Fig. 2-2b- d). These phenomena were also observed for PVC. An example of the transitional Δz for PVC is shown in Figure 2-4 for the funnel shape with $R_f = 12$ *mm*.

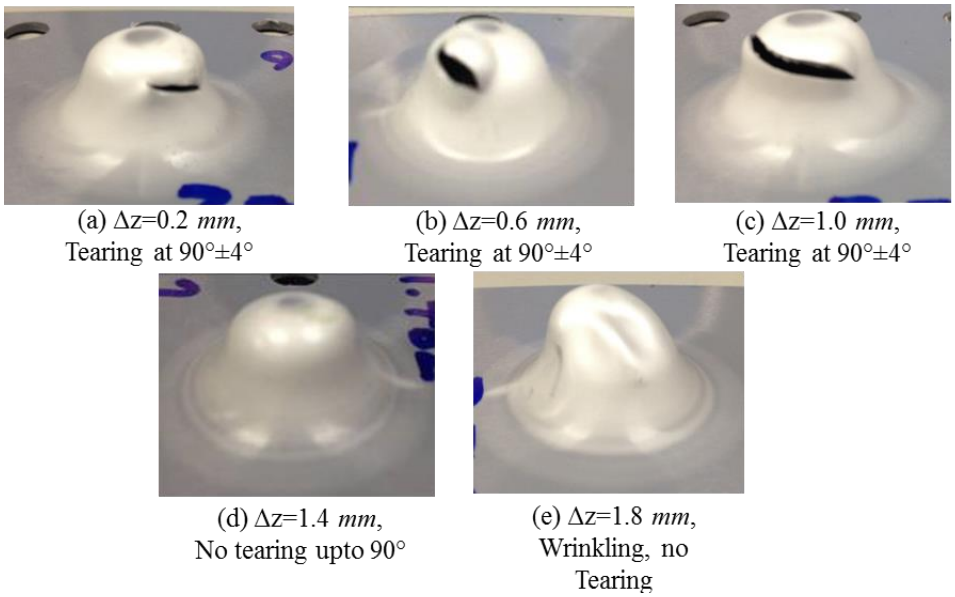

Figure 2-4: Formed parts showing the effect of Δz on sheet tearing or wrinkling for SPIF of PVC funnel part with R_f = 12 *mm*

Figures 2-5 and 2-6 show the effect of increasing the tool rotation speed ω on the failure modes for the PLA funnel shape with R_f =12 *mm*. It can be seen that increasing the tool rotation speed has very little positive effect on increasing the formability with Mode 1 failure (e.g., for Δz = 0.2 *mm* at 1250, 5000 and 7000 rpm in Fig. 2-6a, and for Δz = 0.6 *mm* at 1250 rpm in Fig. 2-6b).

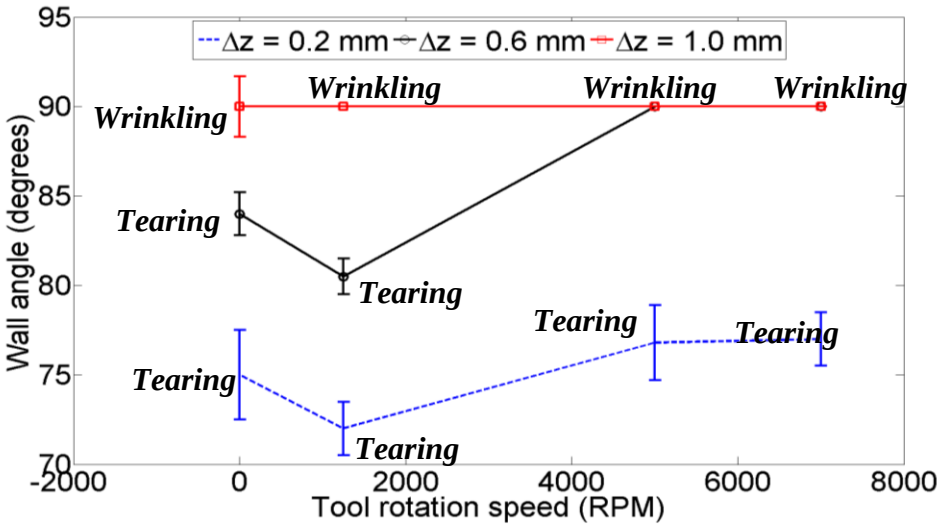

Figure 2-5: Change in wall angle at tearing/wrinkling with *Δz and ω* for PLA funnel part

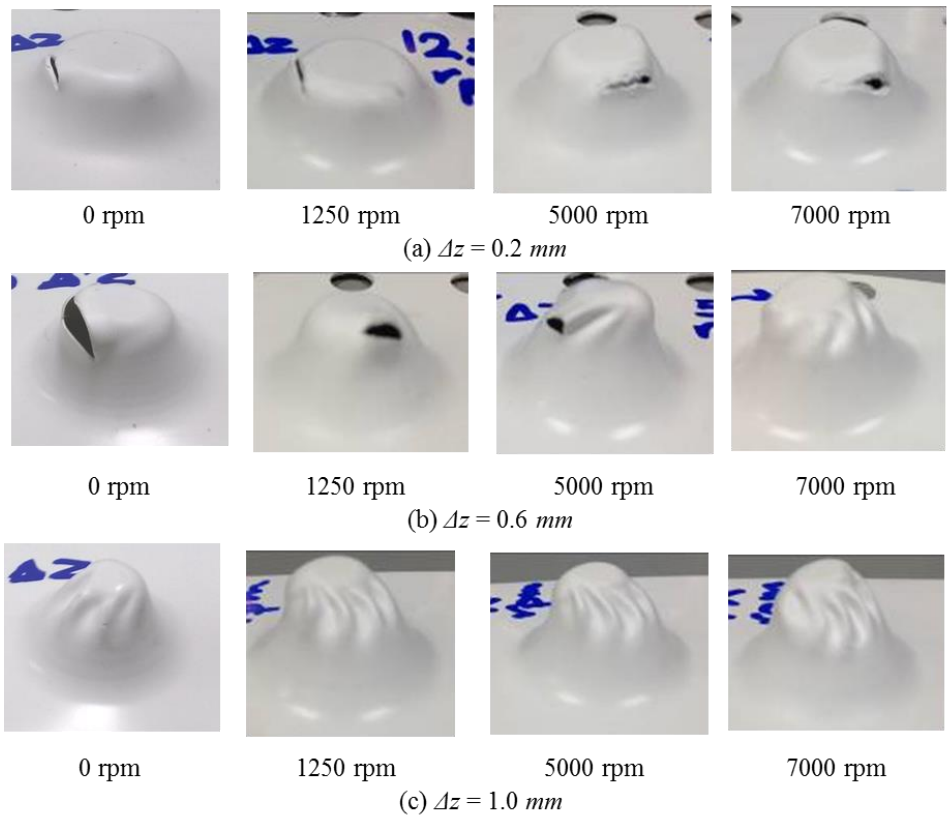

Figure 2-6: Formed PLA funnel parts showing change in failure mode with change in *Δz* and *ω*

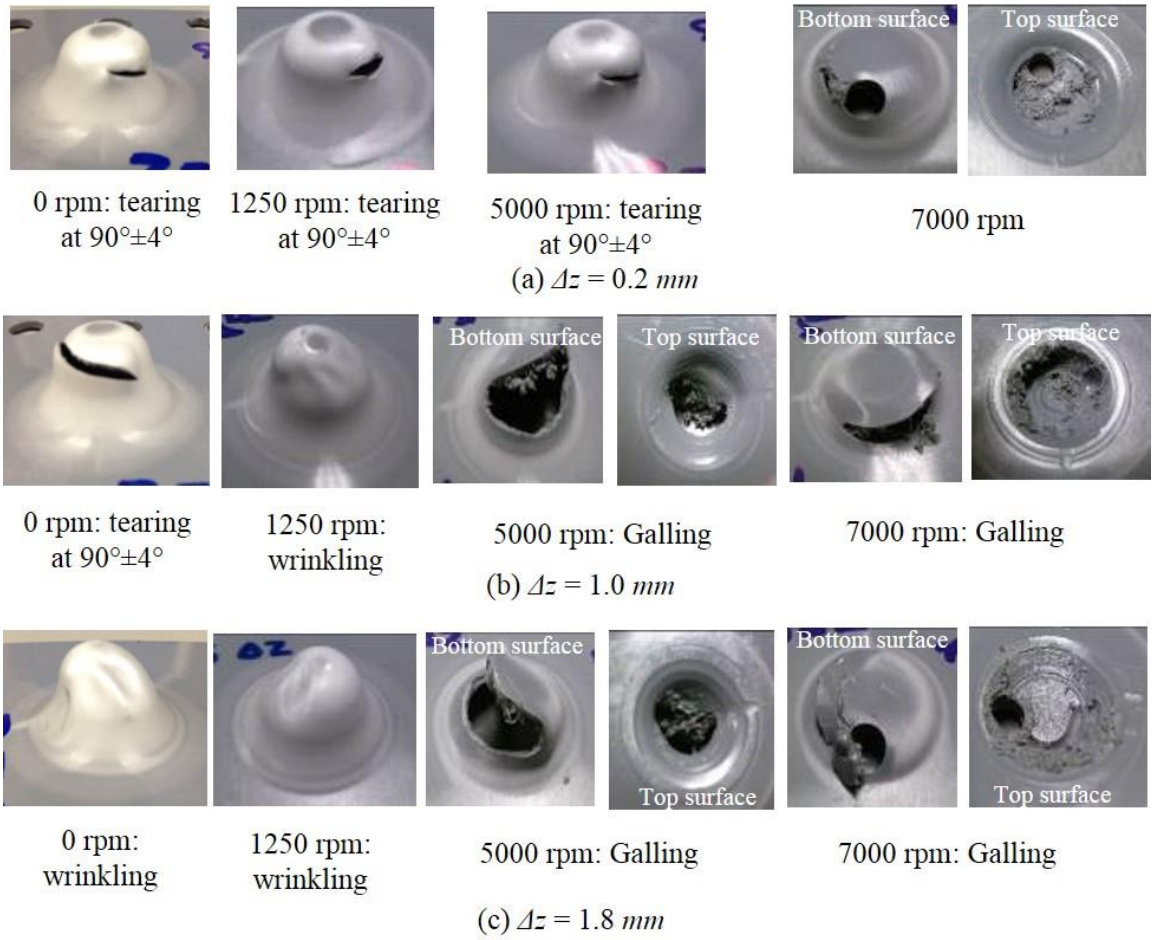

Figure 2-7: Formed PVC funnel parts showing change in failure mode with change in Δz and ω

On the other hand, at a constant Δz an increase in ω increases the tendency for sheet wrinkling to occur (e.g., Δz = 0.6 *mm* at 5000 and 7000 rpm in Fig. 2-6c). For larger incremental depths (Δz = 1.0 *mm*) the increase in ω is unable to alleviate the occurrence of Mode 2 failure. Similar effects where observed when forming the funnel part with R_f= 12 *mm* on PVC sheets (Fig. 2-7).

Further, during SPIF of the PVC funnel shape it was observed that sheet galling occurred at tool rotation speeds of 5000 *rpm* and above, resulting in premature sheet failure.

Similar effects of ω were observed for PLA and PVC for funnel shapes with different R_f values and for the cone parts as well. To summarize, tool rotation in polymer SPIF has minimal effect on the mode 1 failure and greater tool rotation speed can increase the tendency of the sheet to undergo Mode 2 failure or galling during FPI.

2.4.2 Forming Forces

Past work (Filice et al. 2006 [55], Duflou et al. 2007 [56], Bouffioux et al. 2008 [57]) in metals SPIF has shown that the forming forces in SPIF indicate key characteristics of the process mechanics. Further forming forces are a critical process metric needed for process model calibration and machine design. Figures 2-8 and 2-9 show representative in-plane and Z forces as a function of Δz when ω =0 for R_f=12 *mm* funnels.

The in-plane forces were obtained as the magnitude of the resultant of the X and Y forces. As typically seen in a contour toolpath (Duflou et al., 2007 [56]), after completion of one contour the Z force drops when the tool moves to the next contour, reaches its peak value at the step down and finally stabilizes when the tool moves along the contour.

The stable portions of the in-plane and Z forces were obtained for the above-performed experiments after filtering out the spikes at the step down of the contour path. The filtering was done via a nonlinear median filtering algorithm, which applies a sliding window to a sequence of data and replaces the center value in the window with the median value of all the points within the window (Pratt et al., 1991 [58]). Figure 2-10 compares the peak in-plane and Z forces over a range of Δz and ω for R_f= 12 *mm* funnels formed on both PLA and PVC. Figure 2-10 shows that there is an increase in the in-plane and the Z

forces with an increase in Δz. This is a typical trend that is also seen in SPIF of metals and is related to a larger amount of material being deformed in each contour as the Δz increases. Further, there is a steady reduction in the in-plane and Z forces with an increase in tool rotation speed.

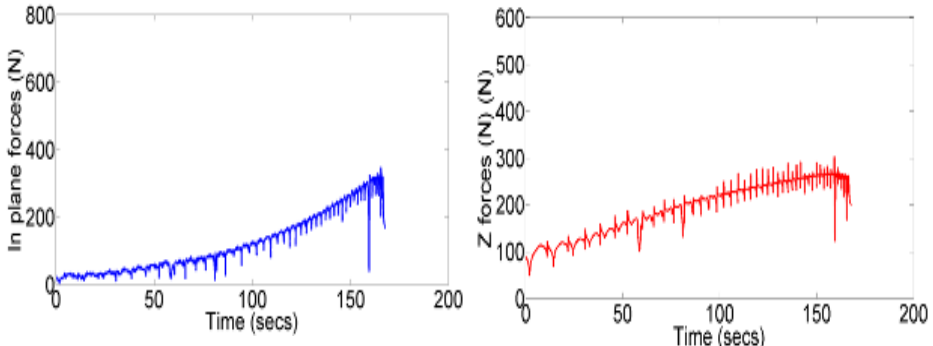

(a) Δz = 0.2 *mm*; Tearing seen

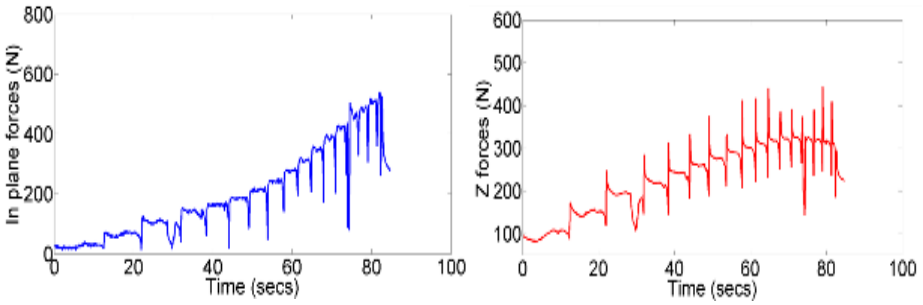

(b) Δz = 0.6 *mm*; Tearing seen

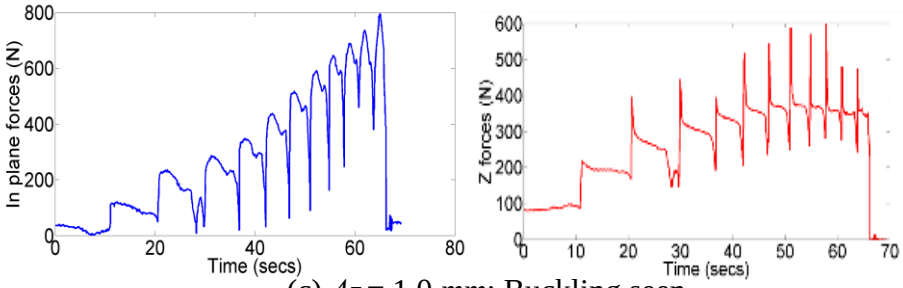

(c) Δz = 1.0 *mm*; Buckling seen

Figure 2-8: In-plane forces and Z forming forces for PLA funnel part with R_f = 12 *mm*

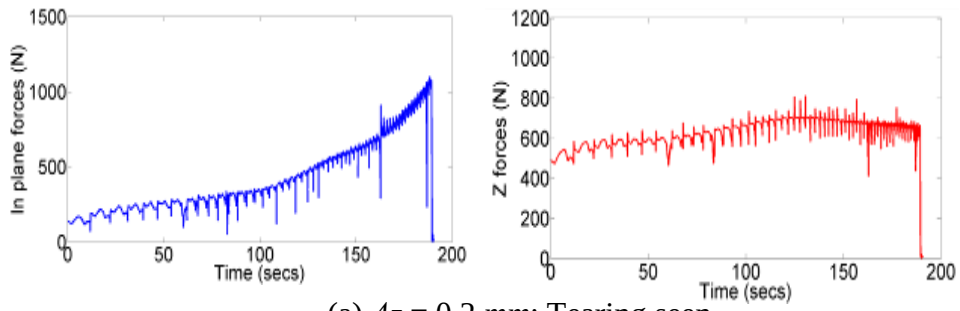

(a) Δz = 0.2 *mm*; Tearing seen

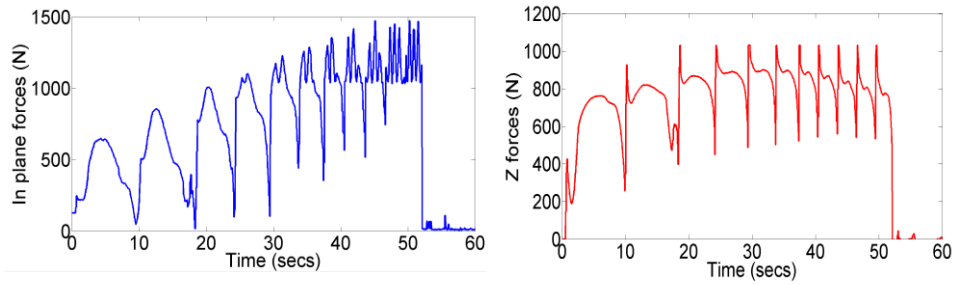

(b) Δz = 1.0 *mm*; Tearing seen

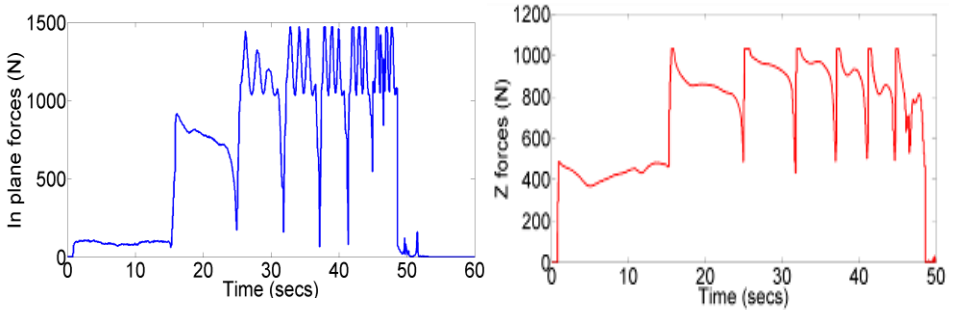

(c) Δz = 1.8 *mm*; Buckling seen

Figure 2-9: In-plane forces and Z forming forces for PVC funnel part with R_f = 12 *mm*

This is probably due to frictional heat generated at the tool-sheet interface. Further, this implies that if formability constraints can be met and the occurrence of buckling or galling can be prevented, then increasing tool rotation speed can enable forming of thicker sheets with lower forming forces.

Note that the increase in the in-plane forming forces with an increase in Δz is more significant than that for the Z forces, and is simultaneously accompanied by a transition

from tearing to wrinkling (Figs. 2-6 and 2-7). It might be hypothesized that these increased X and Y forces are responsible for sheet wrinkling due to dragging the sheet along with the tool. However, there is also a reduction in in-plane forces with an increase in tool rotation speed but no alleviation of wrinkling which shows that the above hypothesis may not always be true.

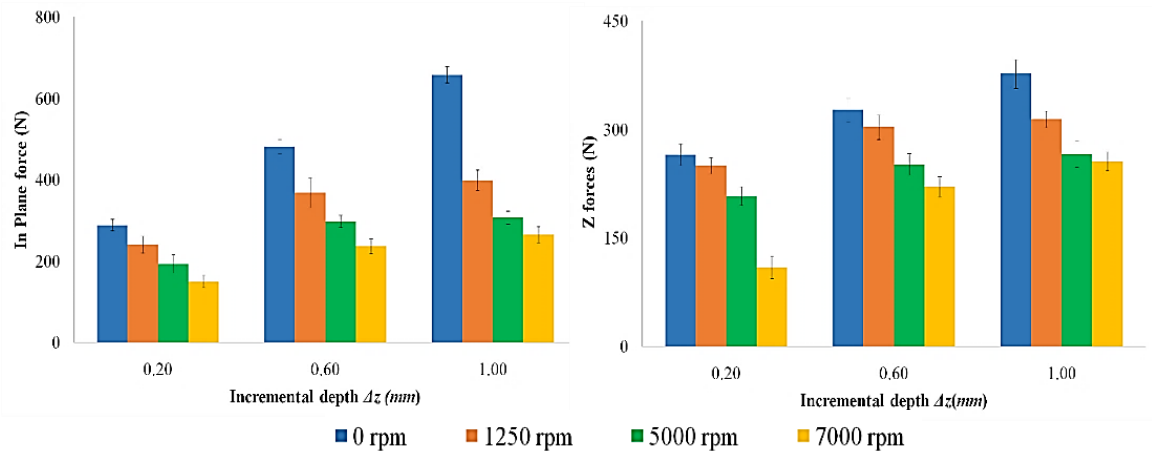

(a)

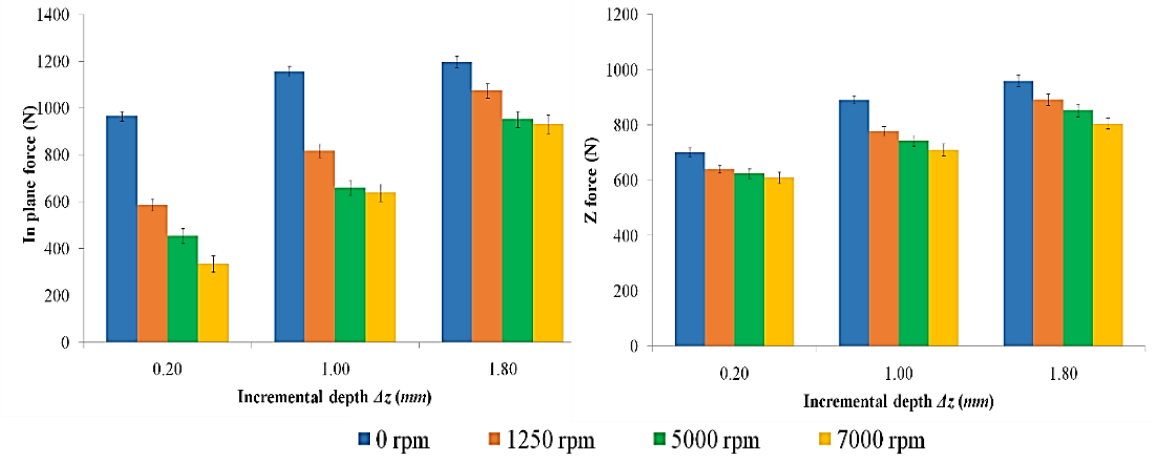

(b)

Figure 2-10: Comparison of maximum stable in-plane and Z forces at different incremental depths and tool rotation speeds for funnel part with R_f = 12 *mm* formed on (a) PLA (b) PVC

2.4.3 Void Structure in Formed Material

Figures 2-11 and 2-12 show representative scanning electron microscope images of the formed and as received material for the funnel parts with R_f = 12 *mm*, on PLA and PVC respectively. The outer surface of the formed material (the side of the sheet that was not in contact with the tool during SPIF) was examined as this is the region of the material where material fracture initiates (Malhotra et al., 2012 [30]). The samples were taken from the middle of the formed wall of the funnel parts. Note that for PVC we ignore the cases where sheet galling occurred (Δz = 0.2 *mm* at 7000 *rpm*; Δz = 1.0 *mm* at ω = 5000, 7000 rpm; Δz = 1.8 *mm* at ω = 5000, 7000 rpm). This is because galling resulted in premature failure so that insignificant changes in void structure were observed because of an insignificant amount of deformation.

Figures 2-13a and 2-13b show the void density and average void area obtained by averaging over a larger number of SEM images. Given that the average cell area is fairly constant for different Δz and tool rotation speeds the trends for the void area fraction, i.e., the surface area of voids to the total surface area, is expected to follow the trends for the void density. For Δz=0.2 *mm* the void density at ω=1250 *rpm* is lower than that at ω=0 rpm. There is again a slight increase when the ω =7000 rpm. This reflects the trend for dependence of formable wall angle on tool rotation speed at Δz = 0.2 *mm* (Fig. 2-5) where the maximum formable wall angle by tearing sees a slight dip at 1250 *rpm* and then an increase at 7000 *rpm*. The dependence of void density on tool rotation speed is similar for Δz =1.0 *mm* (Fig. 2-10a). However, an anomaly is noticed for the Δz = 0.6 *mm* case at 7000

rpm where the void density is lowest as compared to that at the other tool rotation speeds $\Delta z = 0.6\ mm$.

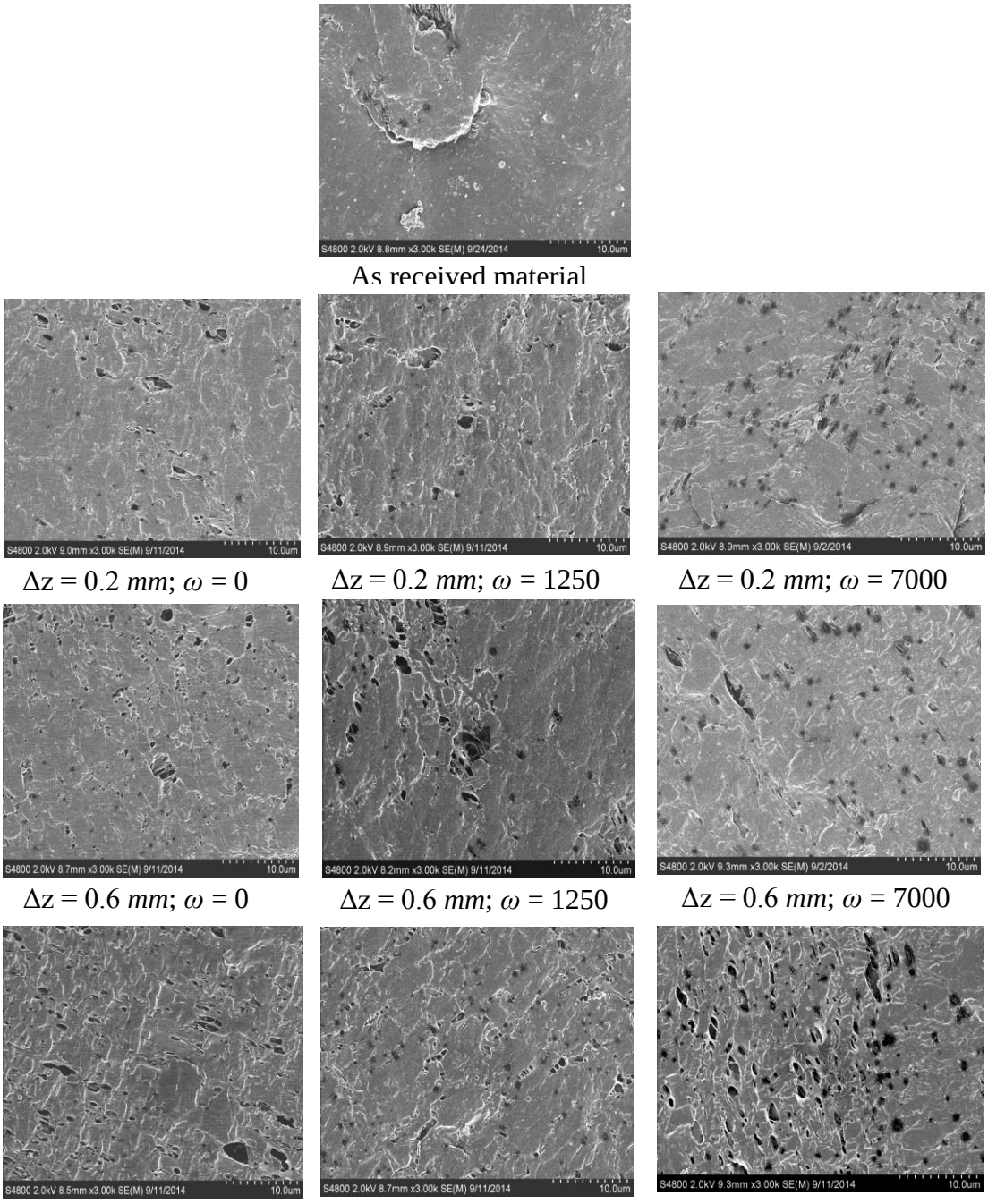

Figure 2-11: SEM micrographs of PLA funnel part at different Δz and ω

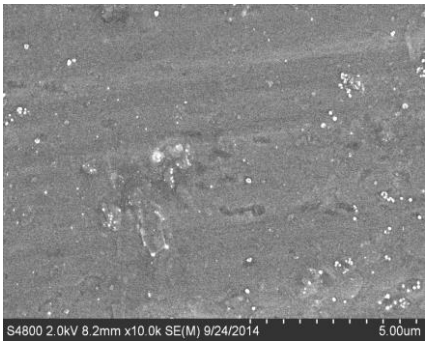

As received material

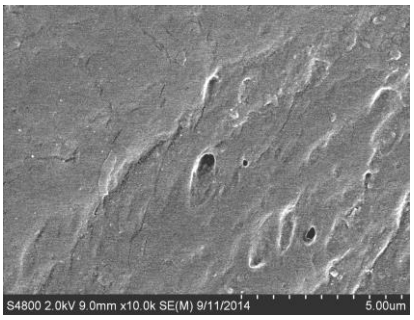

$\Delta z = 0.2\ mm$; $\omega = 0$ rpm

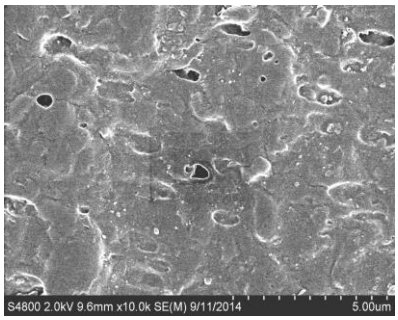

$\Delta z = 0.2\ mm$; $\omega = 1250$ rpm

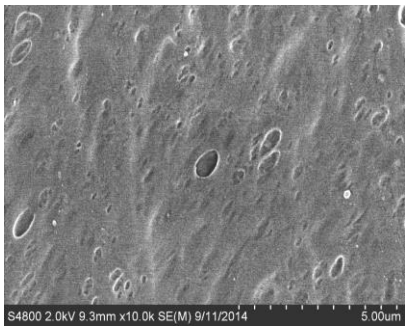

$\Delta z = 1.0\ mm$; $\omega = 0$ rpm

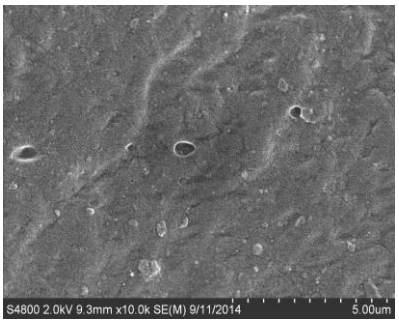

$\Delta z = 1.0\ mm$; $\omega = 1250$ rpm

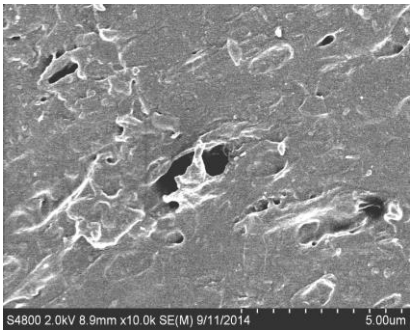

$\Delta z = 1.8\ mm$; $\omega = 0$ rpm

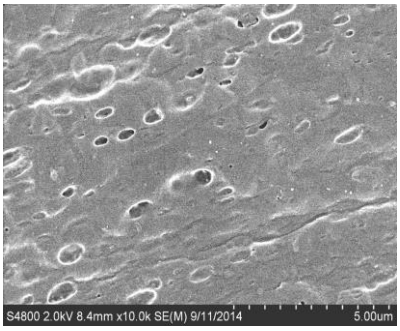

$\Delta z = 1.8\ mm$; $\omega = 1250$ rpm

Figure 2-12: SEM micrographs of PVC funnel part at different Δz and ω

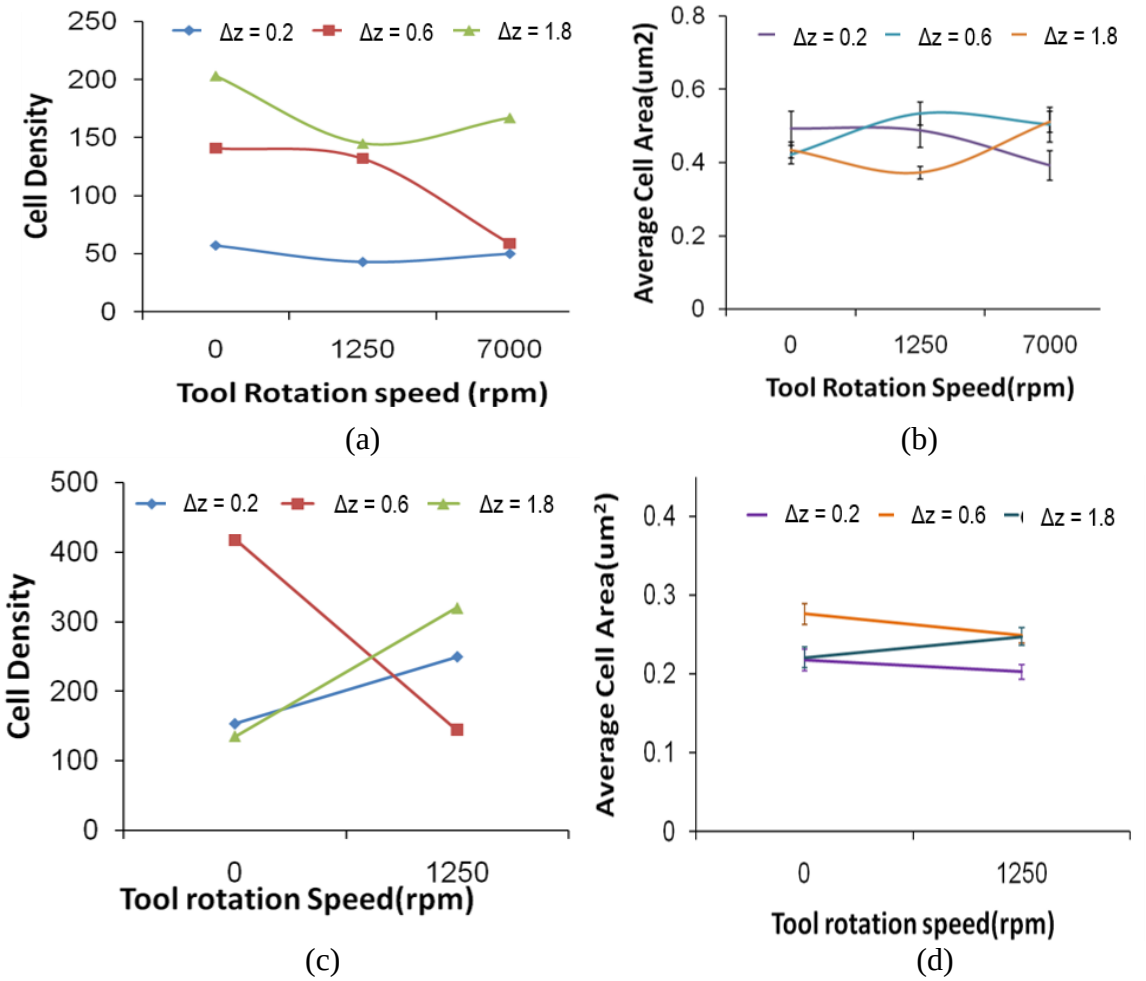

Figure 2-13: (a) Void density for PLA (b) average void area for PLA (c) void density for PVC (d) average void area for PVC

A key point to note is that despite the above anomaly the void density, and thus the void area fraction, is consistently higher at greater *Δz*. This is despite the fact that at higher *Δz* the wall angle at tearing and therefore the formability is higher (Fig. 2-5). In the case of PVC (Figs. 2-13c and 2-13d) for *Δz* = 0.2 and 1.8 *mm* an increase in the tool rotation speed to 1250 *rpm* results in increased void density. An anomalous trend is seen for *Δz* = 0.6 *mm* where the void density reduces with an increase in the tool rotation speed. Since failure in

PVC occurs at similar wall angles irrespective of the value of Δz or ω it is difficult to correlate void density to formability.

2.4.4 Thermal Properties and Crystallinity

The crystallization behavior of the formed and as-received PLA and PVC materials was studied using differential scanning calorimetry (TA Instruments, Q2000) via heat/cool/heat cycles. The samples were heated from 40°C to 180°C and kept isothermal for 3 minutes before cooling to 0°C and then reheating up to 200°C. The temperature ramp rate in all the cycles was 10°C/min. The thermograms for PLA obtained from the first and second heating cycles are shown in Fig. 2-14a and 2.14b respectively. The data obtained from the first heating cycle provides information on the crystallinity of the PLA material formed by SPIF, whereas the data obtained from the second heating cycle allows for a direct comparison of the crystallization behavior after erasing any previous thermal history (caused by SPIF) through the first heating cycle. The crystallinity of PLA is computed using the following equation (Pilla et al., 2008 [59]).

$$\chi_c = \frac{\Delta H_m - \Delta H_{CC}}{\Delta H_m^0} \cdot \frac{100}{w} \tag{2-1}$$

where χ_c= Percentage of crystallinity, $\Delta H_m^0 = 93.7\, J/g$, w = Weight fraction of PLA in sample, ΔH_{CC}= Cold-Crystallization Enthalpy. For the present study, the weight fraction of PLA was taken to be same for all the samples i.e. 100.

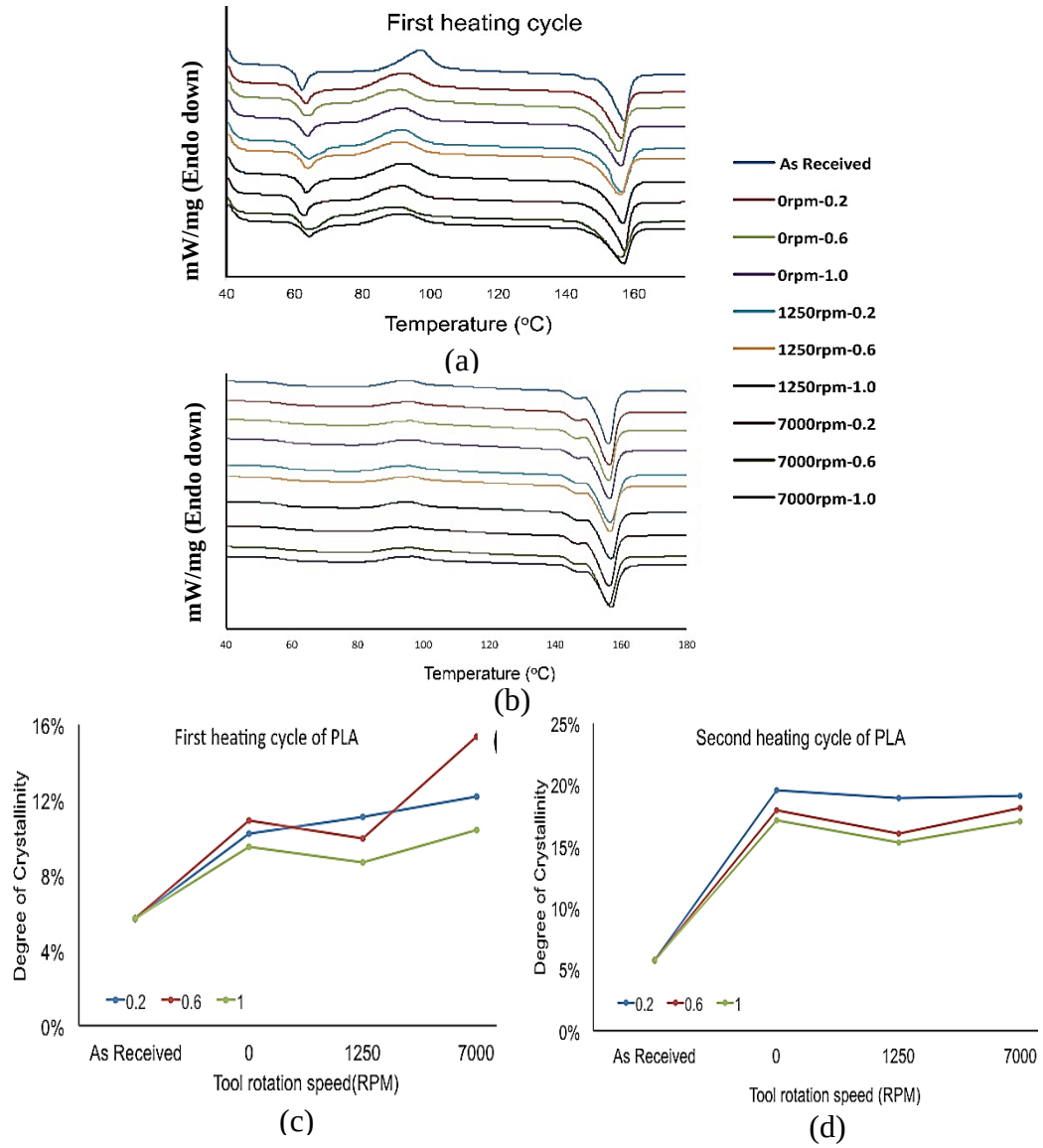

Figure 2-14: Melting curves of PLA with different Δz and ω from the DSC measurements: (a) first heating cycle, (b) second heating cycle, (c) the crystallinity from the first heating cycle and (d) the crystallinity from the second heating cycle

The PLA thermograms obtained from the first heating cycle show an endothermic peak (in all the specimens) near the glass transition (T_g) phase because of physical aging of the polymeric materials (Hodge et al. (1983a) [60], Hodge et al. (1983b) [61], Hodge et al. (1982) [62]). This phenomenon is related to the inherent distribution of the relaxation

times of polymer chains (Turi et al. (1997) [63]). On the other hand, during the second heating cycle, the endotherm peaks near Tg were not observed. This is because the enthalpic recovery that occurred during the first heating cycle is kinetic in nature (Pilla et al., (2009) [64]). Figure 2-14c shows that the SPIF process has enhanced the degree of crystallinity of as received PLA from 5.7% to ~10.5%.

Moreover, the increase in ω (0-7000 rpm) results in an even greater enhancement of the degree of crystallinity. A similar trend was observed for the degree of crystallinity computed from second heating cycle (Fig. 2-14d). However, the observed crystallinity is much higher than the first cycle. As mentioned, the first heating crystallinity reflects the crystal morphology induced by SPIF process while the second heating crystallinity is induced due to cooling rate of cooling cycle. As discussed in the next section, the enhancement in crystallinity of PLA due to the SPIF process has significant implications especially on the mechanical properties of the formed material. The PVC material investigated in this study was completely amorphous (Fig. 2-15) and hence, unlike PLA, no crystal morphology was observed.

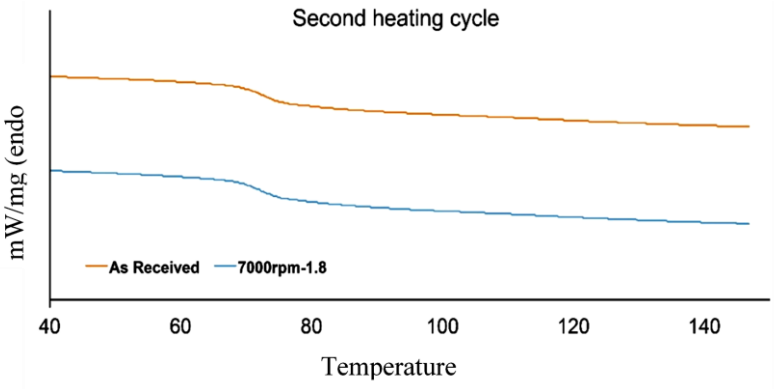

Figure 2-15: Representative melting curves of PVC from the DSC measurements (as received material and from SPIF at $\Delta z = 1.8$ *mm* and $\omega = 7000$rpm)

2.5 Discussions and Future Work

This section discusses the implications of the above experimental observations on polymer SPIF. Figures 2-2 and 2-4 show that unlike SPIF of metals, in polymer SPIF there is an increase in the formability with increase in the incremental depth. This implies a dual advantage of increasing both the formability and the process throughput at the same time. However, Figs. 2-2 and 2-4 also show that there is a limit on this increase in incremental depth in the form of a transitional incremental depth beyond which the failure mode transitions from Mode 1 tearing failure to Mode 2 wrinkling failure. At the same time, Fig. 2-2 shows that this transitional incremental depth depends on the radius of curvature R_f of the part and Fig. 2-3 shows that the Mode 2 failure is absent in the forming of a cone shape. This implies that this transitional incremental depth depends on the part shape being formed. In summary, increasing the incremental depth increases the formability of the material in polymer SPIF while being limited by the occurrence of sheet wrinkling at high incremental depths, and the occurrence of this wrinkling additionally depends on the overall part shape as well. Therefore, there is an optimum value of the incremental depth, i.e., the transitional incremental depth at which formability and throughput can be simultaneously maximized. An investigation of the deformation mechanics that causes this phenomena and mechanics based prediction of this transitional incremental depth for any given part shape is needed.

Figures 2-5, 2-6 and 2-7 show that an increase in tool rotation speed does not significantly increase the formability of the material in polymer SPIF. On the other hand

increasing the tool rotation speed causes an increased tendency for wrinkling. Further, in the case of PVC too high a tool rotation speed can also cause galling and premature failure of the sheet during forming.

Figures 2-8, 2-9 and 2-10 show that the forming forces rise with an increase in the incremental depth which is also observed in metals SPIF. Furthermore, with an increase in the tool rotation speed a reduction in the forming forces is observed (Fig. 2-10) which is probably due to greater friction at the tool-sheet interface. The simultaneous transition to wrinkling and the relatively larger increase in the in-plane forces at higher incremental depths might indicate that wrinkling is due to higher in-plane forces. However the alleviated occurrence of wrinkling despite a reduction in the in-plane forces with higher tool rotation speed does not agree with this hypothesis. At the same time if wrinkling or galling can be prevented then tool rotation might be usable for keeping process forces within machine limitations, especially when forming a thicker polymer or a polymer with higher yield stresses.

In Fig. 2-12 the relationship between void density and formability is not clear for PVC since the PVC funnels with $R_f = 12\ mm$ are almost always formed to nearly the same wall angle whether failure occurs or not (Fig. 2-4). However, the results shown for PLA in Fig. 2-11 and Fig. 2-2 show that an observably increased formability by tearing is accompanied by a corresponding increase of the void density in the formed material. The underlying deformation mechanics that cause this paradoxical effect need to be investigated further. Additionally, these observations suggests that due to greater void

content a material formed with higher incremental depth may undergo earlier failure under mechanical loading conditions during part operation.

The enhanced crystallinity of the formed material as compared to the base material (Figs. 2-14c and 2-14d) might be due to strain-induced crystallization (SIC) that is observed in solid polymers (Dargazany et al., (2014) [65]). In Strain Induced Crystallization, the crystal morphology maybe fringed-micelle, folded-chain, extended-chain, or a combination of these and further investigations are needed to elucidate the polymer-chain orientations. The type of orientations may have an influence on the mechanical properties of the formed material. In general, SIC results in anisotropy in the mechanical response and enhances the tensile stiffness and/or strength (Rao et al., (2001) [66]). This enhancement in crystallinity of the material formed using SPIF indicates tremendous potential for using SPIF to form thermoplastic polymers.

Our future work will investigate methods to predict the maximum incremental depth that can be used without causing wrinkling or tearing of the sheet, with the goal of developing toolpath planning techniques for polymer SPIF that take this process mechanics into account. We will also perform experimental and computational work to investigate the damage evolution in polymer SPIF and evaluate the quantitative effects of shear and pressure on formability in the process. Additionally, we will investigate the crystal morphology and the thermo-mechanical properties of the material formed with SPIF to understand how the SPIF process parameters affect the properties of the formed material.

Influence of Single Point Incremental Forming on Mechanical Properties and Chain Orientation in Thermoplastic Polymers

Mohammad Ali Davarpanah, Shalu Bansal and Rajiv Malhotra

Journal of Manufacturing Science and Engineering

DOI: 10.1115/1.4034036

Volume 139, Issue 2, September 21, 2016, Pages 021012-1-021012-9

3 CHAPTER 3: INFLUENCE OF SINGLE POINT INCREMENTAL FORMING ON MECHANICAL PROPERTIES AND CHAIN ORIENTATION IN THERMOPLASTIC POLYMERS

3.1 Abstract

Incremental forming of thermoplastic surfaces has recently received significant interest due to the potential for simultaneous reduction in thermal energy consumption and in part-shape specific tooling. This paper examines the mechanical properties and the chain orientation of the formed material in Single Point Incremental Forming (SPIF) of amorphous PVC and semi-crystalline Polyamide sheets. Tensile and stress relaxation properties of the formed polymers are compared to those of the unformed polymer. The effect of incremental depth and tool rotation speed on the above properties, and on the temperature rise of the sheet during SPIF, are quantified. Differential Scanning Calorimetry and X-ray Diffraction are used to compare the chain orientation and crystallinity of the formed and the unformed polymers. It is observed that the formed material has greater toughness and ductility, but lower yield stress and reduced Young's modulus, as compared to the unformed material. We also observe deformation-induced chain reorientation in the formed polymer, with minimal change in the degree of crystallinity. The link between the SPIF process parameters, temperature rise of the polymer during SPIF, change in chain orientation and change in mechanical properties of the polymer is discussed.

3.2 Introduction

Single Point Incremental Forming (SPIF) is a process in which a fully peripherally clamped sheet of material is locally deformed by a small hemispherical ended tool moving along a pre-defined three dimensional toolpath. These local deformations accumulate to

give the sheet its final desired shape. In SPIF the incremental depth (Δz) is defined as the step down of the tool in the direction perpendicular to the plane of the sheet, in consecutive passes of the tool (Fig. 3-1). Past work has uncovered the possibility of expanding the materials capability of SPIF beyond metals, by demonstrating SPIF of thermoplastic polymers without any external heating of the polymer. While typical polymer sheet forming processes such as injection molding and hot forming create the desired shape using part-shape-specific tooling and using external heating of the polymer, SPIF of polymers offers the dual advantages of eliminating part-shape-specific tooling and reducing the thermal energy used to heat the polymer.

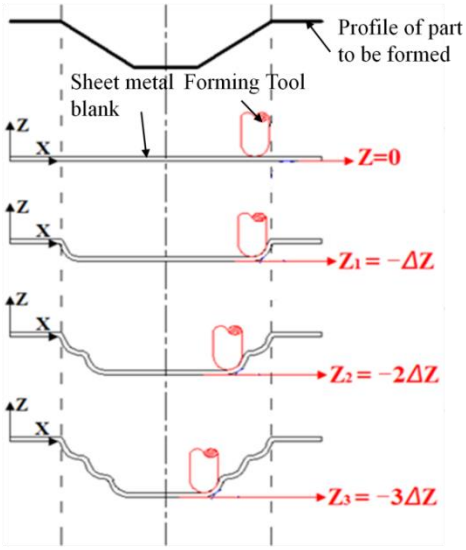

Figure 3-1: Schematic of the SPIF process

These advantages have created significant interest in polymer SPIF. The failure limits, failure modes and springback of the sheet have been the focus of recent work. Franzen et al. [67] experimentally examined the feasibility of forming Polyvinyl Chloride

(PVC) sheets using SPIF. They reported three possible failure modes of the sheet, namely (1) Tearing of the sheet along the circumferential direction, at the transition between the wall and the corner radius of the formed wall; (2) Wrinkling of the sheet along the circumferential direction of the part; and (3) Tearing of the sheet in the radial direction, along the wall of the part. The authors also observed stress whitening in the formed PVC, probably due to deformation induced crazing in the polymer. Davarpanah et al. [68] showed that greater Δz increased the formability of the sheet in the tearing mode of failure. This is contrary to the trends seen in SPIF of metals. They also reported that too large an incremental depth or too high a tool rotation speed causes a change in the mode of failure from tearing to wrinkling. Franzen et al. [69] performed SPIF of five different polymers with varying degrees of crystallinity. They reported that the reduction in density of the formed material was greater for amorphous PVC than for semi-crystalline polymers. The authors also related the springback of the sheet to the yield stress, thickness and elastic modulus of the sheet material. Silva et al. [70] developed an analytical model based on membrane analysis to predict stresses in the polymer due to SPIF. They used a pressure dependent yield criterion for amorphous polymers along with a hydrostatic pressure based fracture criterion, and were able to model the tearing mode of failure in SPIF of PVC.

Yonan et al. [49] employed a pressure modified version of Von Mises yield criterion, with the Ludwik-Hollman law to approximate plastic flow and a hydrostatic pressure dependent damage evolution law, to capture the tearing mode of failure in SPIF of axisymmetric parts. Their experimentally derived fracture forming limit was able to

successfully capture tearing in SPIF of PVC. They also demonstrated that significant anisotropy was induced in the formed material after deformation, with greater yield stress along the meridional direction and lesser yield stress along the circumferential direction. Bagudanch et al. [71] showed that increasing the tool rotation speed results in higher sheet temperatures during forming. This can increase the sheet temperatures beyond the glass transition temperature of the polymer, thus reducing the forming forces and increasing the formability.

Very few works have concurrently investigated the effect of SPIF on the mechanical properties and the underlying chain orientation of the polymer, which is the focus of this paper. Uniaxial tensile tests and stress relaxation tests are performed to examine the mechanical behavior of two polymers, amorphous PVC and semi-crystalline Polyamide 6.6, formed with SPIF. PVC is a commodity thermoplastic and Polyamide is frequently used in structural applications in the automotive and aerospace industries. The rise in the temperature of the polymer during SPIF is quantified. The chain orientation and degree of crystallinity of the formed and unformed polymers are characterized via X-ray Diffraction (XRD) and Differential Scanning Calorimetry (DSC). The above properties of the formed and unformed polymers are compared for different incremental depths (Δz) and tool rotation speeds (ω) used in SPIF. Finally, we discuss the underlying connection between the SPIF process parameters, the temperature rise of the polymer during SPIF, the change in mechanical properties and the change in chain orientation of the polymer as a consequence of forming with SPIF.

3.3 Experiments

An SPIF setup with a square forming area of 150 x 150 mm^2 was assembled on a HAAS CNC machine platform (Fig. 3-2a).

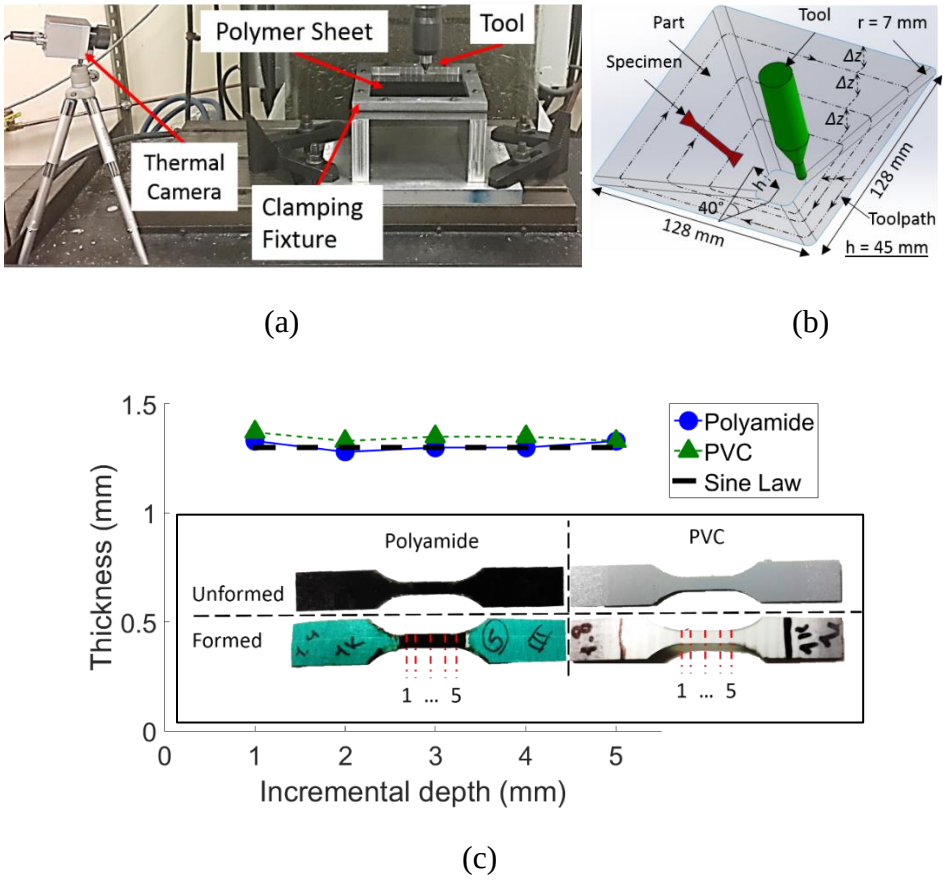

Figure 3-2: (a) Experimental SPIF setup (b) schematic of part, specimen, tool, toolpath and incremental depth in SPIF (c) unformed and formed tensile test samples of Polyamide and PVC and inset: Thickness distribution along gauge length at 5 different points

This setup consisted of the polymer sheet, the clamping fixture, a 5 mm diameter SPIF tool mounted on the CNC spindle, and a thermal camera for measuring sheet temperature during forming. A PTFE-based grease was used as the lubricant to reduce friction between the tool and the sheet during SPIF. A pyramid shape (Fig. 3-2b) was

formed for all the experiments. Since a tool of 5 mm diameter was used in all the experiments there was no interference of the tool with the already formed region of the sheet during SPIF. The nominal thickness of the as-received PVC and Polyamide sheets was 1.5 mm. Table 3-1 summarizes the Δz and ω values used in experiments. All experiments were performed using contour (constant z) toolpaths.

Table 3-1 Summary of SPIF process parameters used in this work

Material	ω (rpm)	Δz (mm)
PVC	0, 500, 1000	1.4, 1.8, 2.0
Polyamide	0, 1000, 5000	

Previous work [68] has shown an increase in formability of the polymer when Δz is higher than the sheet thickness, as compared to when Δz is lower than sheet thickness. Therefore, for completeness the Δz was varied from lesser than to greater the sheet thickness in our experiments. Since galling occurs during SPIF of PVC with ω greater than 1000 rpm [68], the ω for SPIF of PVC was restricted to 1000 rpm. Higher ω were used for Polyamide since no galling is observed with Polyamide. Each set of experiments was repeated 5 times and none of the aforementioned modes of sheet failure were observed during the forming process. The feed rate of the tool was fixed at 5 mm/sec for every experiment. A Micro-Epsilon TIM-200 thermal camera (Fig. 3-2a) was used to record temperature evolution of the sheet during SPIF. This camera records temperatures upto 1500°C with a maximum error of ±2°C, spatial resolution of 96 pixels per inch and

acquisition frequency of 128 Hz. To calibrate the camera, a black band was marked on the polymer sheet and the emissivity of the band was set to 0.99 (black body). Since the unmarked polymer next to the band would have approximately the temperature as the band, the emissivity of the unmarked polymer surface was calibrated till the temperatures of the band and of the unmarked polymer next to the band matched up.

Tensile test specimens conforming to the ASTM D638 (Specimen type V) were extracted from the formed part walls, along the radial direction (Fig. 3-2b). As shown in Fig. 3-2c, the measured thickness of the gauge region of the formed specimen was uniform and matched well with the thickness calculated from the sine law [72]. This is because the tensile specimen was extracted from the formed part such that the corner of the part base, at which significant deviation from uniform thickness is typically observed in SPIF, was far away from the edge of the tensile test specimen. This uniform formed material thickness was used to calculate stresses and strains in the tensile and relaxation tests for the formed specimens. The unformed material thickness was used to calculate stresses and strains in the same tests for the unformed specimens.

Specimens conforming to the same ASTM standard were also extracted for performing the stress relaxation tests. An Instron (Model 5969) tensile test machine with maximum load capacity of 30 kN was used for both tensile and relaxation tests. The strain rate of the specimen was fixed at 0.0174 s^{-1} for tensile tests. The stress relaxation test was performed by extending the material to a constant true strain percentage above the yield strain, and holding the material at that strain for 60 minutes to observe the drop in stresses.

For PVC the strain at the beginning of the stress relaxation test was approximately 50% higher than the strain at yield. As will be shown later, the unformed Polyamide had a very small plastic portion of deformation during the tensile test, as compared to the formed polymer. Thus, the maximum true strain at the beginning of the relaxation test for the unformed material was restricted to 8%. Wide angle X-ray diffraction of samples, cut out from the walls of the formed part and from the unformed polymer sheets, was performed using a Bruker-AXS D8 Discover X-ray diffraction instrument. The degree of crystallinity of the formed and unformed polymers was measured using a TQ 2000 differential scanning calorimeter. The PVC samples were heated from 40˚C to 200˚C with 10˚C/minute temperature ramp and then held isothermally for 3 minutes at 200˚C. For Polyamide the rate of temperature rise was similar to PVC but the temperature was raised from 40˚C to 300˚C and then the polymer was held under isothermal conditions for 5 minutes at 300°C. Since only the data obtained from the first heating cycle is needed to measure the crystalline content of the polymer after the SPIF process [68], only the first heating cycle was used here. The crystallinity of the polymer samples was computed using equation (3-1) below.

$$Degree\ of\ crystallinity = \frac{\Delta H_m - \Delta H_{cc}}{\Delta H_m^0} \tag{3-1}$$

where ΔH^0_m = 255.8 J/g, ΔH_{cc} is cold-crystallization enthalpy and ΔH_m is melting enthalpy [73, 74].

3.4 Results

Uniaxial Tensile Tests: Representative true stress-strain curves from uniaxial tensile testing of formed and unformed PVC are shown in Fig. 3-3. Figure 3-4 shows the

average value and standard deviation of yield stress, UTS, strain at fracture and elastic modulus for the formed and unformed PVC. It can be seen that the formed PVC has greater toughness than the unformed material, while the unformed material shows higher elastic modulus and yield stress. A comparative reduction in toughness can be observed at at ω = 1000 rpm and Δz =1.8 mm. However, uniform trends that relate the the yield stress, elastic modulus, UTS and fracture strain to the Δz and ω cannot be observed.

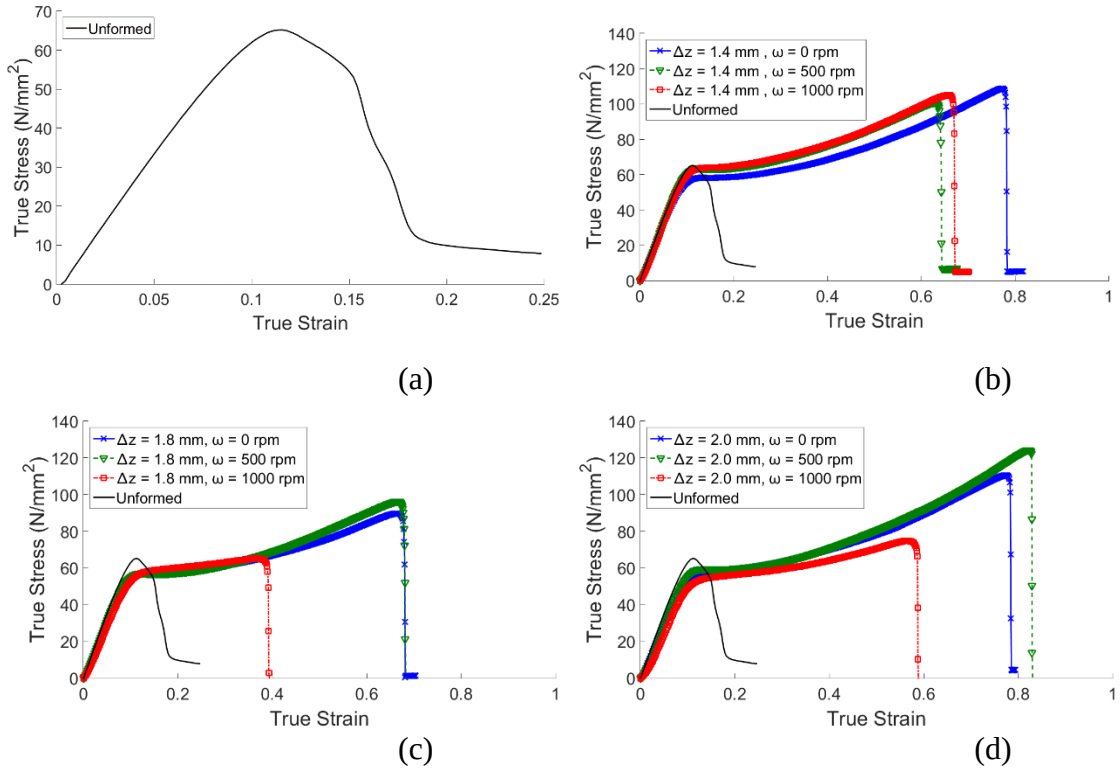

Figure 3-3: Tensile stress- strain curves for (a) unformed PVC; and Formed PVC with (b) Δz = 1.4 mm (c) Δz = 1.8 mm (c) Δz = 2.0 mm at different ω

Figure 3-5 shows representative true stress-strain curves from uniaxial tensile testing for Polyamide, and Fig. 3-6 summarizes the effects of Δz and ω on the mechanical properties. Similar to PVC, the formed Polyamide has significantly greater toughness, but

lower elastic modulus and yield stress, than the unformed Polyamide. Again, no clear trend that relates the Δz and ω to the above properties is apparent from these experiments.

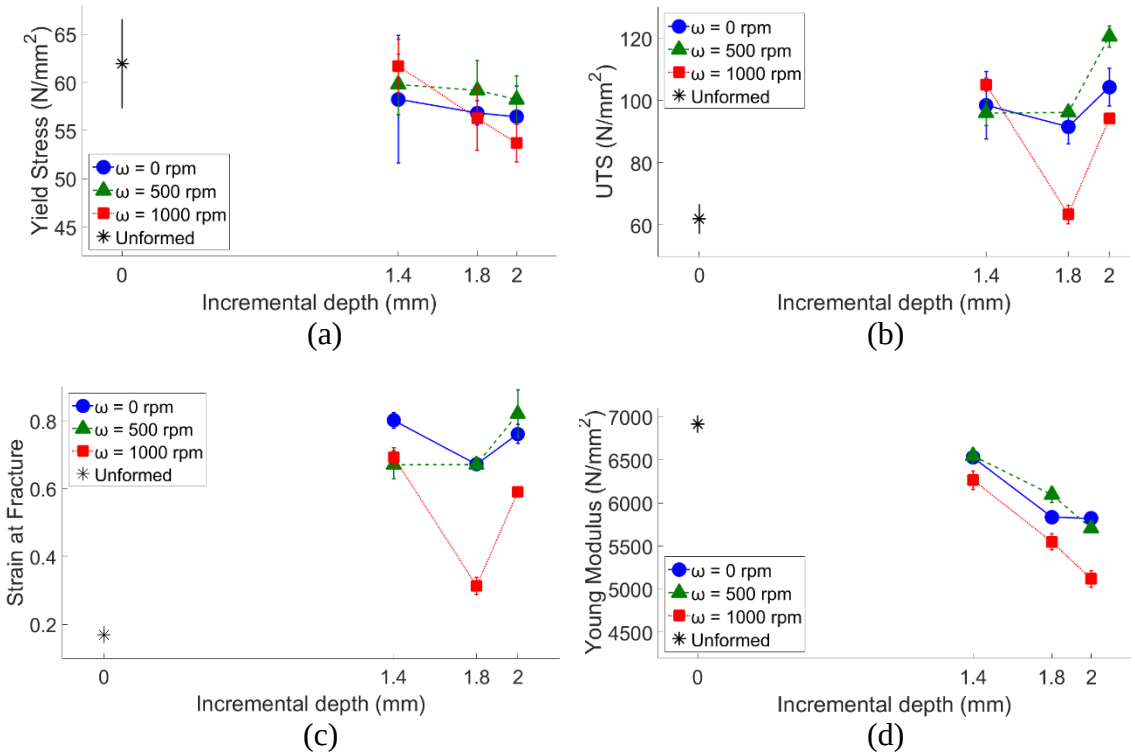

Figure 3-4: (a) Yield stress (b) UTS (c) strain at failure (d) elastic modulus for formed and unformed PVC

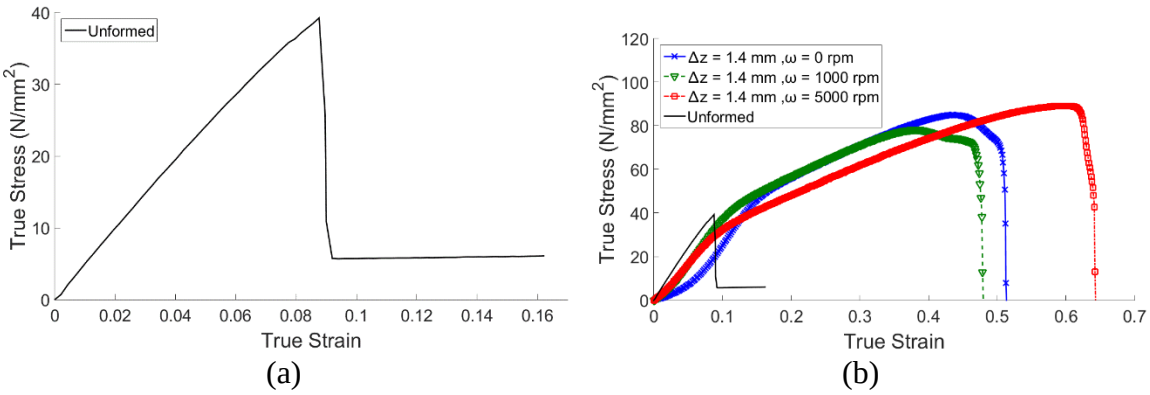

(Continued)

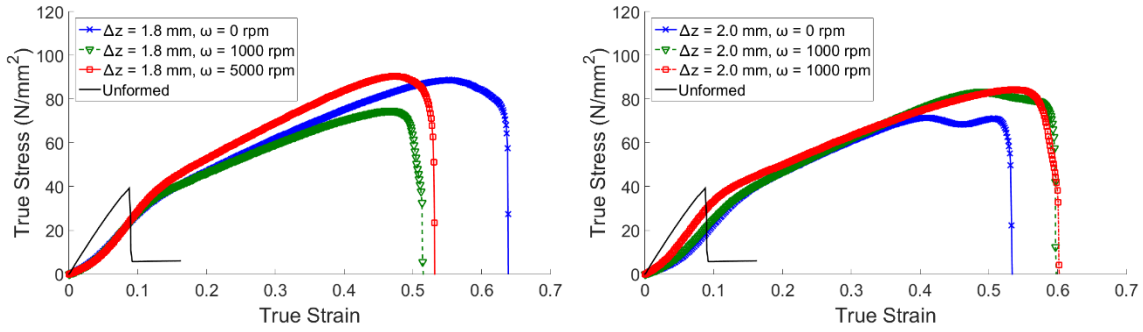

(c) (d)

Figure 3-5: Tensile stress-strain curves for (a) unformed Polyamide and formed Polyamide with (b) Δz = 1.4 mm (c) Δz = 1.8 mm (d) Δz = 2.0 mm at different ω

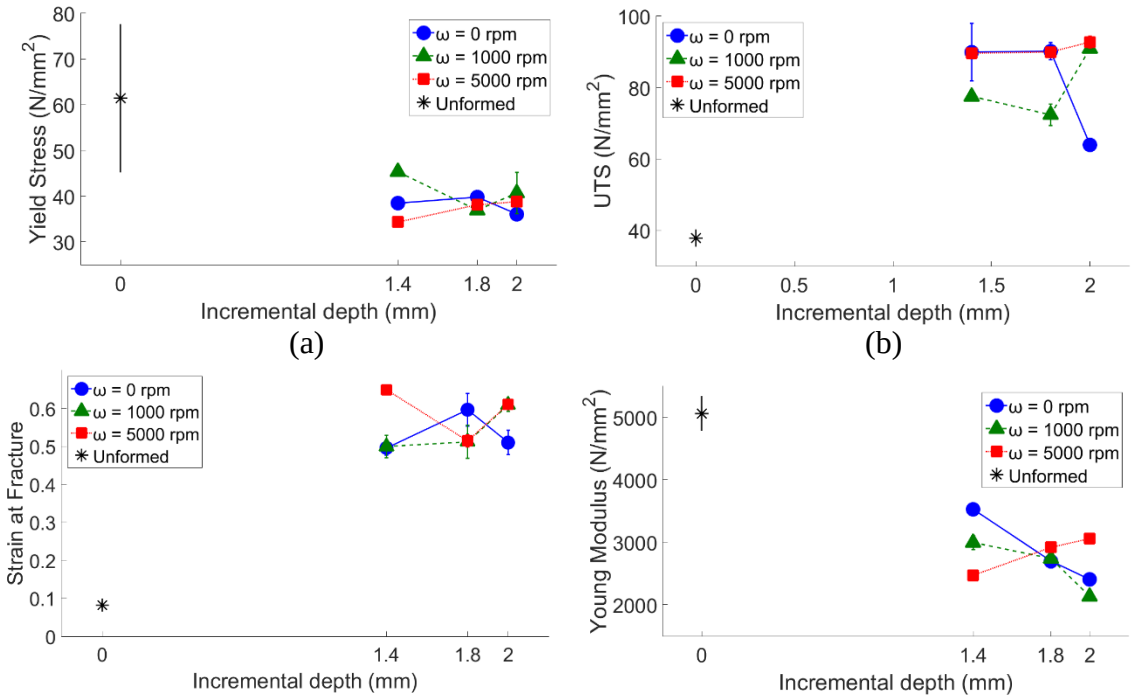

(a) (b)

(c) (d)

Figure 3-6: (a) Yield stress (b) UTS (c) strain at failure (d) elastic modulus for formed and unformed Polyamide

Relaxation Tests: Figure 3-7a shows representative true stress vs. time curves from stress relaxation tests of PVC. The average values of percentage stress reduction, i.e., the change in stress during hold time expressed as a percentage of the stress at the beginning

of hold time, are shown in Fig. 3-7b. There is an increase in the percentage of stress reduction for the formed PVC, as compared to the unformed PVC. Figure 3-8 shows similar data from stress relaxation tests of formed and unformed Polyamide. Again, the formed material shows a higher percentage of stress reduction as compared to the unformed material. However, for different ω and Δz the difference in percentage stress reduction for the formed samples is relatively smaller for both PVC and Polyamide. Thus, while SPIF has an effect on the stress relaxation behavior of the formed polymer as compared to the unformed polymer, the Δz and ω used may not have a significant effect by themselves.

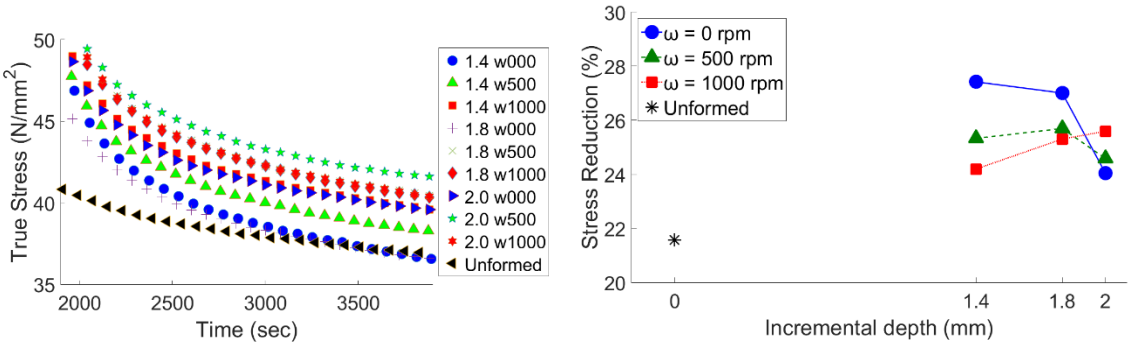

(a) (b)

Figure 3-7: (a) Relaxation test curves (b) percentage stress reduction for the formed and unformed PVC

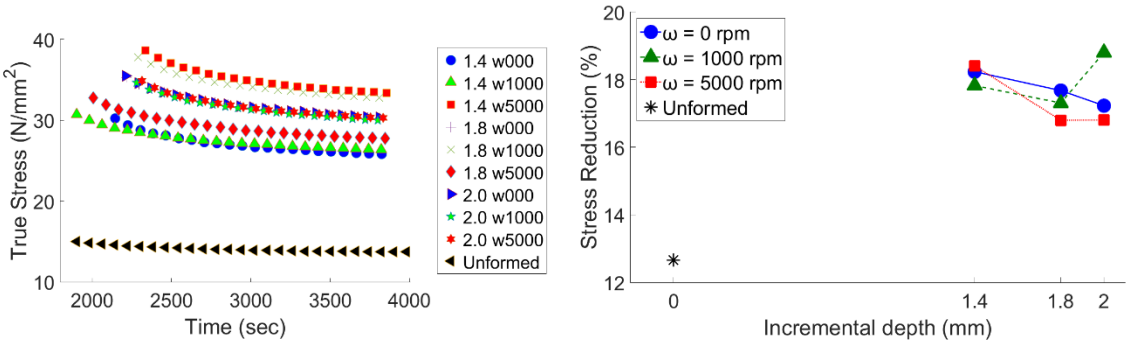

(a) (b)

Figure 3-8: (a) Relaxation test curves (b) percentage stress reduction for the formed and unformed Polyamide

Temperature Measurement: Figure 3-9 shows the maximum measured temperatures of the PVC sheet for various Δz and ω. For all the Δz and ω used for PVC the measured temperature (Fig. 3-9c) is lower than glass transition temperature of PVC (i.e., 85°C).

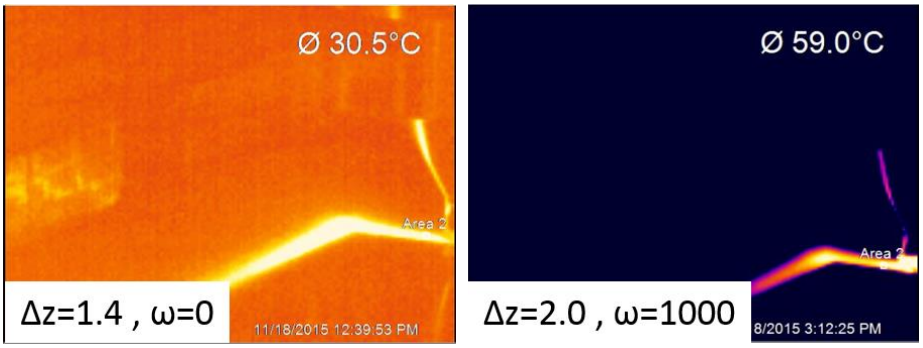

(a) (b)

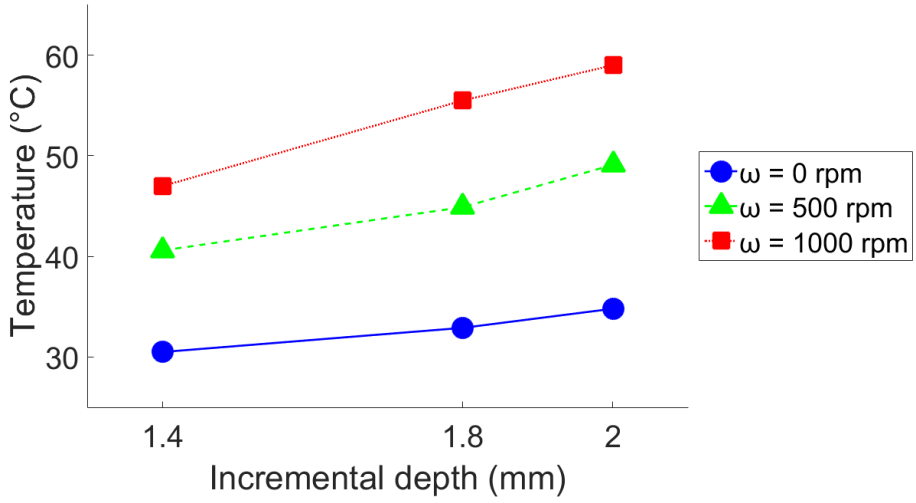

(c)

Figure 3-9: Thermal image of PVC during SPIF at (a) Δz = 1.4 mm, ω = 0 rpm (b) Δz = 2.0 mm, ω = 1000 rpm (c) PVC temperatures at different Δz and ω

Figure 3-10 shows the maximum measured temperatures of the Polyamide sheet during SPIF. At ω = 5000 rpm, for all Δz, the measured temperature is higher than glass

transition temperature of Polyamide (i.e., 50°C). For ω =1000 rpm the temperature is lower than the glass transition temperature, except for Δz = 2.0 mm where the temperature (50.2°C) is slightly higher than glass transition temperature. Figures 3-9 and 3-10 show that, at the same Δz, greater ω increases the sheet temperature during forming, similar to observations in [37].

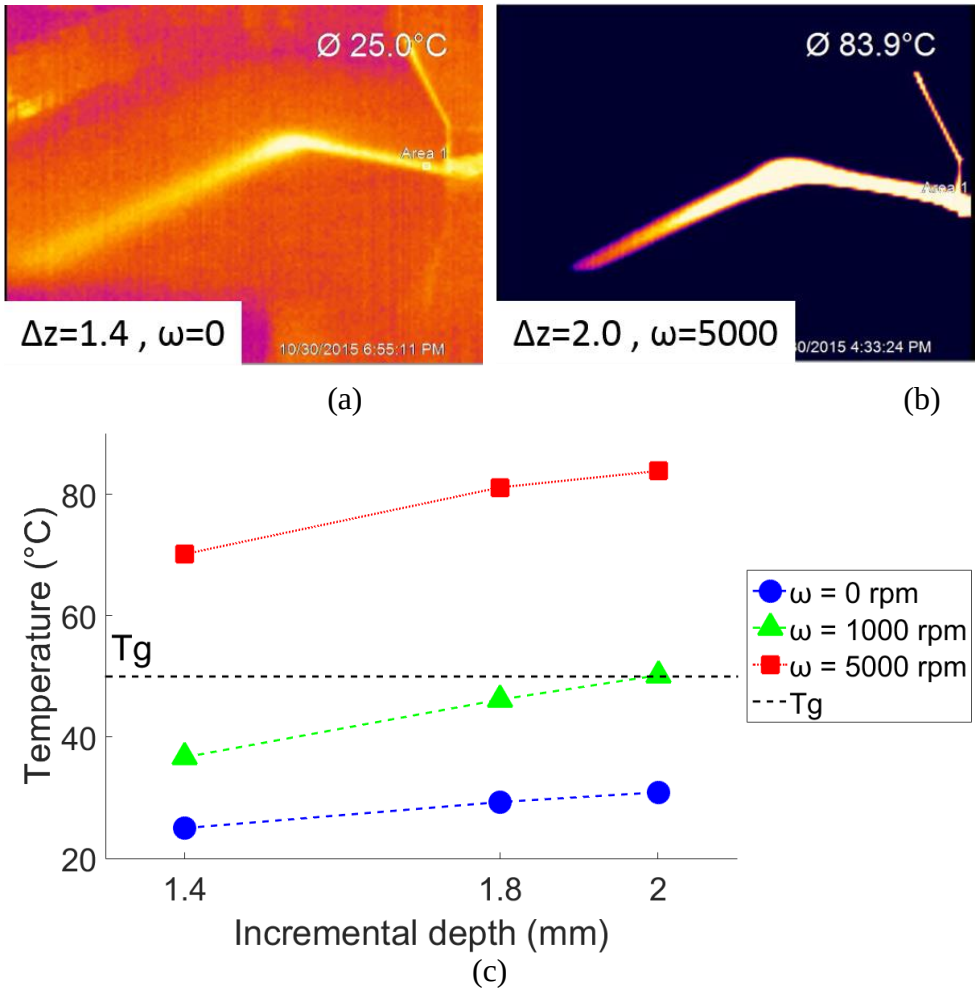

Figure 3-10: Thermal image of Polyamide during SPIF at (a) Δz = 1.4 mm, ω = 0 rpm (b) Δz = 2.0 mm, ω = 5000 rpm (c) Polyamide temperatures at different Δz and ω

This is due to increased frictional energy per unit area of tool-sheet contact due to increased relative speed between the sheet and the tool. Some of this energy is dissipated

as heat into the sheet. At the same ω, greater Δz results in higher temperatures even though the frictional energy dissipation per unit area of tool-sheet contact should stay the same. This is because higher Δz results in greater contact area between the tool and the sheet, which increases the total frictional energy that is dissipated as heat into the sheet.

Chain orientation and crystallinity: Figure 3-11 plots the integrated intensity vs. 2θ curves obtained from XRD of formed and unformed PVC. At the major peaks (2θ=16°, 26°) the intensities are generally higher for the formed polymer as compared to the unformed polymer. This indicates greater chain orientation in the formed PVC along these directions, as compared to the unformed PVC. Figure 3-12 shows similar data for the formed and unformed Polyamide, with significant peaks at 2θ=20° and 2θ=24°. In general, for the formed material the peak at 2θ=24° is higher than or equal to that at 2θ=20°, while in the unformed material the peak at 2θ=24° is lower than that at 2θ=20°. This indicates a change in orientation of crystalline lamella and molecular chain orientation in Polyamide, due to forming with SPIF.

The thermograms obtained from DSC, for both PVC and Polyamide, are shown in Fig. 3-13. The degree of crystallinity observed in the PVC was zero, since the PVC used in this work is primarily amorphous [68]. While the polyamide did show a non-zero degree of crystallinity, there was no significant change in degree of crystallinity between the formed and the unformed polymer (Fig. 3-13c). This indicates that there is little change in the total crystalline content in the PVC or Polyamide, even though there is a change in the molecular chain orientation as indicated by XRD.

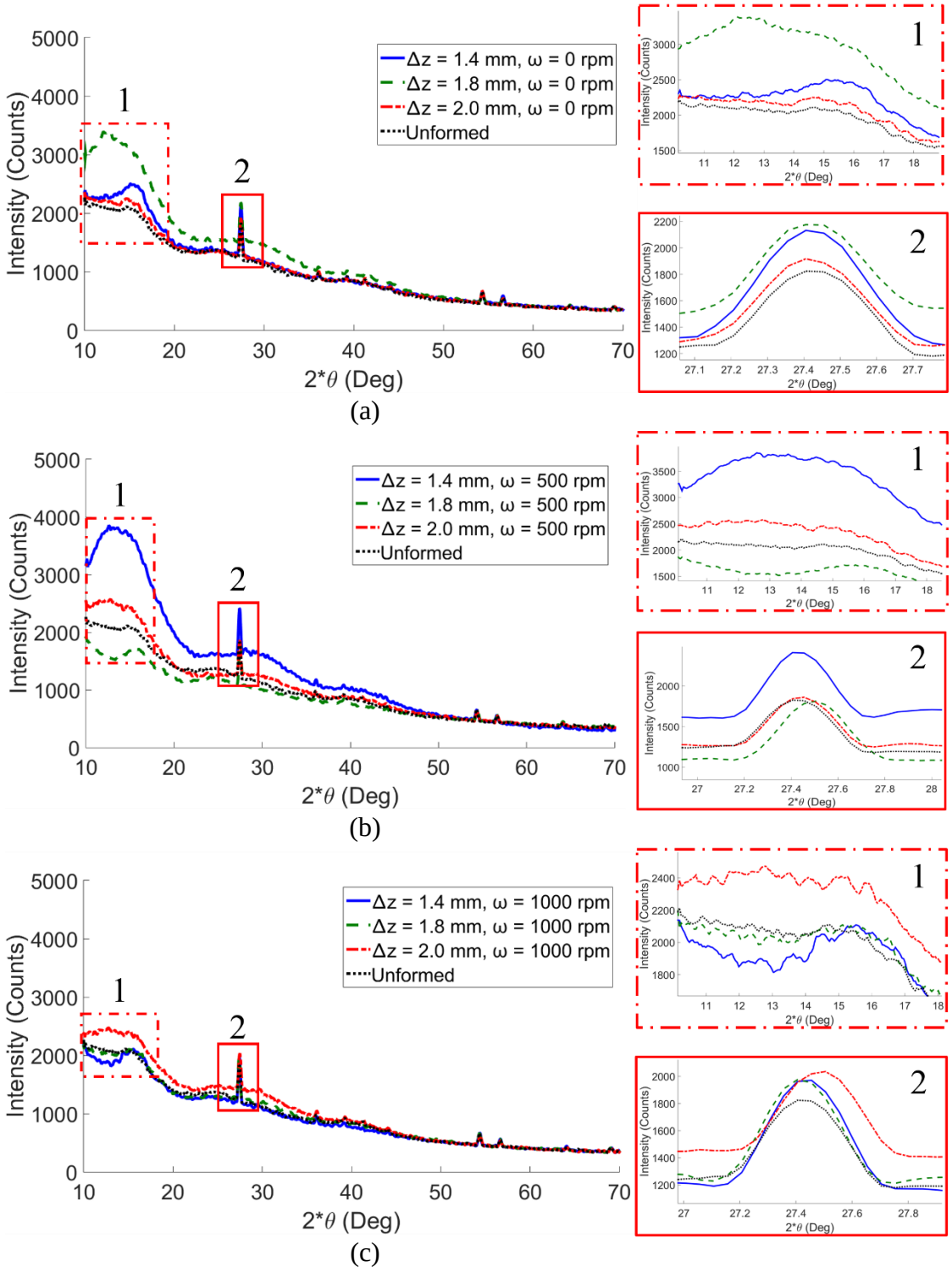

Figure 3-11: Integrated intensity vs. 2θ curves of unformed PVC and formed PVC for (a) ω= 0 rpm (b) ω = 500 rpm (b) ω= 1000 rpm at different Δz

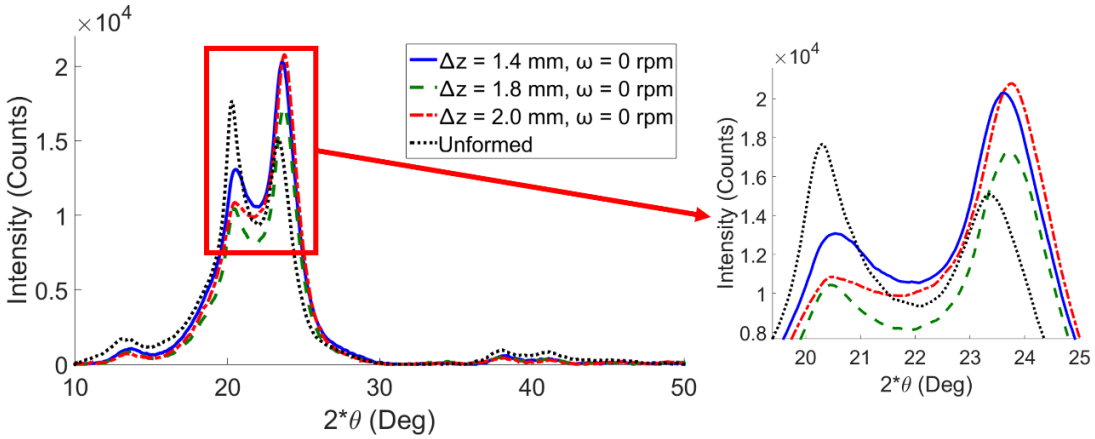

(a)

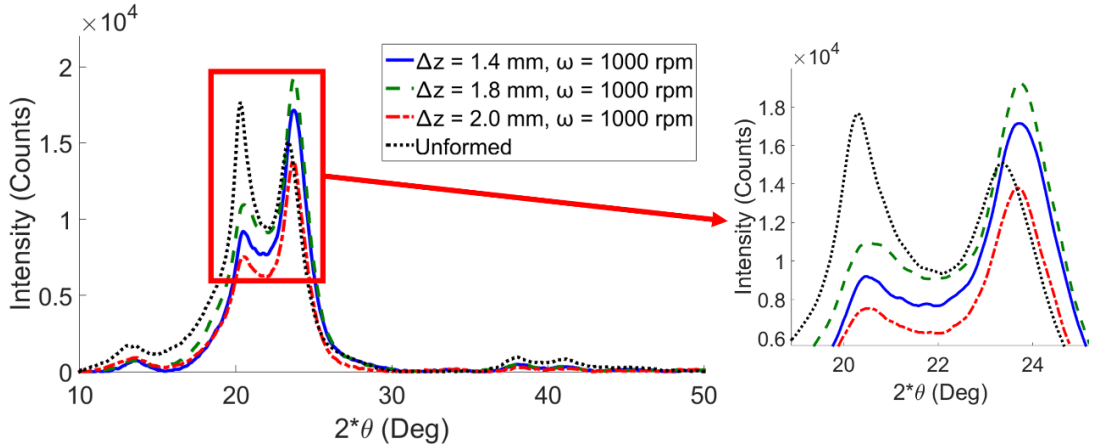

(b)

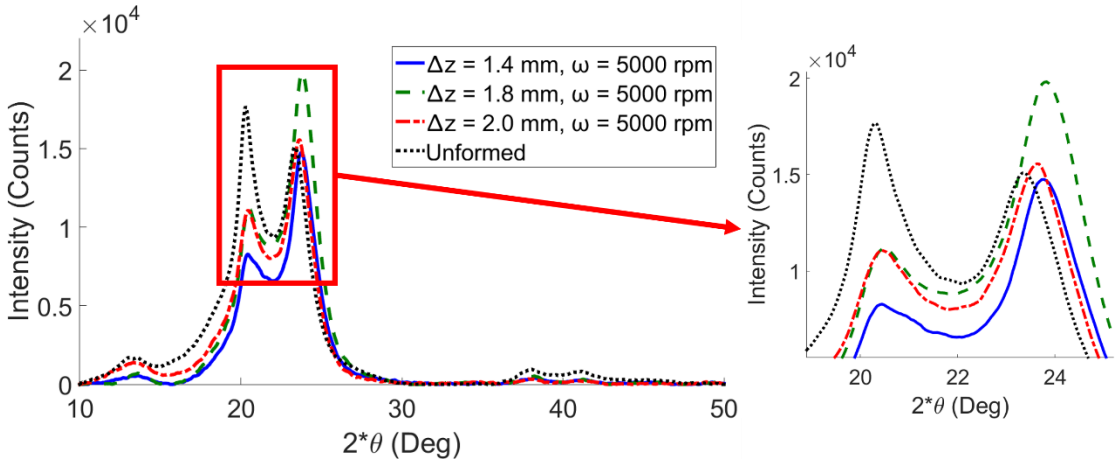

(c)

Figure 3-12: Integrated intensity vs. 2θ curves for the unformed Polyamide and the formed Polyamide for (a) ω = 0 rpm (b) ω = 1000 rpm (b) ω = 5000 rpm at different Δz

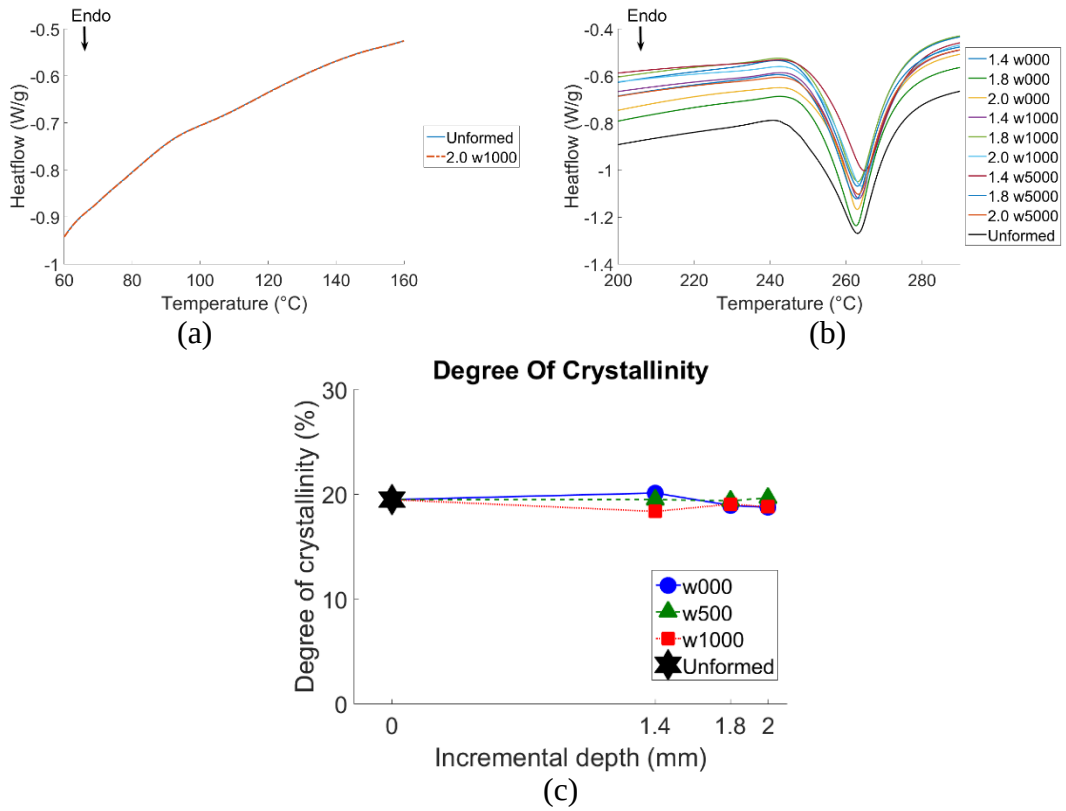

Figure 3-13: (a) Representative thermograms of PVC for the unformed material and for the material formed at Δz = 2.0 mm and ω = 1000 rpm (b) thermograms of Polyamide with different Δz and ω (c) degree of crystallinity of formed and unformed Polyamide

3.5 Summary and Discussion

In the case of amorphous PVC the increase in chain orientation and the absence of glass transition during forming is observable in Fig. 3-11 and Fig. 3-9c respectively. It has been shown [75, 76] that deformation of amorphous polymers at temperatures lower than the glass transition, results in retention of chain orientation in the major stress direction. In the case of SPIF the major principal stress is along the meridional direction of the part wall.

Figures 3-4a and 4d show that the yield stress and the Young's modulus are lower for the formed PVC as compared to the unformed PVC. The yield stress and Young's

modulus of amorphous polymers depend significantly on orientation of molecular chains in the polymer [77, 78]. Greater degree of orientation enables molecular chains to slide past each other easily during deformation, resulting in lesser elastic stiffness and yield stress. The increased orientation of the molecular chains in the polymer in SPIF is probably why the yield stress and the Young's modulus of the formed PVC are lower than that of the unformed PVC. Since the temperature of the PVC never rises above the glass transition temperature during SPIF, thermally induced chain mobility effects can be expected to be negligible. The increase in ductility and toughness of formed PVC can be attributed to the cold drawing nature of forming of amorphous polymers. During SPIF, the deformation of the PVC results in multiple stabilized necks that contain more oriented molecular chains, much like in cold drawing of polymers. The growth of crazes and voids in these neck regions is difficult due to the increase in chain orientation [79, 80]. This increases the energy needed to cause failure of the formed PVC during tensile testing, which manifests as an increase in the ductility and overall toughness of the formed material. Note that the reduction in strain softening in the formed PVC (Fig. 3-3) is also indicative of reduced interactions between molecular chains, due to greater chain orientation induced by SPIF.

Stress relaxation tests on PVC (Fig. 3-7b) show that the percentage stress reduction is higher for the formed polymer as compared to the unformed polymer. The stress relaxation behavior of amorphous polymers, is dependent on the degree to which the polymer chains are able to slide past each other to relieve the stresses induced at the beginning of the stress relaxation test [81]. For example, performing stress relaxation tests

at temperatures greater than the polymers glass transition temperatures, provides energy, that encourages sufficient chain mobility for greater percentage stress reduction than that seen at room temperatures [82]. The greater percentage stress reduction for the PVC formed using SPIF is probably due to the increased orientation of molecular chains which makes it easier for the chains to slip and slide past each other, resulting in greater relaxation of the initially imposed stress in the formed material as compared to the unformed polymer.

For Polyamide, the XRD curves in Fig. 3-12 show significant reorientation of the crystalline portion of the polymer after SPIF. The occurrence of this reorientation seems independent of whether the sheet temperature during SPIF exceeds the glass transition temperature. Further, the localized nature of deformation and temperature rise during SPIF, as well as the absence of significant changes in the degree of crystallinity after SPIF (Fig. 3-13c), suggest that there is very little thermally enabled crystallization in the polymer due to SPIF. Thus, the applied stress during SPIF is probably the primary factor responsible for reorientation of chain-folded lamellae in the formed polymer.

Molecular dynamics simulations [83-85] have shown that plastic deformation in semicrystalline polymers occurs via reorientation of crystalline lamellae toward the major principal stress axis, and then fragmentation of largest crystalline lamellae, followed by unfolding and alignment of chains in both amorphous and crystalline portions of the polymer. Considering that the meridional direction is the major principal stress direction in SPIF the above morphological changes in the polymer during SPIF can lead to greater number of lamellae of smaller thickness that are preferentially oriented along the

meridional direction. This reorientation would result in XRD curves of the kind shown in Fig. 3-12. The above proposed morphological changes are also supported by the reduction in yield stress and elastic stiffness of the formed polyamide as compared to the unformed material [86-88], as shown in Fig. 3-6a and Fig. 3-6d respectively. The occurrence of the proposed morphological changes would also result in higher ductility and toughness of the formed Polyamide, as seen in Fig. 3-6b and Fig. 3-6c, since thinner lamellae encourage the fine chain slip mechanism in semicrystalline polymers [86].

In semi-crystalline polymers, like the Polyamide used here, increasing degree of crystallinity of the polymer and increasing temperatures during stress relaxation typically increase the percentage stress drop during stress relaxation [89]. However, the degree of crystallinity of the formed polyamide, is very similar to that of unformed polyamide, irrespective of the process parameters used (Fig. 3-13c). Further, the relaxation tests were performed at room temperature. It is likely that the greater orientation of lamellae is responsible for greater percentage stress reduction for the formed Polyamide as compared to the unformed Polyamide, similar to the case of PVC.

The above discussion primarily deals with the differences in chain orientation and mechanical properties between the formed and unformed polymers. However, universal trends that relate Δz and ω to the change in mechanical or microstructural properties, are hard to see from the experiments performed here.

3.6 Conclusions

This paper investigates the effect of SPIF on the mechanical properties and chain orientation of the formed polymer, for an amorphous PVC and a semi-crystalline Polyamide. It is shown that forming with SPIF increases the ductility and toughness, but reduces the elastic stiffness and the yield stress, of the polymer. Given that thermoplastics are used mainly in applications that mainly require toughness rather than stiffness, as compared to thermosets, the increase in toughness after forming is a positive quality of polymer SPIF. Further, forming with SPIF increases the percentage drop in stress during stress relaxation of the polymer. XRD and DSC measurements are used to show that SPIF induces a change in molecular chain orientation in the formed polymer. This change in chain orientation due to forming is reflected in the change in mechanical properties of the formed polymer. The change in chain orientation seen here, and the well known repetitive nature deformation of the sheet in SPIF, also suggests that dynamic changes in chain orientation and mechanical properties during SPIF may have an influence on sheet failure and forming forces. At the same time, no clear trends relating the incremental depth and tool rotation speed to the mechanical and microstructural properties of the formed polymer can be seen. Our future work will further expand the process parameter space to examine the possibility of existence of such relationships. We will further focus on developing models to capture the evolution of the stresses, temperatures and chain orientation of the polymer during SPIF. We will also work on finding an explanation for some of the deviations in the observed experimental trends, such as the reduction in toughness at Δz = 1.8 mm and ω = 1000 rpm for formed PVC.

3.7 Acknowledgments

The authors would like to acknowledge the Walmart Manufacturing Innovation Fund for the financial support provided for this work and Mr. Roshan Bhandari for manufacturing the fixture.

Formability and Failure Modes in Single Point Incremental Forming of Metal-Polymer Laminates

Mohammad Ali Davarpanah and Rajiv Malhotra

46th SME North American Manufacturing Research Conference, NAMRC 46, Texas, USA

DOI: https://doi.org/10.1016/j.promfg.2018.07.042

Procedia Manufacturing, Volume 26, Issue 2, August 2018, Pages 343-348

4 CHAPTER 4: FORMABILITY AND FAILURE MODES IN SINGLE POINT INCREMENTAL FORMING OF METAL-POLYMER LAMINATES

4.1 Abstract

Single Point Incremental Forming (SPIF) is a sheet forming technique with several advantages compared to conventional sheet forming including low-cost and part-shape-independent tooling, and higher process flexibility. While recent work has demonstrated the feasibility of SPIF of metal-polymer-metal sandwich sheets, the effects of SPIF process parameters on formability have rarely been examined. This work examines how incremental depth, metal thickness and polymer thickness affect formability and failure modes during SPIF of adhesively bonded metal-polymer laminate sheets. It is shown that higher polymer thickness results in higher formability, but this advantage is limited by the occurrence of metal tearing and galling. Further, the mode of failure is found to depend on the metal sheet thickness and polymer sheet thickness. In laminates with thinner metal sheet only two modes of failure, delamination and metal tearing occur. In laminates with thick metal sheet galling of the polymer is also observed, in addition to the above failure modes.

Nomenclature

D	Maximum diameter of funnel (mm)
Δz	Incremental depth (mm)
R_f	Radius of curvature (mm)
t_{Al}	Aluminium sheet thickness (mm)
t_{PA}	Polyamide sheet thickness (mm)

t_{PA_Trans} Transition polyamide sheet thickness (mm)

4.2 Introduction

In Single Point Incremental Forming (SPIF) process, a fully peripherally clamped sheet of material is locally deformed by a small hemispherical ended tool moving along a pre-defined 3D toolpath. The sum of these local deformations gives the sheet its final shape. The step down of the tool in a direction perpendicular to the sheet is called the incremental depth (Δz). A significant amount of work has been performed on SPIF of metals in terms of deformation and fracture mechanics [30, 90], forming forces [56, 91, 92], toolpath planning [93, 94], geometric accuracy [93, 94], finite element and numerical simulation [90, 95], effect of temperature [92, 96] and surface finish [96, 97] in the incremental forming process.

Recent work has shown the feasibility of forming thermoplastic polymer sheets with SPIF without external heating of the sheet [35, 36, 38, 41, 68, 98-100]. Franzen et al. [67] experimentally examined SPIF of polyvinyl chloride (PVC) sheets and reported three modes of sheet failure during forming, i.e., (1) Sheet fracture by ductile tearing along the circumferential direction, similar to that seen in SPIF of metals; (2) Wrinkling of the sheet along the wall of the part, which is not seen in SPIF of metals; and (3) Tearing of the sheet in the radial direction, along the wall of the part, due to surface defects in the as-received sheet. Martins et al. [39] performed SPIF of five different polymers, polyoxymethylene (POM), polyethylene (PE), polyamide (PA), polyvinylchloride (PVC) and polycarbonate (PC). It was shown that PE and PA have high formability and are suitable for part shapes with high wall angles. POM performed the lowest formability in comparison to other four

polymers. Maass et al. [40] showed that increasing tool diameter sheet thickness increases sheet formability. Davarpanah et al. [68] showed that in polymer SPIF increasing Δz in the toolpath increases the formability of the polymer, contrary to observations in SPIF of metals. Yonan et al. [49] showed that the formed polymer develops significant anisotropy and Davarpanah et al. [101] demonstrated the effect of SPIF on mechanical properties of polymers formed with SPIF. Davarpanah et al. [102] also demonstrated Double Sided Incremental Forming of polymers and showed that the process resulted in higher formability than SPIF.

On the other hand, there is relatively little work on SPIF of adhesively bonded metal-polymer sheets despite potential applications including sound absorption, vibration absorption, thermal insulation and impact absorption with reduced part weight in the aerospace and automotive industries [52]. Jackson et al. [52] demonstrated the feasibility of forming laminated sandwich panels consisting of Polypropylene (PP) core material with mild steel and aluminium (AA5182) faceplate materials. It was also shown that effect of incremental depth and tool radius in sandwich panel SPIF is similar to metal sheet SPIF. However, the effect of the sheet thickness was not examined and only a tearing mode of failure was observed.

This work focuses on SPIF of Polymer-Metal laminates, i.e., a polymer sheet and a metal sheet joined with an adhesive. The metal and polymer sheet thickness and incremental depth are varied to uncover their effect on formability and failure modes.

4.3 Experimental work

An SPIF setup with a square forming area of 130 x 130 mm was assembled on a HAAS CNC machine (Fig. 4-1a). This setup included the clamped metal-polymer laminate, the clamping fixture and a 5 mm diameter forming tool mounted on the CNC tool holder.

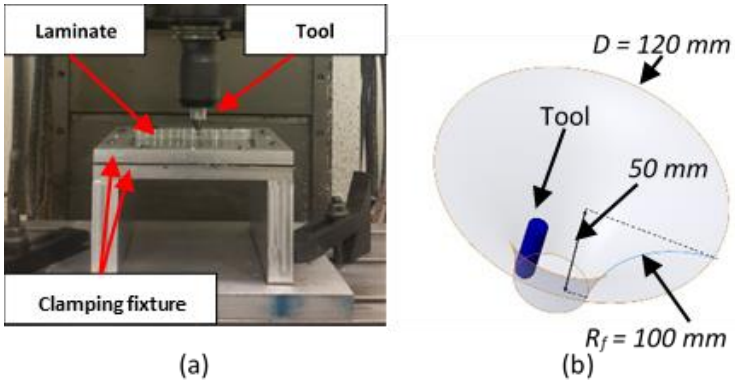

Figure 4-1: (a) SPIF setup (b) schematic of funnel part shape and tool

A PTFE-based grease was used as the lubricant at the tool-laminate interface, i.e., the polymer face of the laminate, to reduce friction during forming. A funnel shape with varying wall angle from 30° to 68.5°, 50 *mm* depth and 100 *mm* radius of curvature (R_f) was formed (Fig. 4-1b). This shape has been frequently used to examine formability in SPIF [54, 68]. This geometry enables a continuously increasing strain to be imposed on the sheet during SPIF. The feed rate of the tool was fixed at 300 *mm/min*. No tool rotation was used.

The laminates consisted of a sheet of semi-crystalline Polyamide (Nylon 66) and AA5052 Aluminium sheet joined with a neoprene contact adhesive (3M Scotch-Weld 1357). Figure 4-2 shows the method for fabrication of such a metal-polymer laminate.

Polyamide and aluminium sheets were cut into 203 x 203 *mm* squares. The aluminium and polyamide sheets' faces that were joined to each other were cleaned with Methyl Ethyl Ketone (MEK) before application of the adhesive.

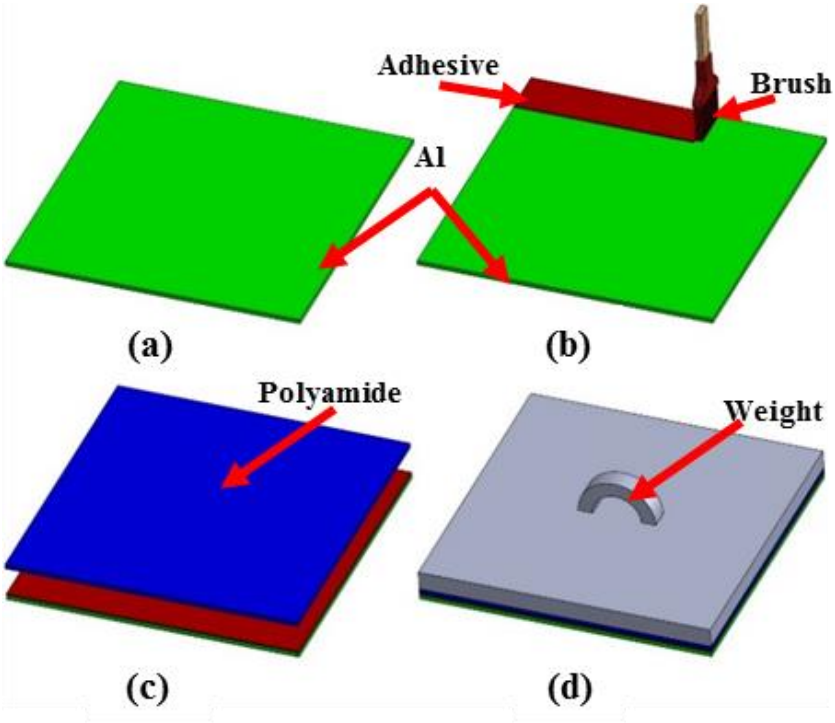

Figure 4-2: Sample preparation steps (a) placing aluminum sheet on the work table; (b) applying adhesive; (c) positioning the polyamide sheet on the adhesive layer; (d) placing the steel plate to maintain uniform static load on the laminates

The adhesive was applied on the cleaned face of aluminium sheet (Fig. 4-2b) and the cleaned face of the polyamide sheet faced the adhesive layer (Fig. 4-2c). Then the whole laminate assembly was kept under static pressure for 48 hours (Fig. 4-2d) using a 10 kg weight steel plate with same width and length as laminate sheets to make sure the whole laminate was under homogeneous pressure.

To investigate the effect of polymer and metal sheet thickness, two different aluminum sheet thicknesses (0.8 *mm* and 1.0 *mm*) and five different polyamide sheet thicknesses (0.79, 1.19, 1.58, 1.98 and 2.38 *mm*) were used to make the above laminates. Further, two Δz (0.2 *mm* and 0.4 *mm*) were used to investigate the effect of incremental depth. Each set of experiments was repeated at least 3 times.

4.4 Results and Discussion

4.4.1 Experimental Results

Figure 4-3 shows formed parts at t_{Al}= 1.0 *mm* and Δz=0.4 *mm* with various t_{PA}.

(a) (b) (c)

Figure 4-3: Shows effect t_{PA} on formed laminates at t_{Al}= 1.0 *mm* and Δz= 0.4 *mm* (a) t_{PA}= 1.19 *mm*, Delamination (D) at 35˚ wall angle; (b) t_{PA}= 1.98 *mm*, Metal tearing (M) at 63˚ wall angle; (c) t_{PA}= 2.38 *mm*, Galling (G) at 62˚ wall angle

Three distinct modes of failure were observed during the above experiments. These were

(1) Delamination at the metal-polymer interface (denoted by D);

(2) Tearing of the aluminium sheet along the circumferential direction (denoted M); and

(3) Galling of polyamide surface which is in contact with the forming tool (denoted as G).

Examples of these failure modes are shown in Fig. 4-4 and this kind of description is used in all the plots in this paper. Previous work [52] did not observe delamination and

galling modes of failure and effect of polymer sheet thickness on formability was not investigated.

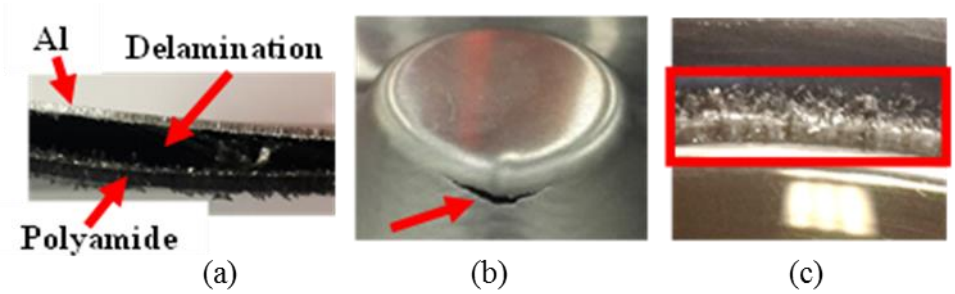

Figure 4-4: Modes of failure (a) Delamination; (b) Metal tearing; (c) Galling

Figure 4-5 shows the effect of t_{PA} and incremental depth (Δz) on formability and mode of failure for the laminates with constant t_{Al}= 0.8 *mm*. At Δz= 0.2 *mm* increasing the polyamide thickness (t_{PA}) increases the formability significantly by reducing the wall angle at which delamination occurs, but only till t_{PA}= 1.58 *mm*. At t_{PA}= 1.58 *mm* the failure mode changes from delamination (D) to metal tearing (M) and the maximum formability is observed. For t_{PA} > 1.58 *mm*, failure mode is still metal tearing (M), but with slightly reduced formability. Similarly, at Δz= 0.4 *mm* an increase in polyamide thicknesses till t_{PA}=1.98 *mm* increases the formability by increasing the wall angle at delamination. At t_{PA}= 1.98 *mm*, the mode of failure changes from delamination (D) to tearing (M) and the maximum formability is observed. Again, after this critical t_{PA} the formability reduces slightly with increasing t_{PA}.

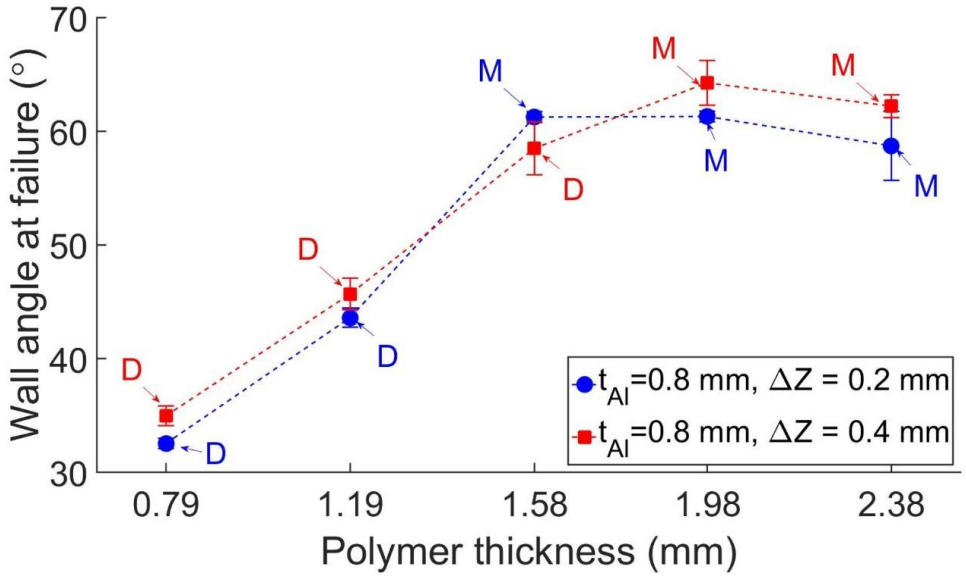

Figure 4-5: Effect of Δz and t_{PA} on failure modes and formed parts for laminates with t_{Al}= 0.8 *mm*

Thus increasing t_{PA} reduces the tendency for delamination but leads to a change in failure mode to tearing. Further, this critical t_{PA} value increases with greater Δz. The polyamide sheet thickness at which the transition in mode of failure occurs will be addressed as the transition polyamide sheet thickness and denoted henceforth as t_{PA_Trans}.

Figure 4-6 shows the effect of polyamide sheet thickness (t_{PA}) and incremental depth (Δz) for laminates with a higher metal sheet thickness, i.e., t_{Al}=1.0 *mm*. At Δz= 0.2 *mm* increasing the polyamide thickness (t_{PA}) increases the wall angle at delamination, and therefore the formability, until t_{PA}= 1.58 *mm*. At this t_{PA} the mode of failure changes from delamination (D) to metal tearing (M) and the maximum formability is observed. For t_{PA} greater than 1.58 *mm*, failure mode changes from metal tearing (M) to galling (G). Similarly, at Δz= 0.4 *mm* an increase in t_{PA} till 1.98 *mm* increases the formability slightly by reducing delamination. At t_{PA}= 1.98 *mm*, the mode of failure changes from delamination

(D) to tearing (M) and the maximum formability is observed. Again, after this critical t_{PA} formability reduces slightly and mode of failure changes from metal tearing (M) to galling (G) with increasing t_{PA}= 2.38 *mm*. At t_{PA_Trans} maximum formability is observed.

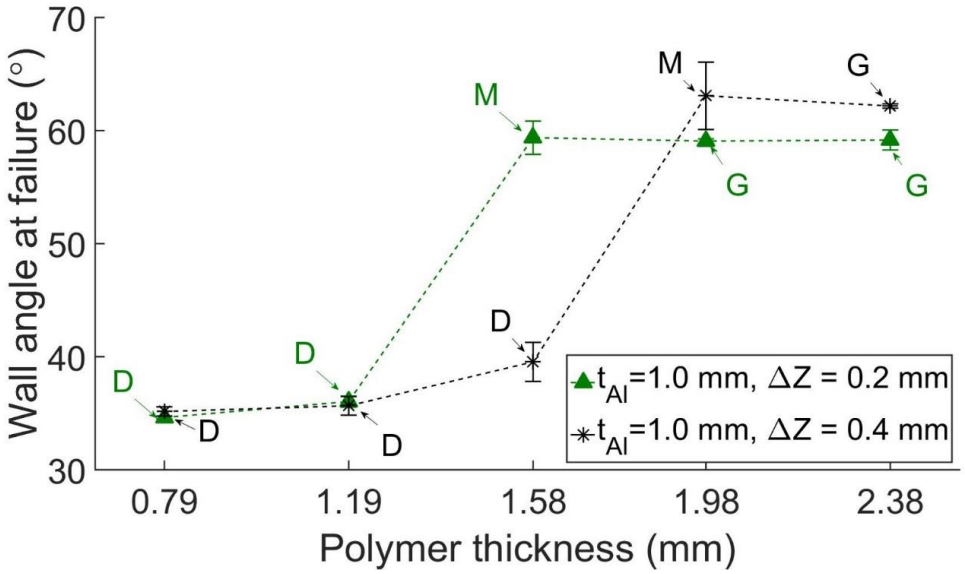

Figure 4-6: Effect of Δz and t_{PA} on failure modes and formed parts for laminates with t_{Al}= 1.0 *mm*

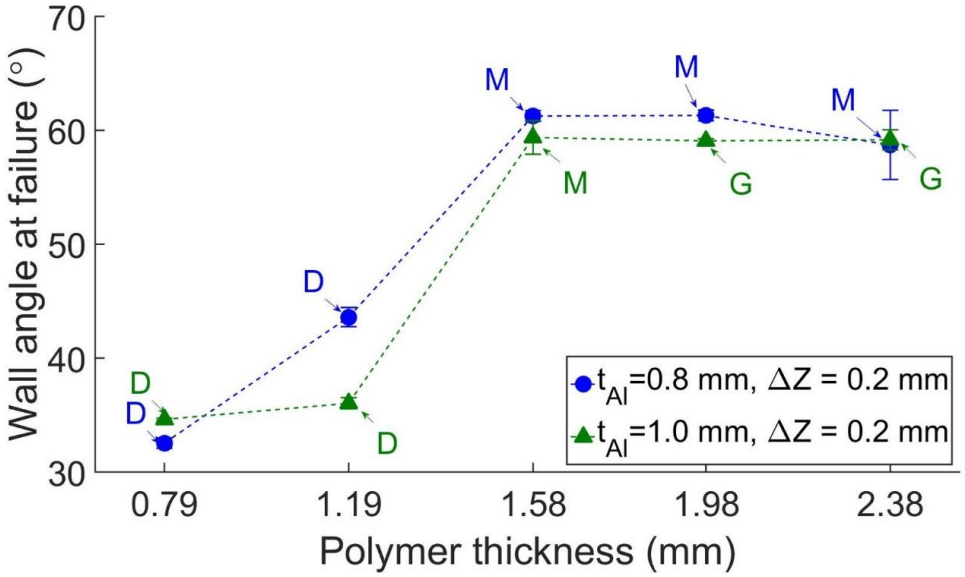

Figure 4-7: Effect of t_{Al} and t_{PA} on failure modes and formed parts for laminates at Δz = 0.2 *mm*

Figure 4-7 shows the effect of aluminium sheet thickness (t_{Al}) and polyamide sheet thickness (t_{PA}) on formability and mode of failure at a constant Δz= 0.2 *mm*. With increasing t_{PA} the formability increases via reduced tendency for delamination until t_{PA}= 1.58 *mm* for both t_{Al}. It shows that no galling is observed in laminates with t_{PA}= 0.8 *mm*.

Figure 4-8 shows a similar indifference of t_{PA} to t_{Al} at a constant Δz= 0.4 *mm*. It should be noted however that at t_{Al}= 0.8 *mm*, formability is significantly higher for t_{PA} lesser than t_{PA_Trans}. It shows that galling is only observed in laminates with t_{Al}= 1 *mm*.

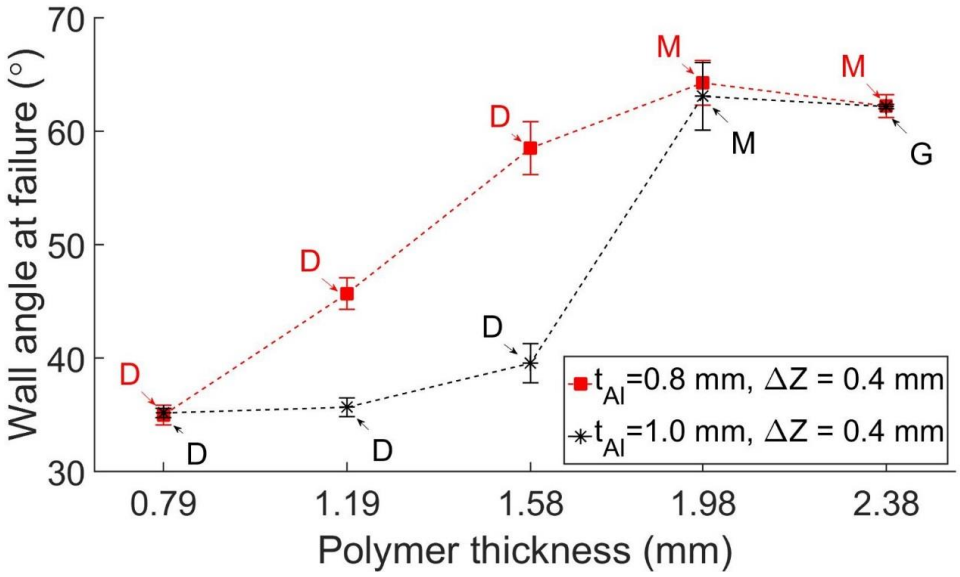

Figure 4-8: Effect of t_{Al} and t_{PA} on failure modes and formed parts for laminates at Δz = 0.4 *mm*

4.5 Conclusion

The summary of the experimental results are as follows:

(1) At low polymer thicknesses, the dominant failure mode is delamination. Increasing polymer thickness increases formability by reducing the tendency for delamination until reaching the *transition polymer thickness* at which mode of

failure changes from delamination to metal tearing and maximum formability is achieved. We believe that this phenomenon is due to lesser bending in unformed area (central area) of the thicker polymer sheet in comparison to thinner polymer sheet which lowers the risk of separation between polymer and metal bonded surfaces, resulting in a lower chance of delamination.

(2) The transition polymer thickness is lesser for smaller incremental depth when the metal thickness is constant. Increasing incremental depth increases the forming force along the forming tool axis, resulting in increasing bending in unformed area and consequently increases the tendency for delamination.

(3) Metal sheet thickness has little effect on the transition polymer thickness. We hypothesize that increasing metal sheet thickness from 0.8 *mm* to 1.0 *mm*, has no significant effect on forming force along forming tool axis, resulting in no significant effect on bending in unformed area. Therefore, metal sheet thickness has no significant effect on delamination.

(4) Increasing polymer thickness beyond transition polymer thickness reduces formability slightly and in laminates with thicker aluminum sheet can change the mode of failure from metal tearing to galling. This is likely because increasing polymer sheet thickness increases the contact pressure between forming tool and polymer sheet, which is results in galling before fracture in thick metal sheet.

4.6 Future work

This work discusses the effect of polymer and metal thickness and incremental depth on formability and failure mode in metal-polymer laminates. However, more research is needed to uncover the effect of other parameters such as adhesive strength and tool rotation speed. A simulation model is needed to predict formability and mode of failure. Our future work will focus on this activity.

4.7 Acknowledgements

The authors would like to acknowledge the Walmart Manufacturing Innovation Fund for the financial support provided for this work.

Preliminary investigations on Double Sided Incremental Forming of thermoplastics

Mohammad Ali Davarpanah, Zixuan Zhang, Shalu Bansal, Jian Cao, and Rajiv Malhotra

Manufacturing Letters

DOI: https://doi.org/10.1016/j.mfglet.2016.05.003

Volume 8, April 2016, Pages 21-26

5 CHAPTER 5: PRELIMINARY INVERSTIGATION ON DOUBLE SIDED INCREMENTAL FROMING OF THERMOPLASTICS

5.1 Abstract

Single Point Incremental Forming (SPIF) of polymers has gained significant attention due to the high material formability, absence of external heating of the polymer, and the use of part-shape-independent tooling. Despite the advantages of Double Sided Incremental Forming (DSIF) of metals, polymer DSIF has not yet been explored. This study examines DSIF of a PVC polymer. Forming forces, formability and void structure of the formed polymer in SPIF and DSIF are compared. Significant advantages of polymer DSIF over SPIF are observed including greater formability, reduced void growth in the material and reduced sheet bending outside the desired forming region.

5.2 Introduction

Single Point Incremental Forming (SPIF) locally deforms a fully peripherally clamped sheet using a small hemispherical ended tool moving along a pre-defined 3D toolpath [18, 19, 103, 104]. Double Sided Incremental Forming (DSIF) uses one such tool on either side of the sheet, such that one tool forms the sheet and the other tool supports or squeezes the sheet locally. Past work on DSIF of metals [25, 105-107] has shown significant advantages over SPIF, including higher formability and improved geometric accuracy. SPIF of commodity and engineering thermoplastics including PVC, PLA, Polyamide, PET, PC and POM has been demonstrated [34, 37-39, 45, 68, 69] without the need for any external heating of the polymer. Currently, thermoplastic surfaces for prototyping and replacement in automobile interiors, low volume fabrication in aircraft interiors [1] and packaging are typically fabricated via injection molding or hot forming.

The reduced cost of thermal energy and tooling in polymer incremental forming can reduce the manufacturing costs in these applications. Furthermore, thermoplastics are more amenable to meeting fire safety standards in the automotive and aerospace industries than thermosets [108]. Despite the above advantages of DSIF, polymer DSIF has not yet been explored. This paper reports preliminary experimental work performed to explore the feasibility of polymer DSIF. SPIF, Conventional DSIF (CDSIF) and Accumulative DSIF (ADSIF, [25]) of commercially obtained PVC are compared in terms of key process and material indexes including forming forces, formability and void content of the formed polymer. These indexes are characterized in terms of the incremental depth (Δz), i.e., the step down in the part depth direction in each consecutive pass of the tool [19], the squeeze factor (s), i.e., the amount by which the two tools squeeze the sheet [24], and the part shape. The feasibility and advantages of polymer DSIF over SPIF are demonstrated and future research directions for polymer DSIF are discussed.

5.3 Experiments

A DSIF machine [25, 105, 106] with a forming area of 250 × 250 mm^2, and two tool-mounted load cells for measuring forming forces, was used to form 1.6 *mm* thick PVC sheets with 10 mm diameter tools. A PTFE based grease was used as the lubricant at the tool-sheet interface with a tool feed rate of 10 *mm/s*. A 60° wall angle cone and a funnel shape, with radius of curvature R_f of 80 *mm* and 150 *mm* and continuously changing wall angle from 30° to 90° (Fig. 5-1a), were formed with CDSIF using Δz = 1.2 *mm* and 1.8 *mm*. Squeeze factors s of 0.8 and 1.0 were investigated. Note that when s = 1.0 the bottom tool is just touching the sheet and when s < 1.0, the tools are actively squeezing the sheet in the

local deformation region between the two tools [105]. SPIF and ADSIF of the cone shape were also performed using $\Delta z = 1.8\ mm$. In CDSIF and ADSIF, the bottom tool was positioned based on the sine law [105]. All experiments were performed using a spiral toolpath (Fig. 5-1b, [19]).

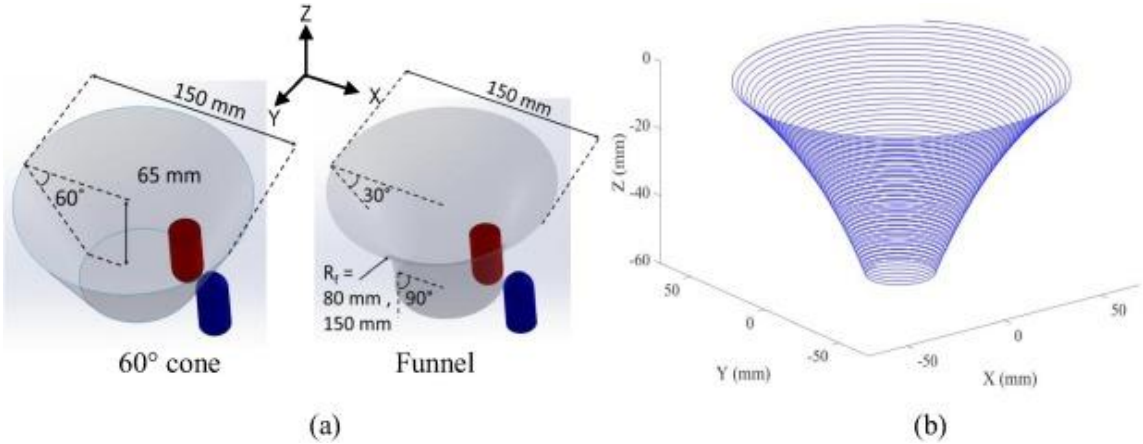

Figure 5-1: (a) Schematic of formed cone and funnel parts. (b) representative example of spiral toolpath used, shown here for a funnel shape

5.4 Results

Figure 5-2a–e shows parts formed with SPIF, CDSIF and ADSIF. The fracture depth and wall angle are commonly used to describe the formability in incremental forming. At the same Δz (Table 5-1) the formed depth of the cone is greater with CDSIF (Fig. 5-2b) and ADSIF (Fig. 5-2c) than with SPIF (Fig. 5-2a), indicating greater formability with DSIF. In fact, no sheet failure is observed with ADSIF. Furthermore, in CDSIF a reduction in s (i.e., greater squeezing of the sheet) and an increase in Δz increases the formability (Table 5-1). Greater formability with greater Δz has also been observed in polymer SPIF [68], which is the opposite trend to that seen in metal SPIF. The formability also seems to depend on the overall part shape, as in polymer SPIF [68], since the funnel

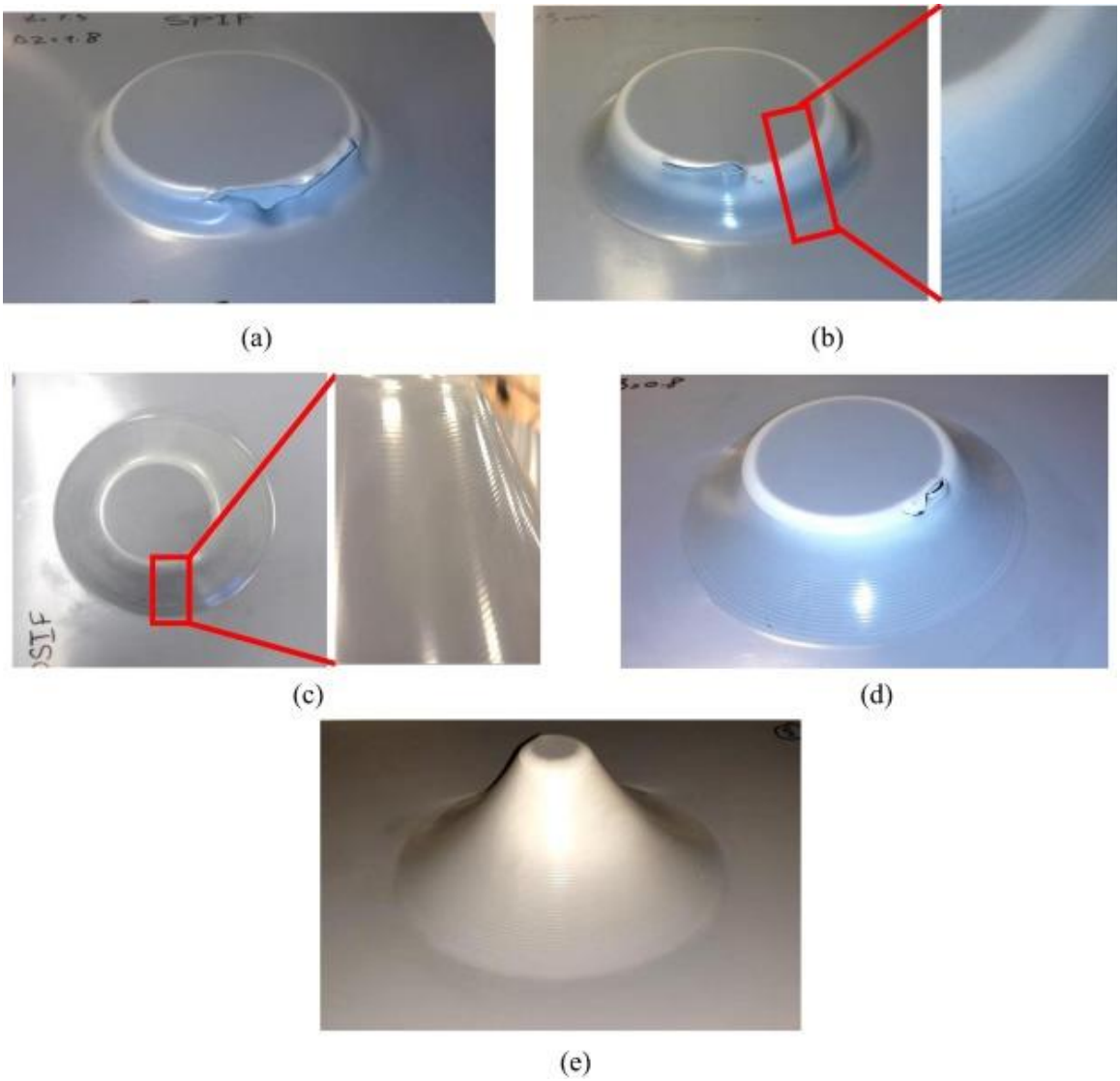

Fig

Figure 5-2: Cone shape formed with (a) SPIF (b) CDSIF (c) ADSIF; (d) R_f = 80 mm funnel formed with CDSIF; (e) R_f = 150 mm funnel formed with CDSIF.

with R_f = 150 mm (Fig. 5-2e) is deformed to a greater wall angle than the funnel with R_f = 80 mm (Fig. 5-2d). A closer observation of the side of the sheet in contact with the bottom tool (Fig. 5-2b) and of the forming forces (Fig. 5-3a) in CDSIF, shows a gradual loss of contact between the sheet and the bottom tool. This phenomenon is also seen in metal CDSIF [23, 24].

Table 5-1: Process parameters and tool tip depths at failure

Part	Process	Δz (*mm*)	Squeeze factor	Z depth at fracture (*mm*)
60˚ Cone	SPIF	1.8	Not applicable	28.2
	CDSIF	1.8	1.0	34.1
		1.8	0.8	35.3
		1.2	1.0	28.2
		1.2	0.8	29.2
Funnel (R_f = 80 *mm*)	ADSIF	1.8	1.0	No failure
	CDSIF	1.8	1.0	37.75 (66.8˚ wall angle)
		1.8	0.8	41.44 (69.6˚ wall angle)
		1.2	1.0	37.8 (66.1 ˚ wall angle)
		1.2	0.8	38.0 (67.2 ˚ wall angle)
Funnel (R_f = 150 *mm*)	CDSIF	1.2	0.8	No failure observed, tool-part interference at 71.0° wall angle prevented continuation of forming

A concurrent change in the color of the sheet was observed, from grey when tool-sheet contact was retained to whitish-grey when tool-sheet contact was lost. This color change indicates the occurrence of crazing [34] after tool-sheet contact is lost in CDSIF, which typically leads to growth of larger voids and fracture. In ADSIF there is no loss of

contact between the bottom tool and the sheet (Figs. 5-2c and 3b) and no change in color of the polymer.

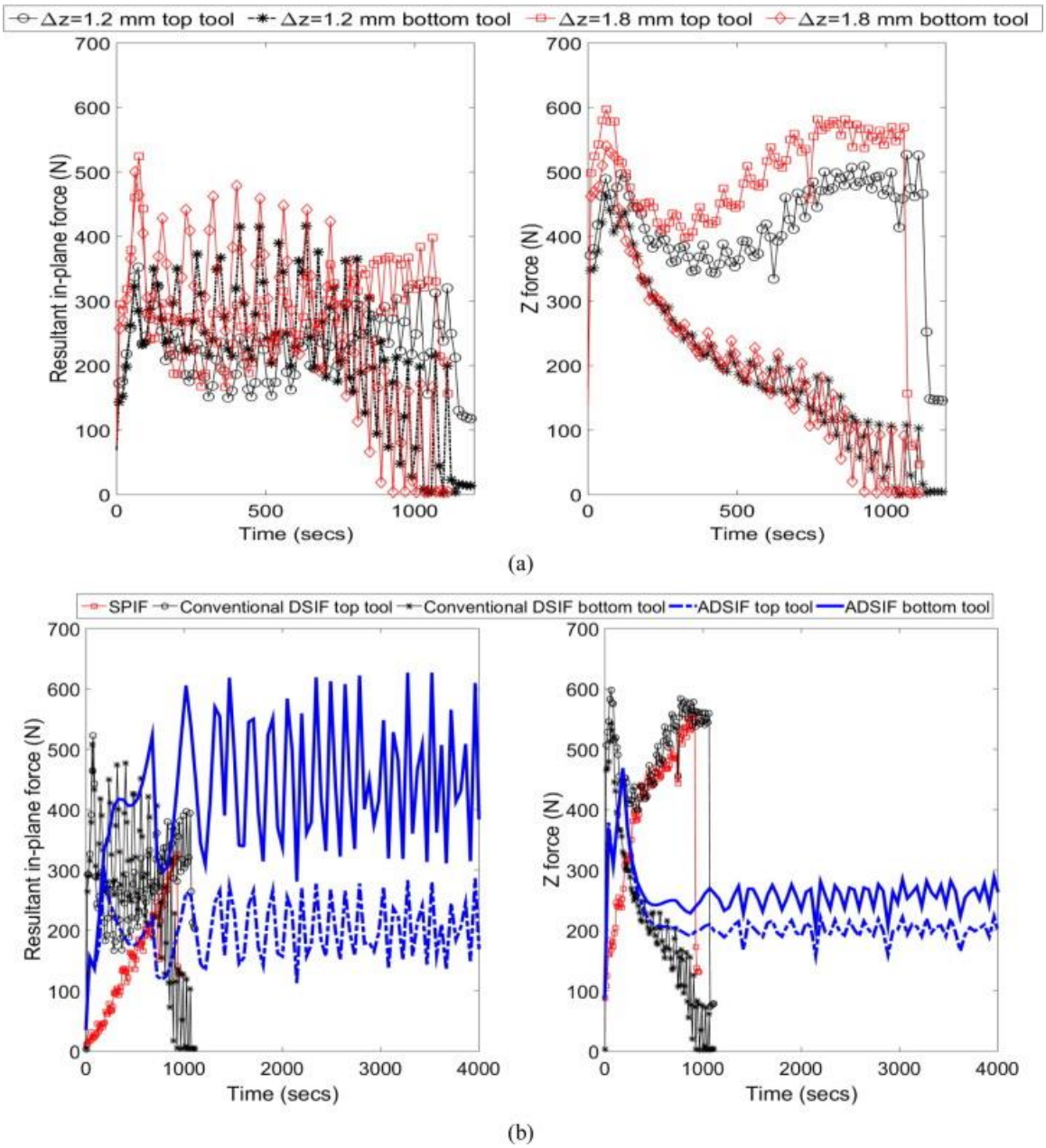

Figure 5-3: Magnitude of forming forces for 60° cone formed (a) by CDSIF with Δz = 1.2 and 1.8 *mm* and s = 1.0 (b) by SPIF, CDSIF and ADSIF with Δz = 1.8 *mm* and s = 1.0

This absence of crazing is probably the reason behind higher formability in ADSIF than in CDSIF. Fig. 5-4a–e shows representative SEM images of the outer surface of the formed parts, along with binary images (inset) obtained after image processing with ImageJ software. Multiple such images were analyzed to calculate the surface void area fraction in the formed material (Fig. 5-4f). The void area fraction is much higher for SPIF than for CDSIF in the region of the part where tool-sheet contact is retained. When contact is lost in CDSIF, the void area fraction rises to levels similar to those in SPIF. Since tool contact is not lost in ADSIF the void area fraction stays low. This observation further supports the hypothesis that retention of tool-sheet contact in ADSIF reduces crazing and resultant void growth in the polymer, resulting in greater formability with ADSIF as compared to CDSIF and SPIF. For the cone shape, the geometric definition of the interface between the wall of the formed part and the ideally flat part of the sheet was observed to be significantly improved with CDSIF and ADSIF than with SPIF (Fig. 5-2a–c). This indicates a reduction in the unwanted bending of the sheet outside the desired deformation zone with DSIF. A similar degree of geometric definition can also be seen in CDSIF of the funnel shape (Fig. 5-2d and e).

5.5 Discussion and Conclusions

The experimental work performed here demonstrates, for the first time, the feasibility of polymer DSIF. Greater Δz and reduction in s result in greater formability in CDSIF. Furthermore, ADSIF has even greater formability than CDSIF. Key advantages of polymer DSIF over SPIF include greater formability, less void growth in the material and reduction in unwanted bending of the sheet outside the desired forming zone.

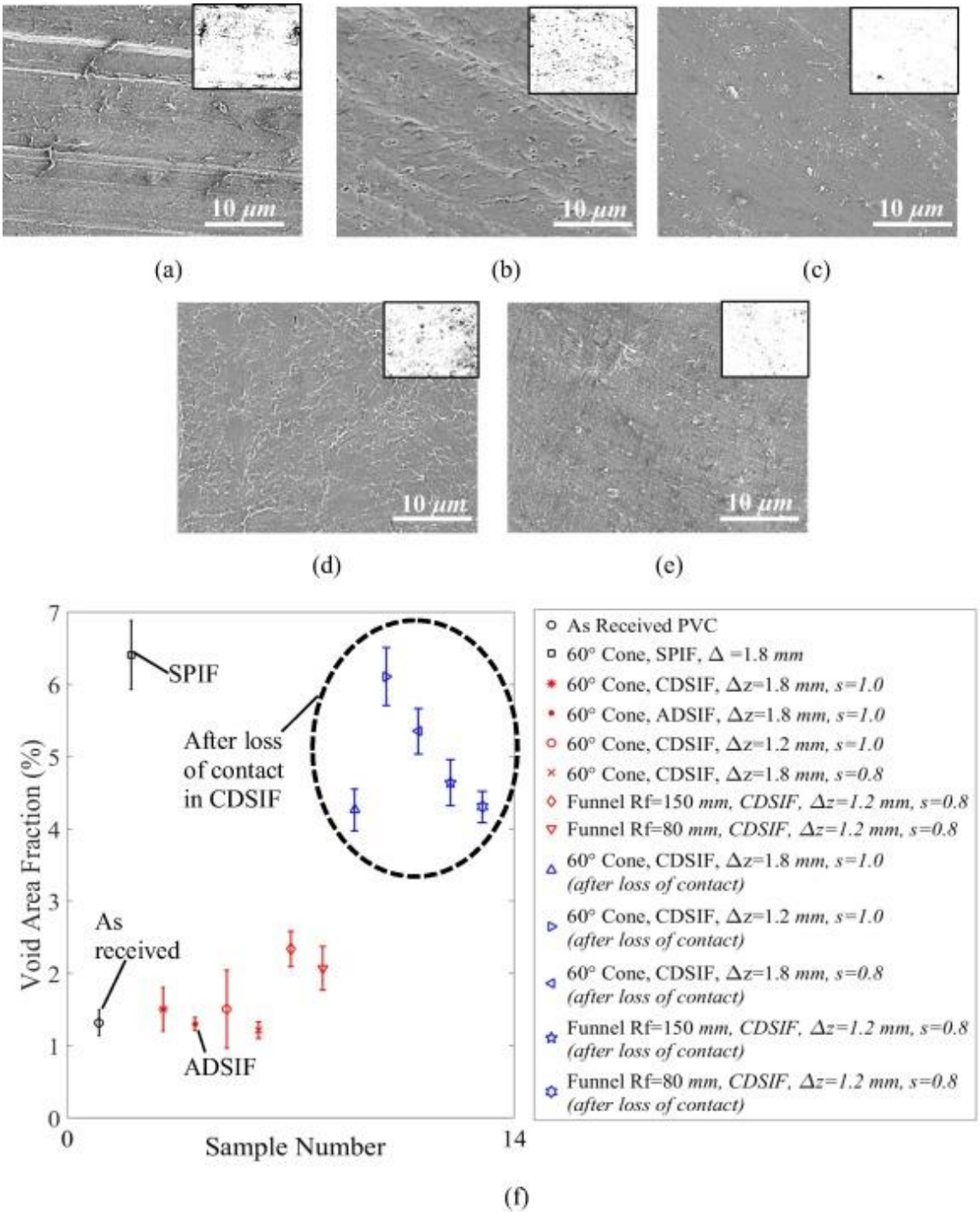

Figure 5-4: Representative SEM images of (a) as received PVC; and PVC formed with (b) SPIF (c) CDSIF at Δz = 1.8 mm and s = 1.0 before loss of tool-sheet contact (d) CDSIF at Δz = 1.8 mm and s = 1.0 after loss of tool-sheet contact (e) ADSIF at Δz = 1.8 mm and s = 1.0; (f) void area fraction calculated from SEM images

Given the past work in polymer SPIF and the observations from this work, it is expected that the above advantages of DSIF can be extended to other thermoplastic polymers as well. At the same time, more research is needed to identify the production batch size at which polymer incremental forming is economically and energetically competitive with hot forming and injection molding. Past work in polymer SPIF [37] has shown that even at a tool feed rate of 50 *mm/s* (compared to 10 *mm/s* used here) the PVC sheet does not reach glass transition temperature. While the use of a second tool in DSIF adds a second source of frictional heat generation as compared to SPIF, given the significantly higher thermal conductivity of the metallic tool as compared to the polymer, it is likely that this additional heat will have a minimal effect on increasing the polymer temperature during DSIF. The temperature of the polymer during DSIF needs to be measured to confirm this hypothesis. There is also a need to identify the mechanisms behind the influence of Δz and s on formability and geometric accuracy, and for techniques to prevent loss of contact between the sheet and the bottom tool during forming in polymer CDSIF [23].

5.6 Acknowledgments

The authors at Oregon State University acknowledge the financial support provided for this work by the Walmart Manufacturing Innovation Fund. The authors at Northwestern University acknowledge the support from the U.S. Department of Energy (Award No. DE-EE0005764).

Chapter 6

6 CONCLUSION AND FUTURE WORK

Effects of incremental depth, tool rotation and part shape on formability and failure modes as well as microstructural properties in SPIF of polymers are investigated experimentally and discussed in chapter 2. The highlighted results are summarized as follows:

- Increasing incremental depth increases the formability and process speed in polymer SPIF. However, this advantage is limited to occurrence of wrinkling at high incremental depths.

- Mode of failure in polymer SPIF depends not only on incremental depth but also on the desired part shape.

- Increasing tool rotation speed results in reduction in the forming forces.

- Comparing the degree of crystallinity of the formed and unformed PLA, which is semi-crystalline polymer, showed that the degree of crystallinity in the formed material is higher than as received material. Higher degree of crystallinity in general results in higher toughness in polymers.

Investigation on effect of SPIF process parameters on polymers continued in chapter 3. In this chapter, effect of SPIF on mechanical properties of the formed polymers was explored. The highlighted results are summarized below:

- SPIF process increases strain at fracture and Ultimate Tensile Strength and reduces yield stress and Young's modulus in formed polymer (amorphous and semi-crystalline polymers) in comparison to unformed polymer.

- SPIF process results in chain orientation in amorphous polymer as well as chain and crystal lamella orientation in semi-crystalline polymers. This phenomenon explains the changes in mechanical properties of the formed polymer as compared to the unformed polymer.

- Degree of crystallinity of the polyamide (semi-crystalline polymer) showed no significant change in formed and unformed material. It shows that SPIF process does not always result in change in degree of crystallinity.

- Increasing tool rotation speed increases temperature near the forming area, which can explain the reduction of measured forming forces in chapter 2.

To further investigate the application of SPIF process, the effect of process parameters on Metal-Polymer laminate SPIF is investigated in chapter 4. The highlighted results are:

- At low polymer sheet thickness, the dominant failure mode is delamination. Increasing the polymer sheet thickness increases the formability until the mode of failure changes from delamination to tearing in metal sheet. This polymer sheet thickness is referred to as transition polymer thickness.

- Increasing the polymer thickness beyond the transition polymer thickness slightly reduces the formability and in laminates with high metal sheet thickness results in galling.

- The transition polymer thickness is lesser at SPIF process with lower incremental depths.

- Metal sheet thickness has little effect on the transition polymer thickness.

The last part of the work focused on preliminary study of polymer DSIF. The results are as follows:

- CDSIF process increases the formability as compared to SPIF process for the polymer sheets.

- Increasing the incremental depth and increasing the squeeze effect increases the formability in polymer CDSIF.

- ADSIF of polymers shows higher formability than CDSIF of polymers.

- Polymer DSIF shows higher formability and lesser void growth, better shape definition as compared to polymer SPIF.

- Only tearing is observed in polymer CDSIF.

Future work will focus on a simulation model needed to predict the formability and failure modes, as well as forming forces in polymer incremental forming. This model can

be used to improve the toolpath parameters and toolpath strategy by predicting the tool elastic deflection and sheet thickness during forming process. The simulation model can be used to understand the deformation mechanism in polymer incremental forming. Effect of adhesive strength and tool rotation speed on formability and failure modes in polymer-metal laminate incremental forming needs to be investigated. A simulation model is needed to predict formability and mode of failure in polymer-metal laminate incremental foming. Further research is needed to investigate the effect of DSIF process parameters on formability and failure mode in polymer DSIF as well as mechanical properties of the DSIF formed polymers.

7 REFERENCES

[1] K.H. Digges, R.G. Gann, S.J. Grayson, M.M. Hirschler4, R.E. Lyon, D.A. Purser, J.G. Quintiere, R.R. Stephenson, A. Tewarson, Human survivability in motor vehicle fires, Fire and Materials, 32 (2008) 249–258.

[2] K. MM, B. KO, B. PJ., Use of Customized Polyetheretherketone (PEEK) Implants in the Reconstruction of Complex Maxillofacial Defects, Arch Facial Plast Surg, 11 (2009) 53-57.

[3] L. Manning, Custom skull implants on demand? Exactly, in, 2011.

[4] United States National Research Council, Elements of Polymer Fire Safety and Guide to the Designer: Report, 1979.

[5] J. Deng, K. Li, E. Harkin-Jones, M. Price, N. Karnachi, A. Kelly, J. Vera-Sorroche, P. Coates, E. Brown, M. Fei, Energy monitoring and quality control of a single screw extruder, Applied Energy, 113 (2014) 1775-1785.

[6] P.G. Lafleur, B. Vergnes, Polymer extrusion, John Wiley & Sons, 2014.

[7] X. Zhou, Y. Zhang, T. Mao, H. Zhou, Monitoring and dynamic control of quality stability for injection molding process, Journal of Materials Processing Technology, 249 (2017) 358-366.

[8] H. Zhou, Computer modeling for injection molding: simulation, optimization, and control, John Wiley & Sons, 2013.

[9] B. Plovie, Y. Yang, J. Guillaume, S. Dunphy, K. Dhaenens, S. Van Put, B. Vandecasteele, T. Vervust, F. Bossuyt, J. Vanfleteren, Arbitrarily shaped 2.5 D circuits using stretchable interconnects embedded in thermoplastic polymers, Advanced Engineering Materials, 19 (2017) 1700032.

[10] P. Klein, Fundamentals of plastics thermoforming, Synthesis Lectures on Materials Engineering, 1 (2009) 1-23.

[11] A. Bandyopadhyay, S. Bose, Additive manufacturing, CRC Press, 2015.

[12] A. Tsouknidas, Friction induced wear of rapid prototyping generated materials: a review, Advances in Tribology, 2011 (2011).

[13] M. Shaw, Cold forming of polymeric materials, Annual Review of Materials Science, 10 (1980) 19-42.

[14] H. Li, P. Koch, D. Prevorsek, H. Oswald, Cold forming of plastics part I. Draw forming of thermoplastic sheets, Polymer Engineering & Science, 11 (1971) 99-108.

[15] J.B. Titus, Solid-Phase Forming (Cold Forming) of Plastics, in, PLASTICS TECHNICAL EVALUATION CENTER PICATINNY ARSENAL NJ, 1972.

[16] T. Mekonnen, P. Mussone, H. Khalilb, D. Bressler, Progress in bio-based plastics and plasticizing modifications, Journal of Materials Chemistry A, 1 (2013) 13379-13398.

[17] J. Smith, R. Malhotra, K.W. Liu, J. Cao, Deformation mechanics in single-point and accumulative double-sided incremental forming, The International Journal of Advanced Manufacturing Technology, 69 (2013) 1185-1201.

[18] A. Attanasio, E. Ceretti, C. Giardini, Optimization of tool path in two points incremental forming, Journal of Materials Processing Technology, 177 (2006) 409-412.

[19] R. Malhotra, N. Reddy, J. Cao, Automatic 3D spiral toolpath generation for single point incremental forming, Journal of Manufacturing Science and Engineering, 132 (2010) 061003.

[20] K. Jackson, J. Allwood, The mechanics of incremental sheet forming, Journal of Materials Processing Technology, 209 (2009) 1158-1174.

[21] Z. Zhang, H. Ren, R. Xu, N. Moser, J. Smith, E. Ndip-Agbor, R. Malhotra, Z.C. Xia, K.F. Ehmann, J. Cao, A mixed double-sided incremental forming toolpath strategy for improved geometric accuracy, Journal of Manufacturing Science and Engineering, 137 (2015) 051007.

[22] D. Xu, B. Lu, T. Cao, H. Zhang, J. Chen, H. Long, J. Cao, Enhancement of process capabilities in electrically-assisted double sided incremental forming, Materials & Design, 92 (2016) 268-280.

[23] N. Moser, Z. Zhang, H. Ren, H. Zhang, Y. Shi, E.E. Ndip-Agbor, B. Lu, J. Chen, K.F. Ehmann, J. Cao, Effective forming strategy for double-sided incremental forming considering in-plane curvature and tool direction, CIRP Annals - Manufacturing Technology, (2016).

[24] R. Malhotra, J. Cao, F. Ren, V. Kiridena, Z. Cedric Xia, N.V. Reddy, Improvement of Geometric Accuracy in Incremental Forming by Using a Squeezing Toolpath Strategy With Two Forming Tools, Journal of Manufacturing Science and Engineering, 133 (2011) 061019-061019.

[25] R. Malhotra, J. Cao, M. Beltran, D. Xu, J. Magargee, V. Kiridena, Z.C. Xia, Accumulative-DSIF strategy for enhancing process capabilities in incremental forming, CIRP Annals - Manufacturing Technology, 61 (2012) 251-254.

[26] Y. Kim, J. Park, Effect of process parameters on formability in incremental forming of sheet metal, Journal of Materials Processing Technology, 130 (2002) 42-46.

[27] G. Hussain, L. Gao, N. Dar, An experimental study on some formability evaluation methods in negative incremental forming, Journal of Materials Processing Technology, 186 (2007) 45-53.

[28] D. Young, J. Jeswiet, Wall thickness variations in single-point incremental forming, Proceedings of the Institution of Mechanical Engineers, Part B: Journal of Engineering Manufacture, 218 (2004) 1453-1459.

[29] G. Ambrogio, L. Filice, F. Gagliardi, F. Micari, Sheet thinning prediction in single point incremental forming, in: Advanced materials research, Trans Tech Publ, 2005, pp. 479-486.

[30] R. Malhotra, L. Xue, T. Belytschko, J. Cao, Mechanics of fracture in single point incremental forming, Journal of Materials Processing Technology, 212 (2012) 1573-1590.

[31] Y. Wang, Y. Huang, J. Cao, N.V. Reddy, Experimental study on a new method of double side incremental forming, in: ASME 2008 International Manufacturing Science and Engineering Conference collocated with the 3rd JSME/ASME International Conference on Materials and Processing, American Society of Mechanical Engineers, 2008, pp. 601-607.

[32] Y. Wang, W. Wu, Y. Huang, N.V. Reddy, J. Cao, Experimental and Numerical Analysis of Double Sided Incremental Forming, in: ASME 2009 International Manufacturing Science and Engineering Conference, American Society of Mechanical Engineers, 2009, pp. 613-618.

[33] I. Cerro, E. Maidagan, J. Arana, A. Rivero, P. Rodriguez, Theoretical and experimental analysis of the dieless incremental sheet forming process, Journal of Materials Processing Technology, 177 (2006) 404-408.

[34] V. Franzen, L. Kwiatkowski, P. Martins, A. Tekkaya, Single point incremental forming of PVC, Journal of Materials Processing Technology, 209 (2009) 462-469.

[35] V. Franzen, L. Kwiatkowski, J. Neves, P. Martins, A. Tekkaya, On the capability of single point incremental forming for manufacturing polymer sheet parts, in: ICTP2008, 9th International Conference on Theory of Plasticity, 2008.

[36] V.S. Le, A. Ghiotti, G. Lucchetta, Preliminary Studies on Single Point Incremental Forming for Thermoplastic Materials, International Journal of Material Forming, 1 (2008) 1179-1182.

[37] I. Bagudanch, M. Garcia-Romeu, G. Centeno, A. Elías-Zúñiga, J. Ciurana, Forming force and temperature effects on single point incremental forming of polyvinylchloride, Journal of Materials Processing Technology, 219 (2015) 221-229.

[38] T.A. Marques, M.B. Silva, P. Martins, On the potential of single point incremental forming of sheet polymer parts, The International Journal of Advanced Manufacturing Technology, 60 (2012) 75-86.

[39] P.A.F. Martins, L. Kwiatkowski, V. Franzen, A.E. Tekkaya, M. Kleiner, Single point incremental forming of polymers, CIRP Annals - Manufacturing Technology, 58 (2009) 229-232.

[40] F. Maaß, S. Gies, A. Tekkaya, Deformation characteristics of thermoplastics in single point incremental forming, in: AIP Conference Proceedings, AIP Publishing, 2017, pp. 050005.

[41] I. Bagudanch, G. Centeno, C. Vallellano, M. Garcia-Romeu, Revisiting formability and failure of polymeric sheets deformed by Single Point Incremental Forming, Polymer Degradation and Stability, 144 (2017) 366-377.

[42] L.M. Lozano-Sánchez, I. Bagudanch, A.O. Sustaita, J. Iturbe-Ek, L.E. Elizalde, M.L. Garcia-Romeu, A. Elías-Zúñiga, Single-Point Incremental Forming of Two Biocompatible Polymers: An Insight into Their Thermal and Structural Properties, Polymers, 10 (2018) 391.

[43] G. Medina-Sánchez, E. Torres-Jimenez, R. Lopez-Garcia, R. Dorado-Vicente, R. Cazalla-Moral, Temperature influence on Single Point Incremental Forming of PVC parts, Procedia Manufacturing, 13 (2017) 335-342.

[44] M. Durante, A. Formisano, F. Lambiase, Incremental forming of polycarbonate sheets, Journal of Materials Processing Technology, 253 (2018) 57-63.

[45] M. Silva, L. Alves, P. Martins, Single point incremental forming of PVC: Experimental findings and theoretical interpretation, European journal of mechanics-A/Solids, 29 (2010) 557-566.

[46] P. Martins, N. Bay, M. Skjødt, M. Silva, Theory of single point incremental forming, CIRP annals-Manufacturing technology, 57 (2008) 247-252.

[47] I. Bagudanch, O. Martínez-Romero, A. Elías-Zúñiga, M.L. Garcia-Romeu, Identifying polymeric constitutive equations for incremental sheet forming modelling, Procedia Engineering, 81 (2014) 2292-2297.

[48] S.A. Yonan, P. Haupt, L. Kwiatkowski, V. Franzen, A. Brosius, A. Tekkaya, Three-dimensional Formulation and Validation of a New Viscoplastic Material Model for the Simulation of Incremental Forming of Thermoplastics Material Characterization Constitutive Modelling, in: 10th International Conference on Technology of Plasticity Aachen, 2011, pp. 973-977.

[49] S.A. Yonan, M.B. Silva, P.A.F. Martins, A.E. Tekkaya, Plastic flow and failure in single point incremental forming of PVC sheets, Express Polymer Letters, 8 (2014) 301.

[50] S.A. Yonan, C. Soyarslan, P. Haupt, L. Kwiatkowski, A. Tekkaya, A simple finite strain non-linear visco-plastic model for thermoplastics and its application to the simulation of incremental cold forming of polyvinylchloride (PVC), International Journal of Mechanical Sciences, 66 (2013) 192-201.

[51] I. Bagudanch, M.L. García-Romeu, I. Ferrer, J. Ciurana, Customized cranial implant manufactured by incremental sheet forming using a biocompatible polymer, Rapid Prototyping Journal, 24 (2018) 120-129.

[52] K. Jackson, J. Allwood, M. Landert, Incremental forming of sandwich panels, Journal of Materials Processing Technology, 204 (2008) 290-303.

[53] D. Xu, W. Wu, R. Malhotra, J. Chen, B. Lu, J. Cao, Mechanism investigation for the influence of tool rotation and laser surface texturing (LST) on formability in single point incremental forming, International Journal of Machine Tools and Manufacture, 73 (2013) 37-46.

[54] G. Hussain, L. Gao, A novel method to test the thinning limits of sheet metals in negative incremental forming, International Journal of Machine Tools and Manufacture, 47 (2007) 419-435.

[55] L. Filice, G. Ambrogio, F. Micari, On-line control of single point incremental forming operations through punch force monitoring, CIRP annals-Manufacturing technology, 55 (2006) 245-248.

[56] J. Duflou, Y. Tunckol, A. Szekeres, P. Vanherck, Experimental study on force measurements for single point incremental forming, Journal of Materials Processing Technology, 189 (2007) 65-72.

[57] C. Bouffioux, P. Eyckens, C. Henrard, R. Aerens, A. Van Bael, H. Sol, J. Duflou, A. Habraken, Identification of material parameters to predict Single Point Incremental Forming forces, International Journal of Material Forming, 1 (2008) 1147-1150.

[58] W. Pratt, Digital Image Processing. New York: John Wiley & Sons, Inc, (1991).

[59] S. Pilla, S. Gong, E. O'Neill, R.M. Rowell, A.M. Krzysik, Polylactide-pine wood flour composites, Polymer Engineering & Science, 48 (2008) 578-587.

[60] I.M. Hodge, Effects of annealing and prior history on enthalpy relaxation in glassy polymers. 4. Comparison of five polymers, Macromolecules, 16 (1983) 898-902.

[61] I.M. Hodge, G.S. Huvard, Effects of annealing and prior history on enthalpy relaxation in glassy polymers. 3. Experimental and modeling studies of polystyrene, Macromolecules, 16 (1983) 371-375.

[62] I.M. Hodge, A.R. Berens, Effects of annealing and prior history on enthalpy relaxation in glassy polymers. 2. Mathematical modeling, Macromolecules, 15 (1982) 762-770.

[63] B. Wunderlich, Thermal characterization of polymeric materials, Turi, EA, Ed, 205 (1997).

[64] S. Pilla, S. Gong, E. O'Neill, L. Yang, R.M. Rowell, Polylactide-recycled wood fiber composites, Journal of Applied Polymer Science, 111 (2009) 37-47.

[65] R. Dargazany, V.N. Khiêm, E.A. Poshtan, M. Itskov, Constitutive modeling of strain-induced crystallization in filled rubbers, Physical Review E, 89 (2014) 022604.

[66] I. Rao, K. Rajagopal, A study of strain-induced crystallization of polymers, International Journal of Solids and Structures, 38 (2001) 1149-1167.

[67] V. Franzen, L. Kwiatkowski, P.A.F. Martins, A.E. Tekkaya, Single point incremental forming of PVC, . Mater. Process. Technol., 209 (1) (2009) 462–469.

[68] M.A. Davarpanah, A. Mirkouei, X. Yu, R. Malhotra, S. Pilla, Effects of incremental depth and tool rotation on failure modes and microstructural properties in Single Point Incremental Forming of polymers, Journal of Materials Processing Technology, 222 (2015) 287-230.

[69] V. Franzen, L. Kwiatkowski, J. Neves, P.A.F. Martins, A.E. Tekkaya, On the capability of single point incremental forming for manufacturing PVC sheet parts, ICTP-2008, International Conference on Technology of Plasticity, Gyeongju, Korea (2008).

[70] M.B. Silva, L.M. Alves, P.A.F. Martins, Single point incremental forming of PVC: Experimental findings and theoretical interpretation, European Journal of Mechanics - A/Solids, 29 (2010) 557-566.

[71] I. Bagudanch, M.L. Garcia-Romeu, G. Centeno, A. Elías-Zúñiga, J. Ciurana, Forming force and temperature effects on single point incremental forming of polyvinylchloride, Journal of Materials Processing Technology, 219 (2015) 221-229.

[72] J. Jeswiet, F. Micari, G. Hirt, A. Bramley, J. Duflou, J. Allwood, Asymmetric Single Point Incremental Forming of Sheet Metal, CIRP Annals - Manufacturing Technology, 54 (2005) 88-114.

[73] R.P. Danner, M.S. High, Handbook of Polymer Solution Thermodynamics, American Institute of Chemical Engineers, 1993.

[74] S. Pilla, S. Gong, E. O'Neill, R.M. Rowell, A.M. Krzy, Polylactide-pine woodflour composites, Polymer Engineering & Science, 48 (2008) 578-587.

[75] E.M. Arruda, M.C. Boyce, Evolution of plastic anisotropy in amorphous polymers during finite straining, International Journal of Plasticity, 9 (1993) 697-720.

[76] E.M. Arruda, M.C. Boyce, R. Jayachandran, Effects of strain rate, temperature and thermomechanical coupling on the finite strain deformation of glassy polymers, Mechanics of Materials, 19 (1995) 193-212.

[77] I. Ward, Structure and Properties of Oriented Polymers, Springer Science + Business Media, BV, 1975.

[78] R.F. Landel, L.E. Nielsen, Mechanical Properties of Polymers and Composites, Second Edition, Macel Dekker, Inc, New York. Basel, 1994.

[79] E. Shin, A. Hiltner, E. Baer, The brittle-to-ductile transition in microlayer composites, Journal of Applied Polymer Science, 47 (2) (1993) 269-288.

[80] J. Takahashi, T. Yamamoto, K. Shizawa, Modeling and simulation for ductile fracture prediction of crystalline polymer based on craze behavior, International Journal of Mechanical Sciences, 52(2) (2010) 266-276.

[81] O. Tim., in: Understanding Polymer Processing: Processes and Governing Equations, Hanser Publications, 2010, pp. 29-54.

[82] A.S. Argon, The Physics of Deformation and Fracture of Polymers, Cambridge University Press, 2013.

[83] I.-C. Yeh, J.W. Andzelm, G.C. Rutledge, Mechanical and structural characterization of semicrystalline polyethylene under tensile deformation by molecular dynamics simulations, Macromolecules, 48 (2015) 4228–4239.

[84] S. Jabbari-Farouji, J. Rottler, O. Lame, A. Makke, M. Perez, J.-L. Barrat, Plastic deformation mechanisms of semicrystalline and amorphous polymers, ACS Macro Lett, 4 (2015) 147–150.

[85] S. Jabbari-Farouji, J. Rottler, O. Lame, A. Makke, M. Perez, J.-L. Barrat, Correlation of structure and mechanical response in solid-like polymers, Journal of Physics: Condensed Matter, 27 (2015).

[86] R. Hiss, S. Hobeika, C. Lynn, G. Strobl, Network stretching, slip processes, and fragmentation of crystallites during uniaxial drawing of polyethylene and related copolymers. A comparative study, Macromolecules 32 (1999) 4390–4403.

[87] W.J. O'Kane, R.J. Young, The role of dislocations in the yield of polypropylene, Journal of Materials Science Letters 14 (1995) 433-435.

[88] W.J. O'Kane, R.J. Young, A.J.J. Ryan, The effect of annealing on the structure and properties of Isotactic polypropylene films, Journal of Macromolecular Science , Part B: Physics, B34 (1995) 427–458.

[89] N. Dusunceli, O.U. Colak, Modelling effects of degree of crystallinity on mechanical behavior of semicrystalline polymers, International Journal of Plasticity, 24 (2007) 1224-1242.

[90] A. Martínez-Donaire, D. Morales-Palma, A. Caballero, M. Borrego, G. Centeno, C. Vallellano, Numerical explicit analysis of hole flanging by single-stage incremental forming, Procedia Manufacturing, 13 (2017) 132-138.

[91] R. Aerens, P. Eyckens, A. Van Bael, J. Duflou, Force prediction for single point incremental forming deduced from experimental and FEM observations, The International Journal of Advanced Manufacturing Technology, 46 (2010) 969-982.

[92] T. Husmann, C.S. Magnus, Thermography in incremental forming processes at elevated temperatures, Measurement, 77 (2016) 16-28.

[93] A.K. Behera, J. Verbert, B. Lauwers, J.R. Duflou, Tool path compensation strategies for single point incremental sheet forming using multivariate adaptive regression splines, Computer-Aided Design, 45 (2013) 575-590.

[94] M. Bambach, B.T. Araghi, G. Hirt, Strategies to improve the geometric accuracy in asymmetric single point incremental forming, Production Engineering, 3 (2009) 145-156.

[95] S. Shanmuganatan, V.S. Kumar, Experimental investigation and finite element modeling on profile forming of conical component using Al 3003 (O) alloy, Materials & Design (1980-2015), 36 (2012) 564-569.

[96] G. Ambrogio, L. Filice, F. Gagliardi, Formability of lightweight alloys by hot incremental sheet forming, Materials & Design, 34 (2012) 501-508.

[97] K. Hamilton, J. Jeswiet, Single point incremental forming at high feed rates and rotational speeds: Surface and structural consequences, CIRP annals-Manufacturing technology, 59 (2010) 311-314.

[98] R. Sridhar, D. Rajenthirakumar, Polymer Sheet Hot Incremental Forming-An Innovative Polymer Forming Approach, Polymers & Polymer Composites, 24 (2016) 447.

[99] I. Bagudanch, L.M. Lozano-Sánchez, L. Puigpinós, M. Sabater, L.E. Elizalde, A. Elías-Zúñiga, M.L. Garcia-Romeu, Manufacturing of polymeric biocompatible cranial geometry by single point incremental forming, Procedia Engineering, 132 (2015) 267-273.

[100] P. Martins, L. Kwiatkowski, V. Franzen, A. Tekkaya, M. Kleiner, Single point incremental forming of polymers, CIRP annals-Manufacturing technology, 58 (2009) 229-232.

[101] M.A. Davarpanah, S. Bansal, R. Malhotra, Influence of Single Point Incremental Forming on Mechanical Properties and Microstructural Morphology of Polymers, ASME Journal of Manufacturing Science and Engineering (Submitted), (2015).

[102] M.A. Davarpanah, S. Bansal, Z. Zhang, R. Malhotra, J. Cao, Preliminary investigations on Double Sided Incremental Forming of thermoplastics, Manufacturing Letters, (2016).

[103] M. Rauch, J.-Y. Hascoet, J.-C. Hamann, Y. Plenel, Tool path programming optimization for incremental sheet forming applications, Computer-Aided Design, 41 (2009) 877-885.

[104] A. Attanasio, E. Ceretti, C. Giardini, L. Mazzoni, Asymmetric two points incremental forming: improving surface quality and geometric accuracy by tool path optimization, Journal of Materials Processing Technology, 197 (2008) 59-67.

[105] Z. Zhang, H. Ren, R. Xu, N. Moser, J. Smith, E. Ndip-Agbor, R. Malhotra, Z. Cedric Xia, K.F. Ehmann, J. Cao, A Mixed Double-Sided Incremental Forming Toolpath Strategy for Improved Geometric Accuracy, Journal of Manufacturing Science and Engineering, 137 (2015) 051007-051007.

[106] R. Xu, X. Shi, D. Xu, R. Malhotra, J. Cao, A preliminary study on the fatigue behavior of sheet metal parts formed with accumulative-double-sided incremental forming, Manufacturing Letters, 2 (2014) 8-11.

[107] N. Moser, E. Ndip-Agbor, H. Ren, Z. Zhang, K. Ehmann, J. Cao, Challenges and Process Strategies Concerning Multi-Pass Double Sided Incremental Forming, Key Engineering Materials, (2015).

[108] United States National Research Council. Elements of polymer fire safety and guide to the designer: report., in, National Academies, 1979.

8 APPENDIX A

This appendix contains extended information related to experiments discussed in chapters 2 to 5.

8.1 Design of Experiments - Chapter 2

8.1.1 Experiments

An SPIF setup (Fig. 2-1a) was used for performing experiments. A dial gauge with 0.0005" accuracy was used to co-center the tool axis with the center of forming area. 0.005" was chosen as the maximum acceptable error, which is less than 0.5% of the part shape diameter. To define the zero offset along incremental depth direction (Z-axis) the forming tool was moved along Z-axis until it touched the blank. The zero offset was redone when the thickness of the sheet was changed.

Figure 8-1 shows the two part shapes with the toolpath strategy, which are used for performing experiments in chapter 2.

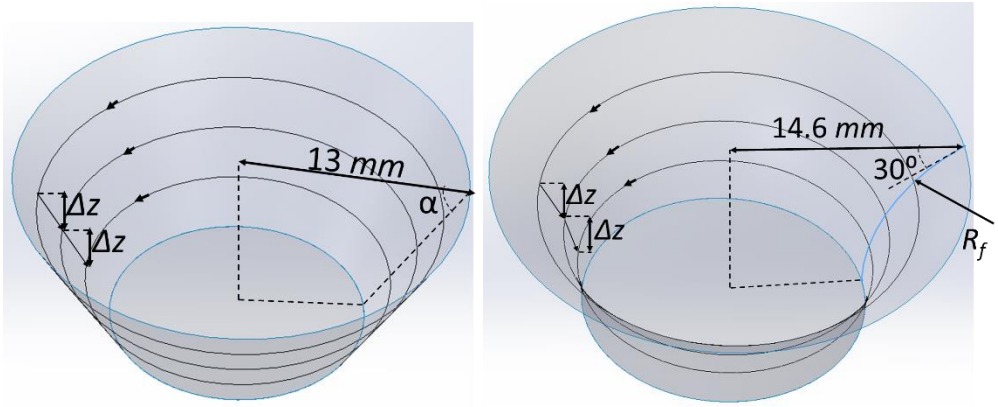

(a) (b)

Figure 8-1: (a) Cone shape and (b) Funnel shape with schematic of the toolpath strategy

To identify the mode of failure the operator observed the specimen during the forming process and after observing any form of failure (Tearing or Wrinkling), the

operator stopped the forming process and recorded the tool position in Z-direction. The recorded tool position in Z-direction was used to calculate the wall angle at failure for the funnel shape and record the depth at fracture for the cone shape experiments (Figure 8-1).

Table 8-1 shows the design of experiment table for experiments in chapter 2. The abbreviation of the table are as follows:

- ID: Each ID represents a set of process parameters
- Mat.: Blank sheet material
- Rep.: Represents how many times each experiment ID has been performed
- Δz: Incremental depth in mm
- d_{tool}: Forming tool diameter in mm
- F: Feedrate in mm/min
- ω: Tool rotation speed in rpm
- t: Initial blank sheet thickness in mm
- α: Cone shape part wall angle in degree
- R_f: Radius of curvature of funnel shape in mm

The toolpath was uploaded to the CNC machine and all the repetitions were completed for an experiment ID before moving to the next experiment ID.

Table 8-1: Design of experiments

ID	Mat.	Rep (#)	Δz (mm)	d_{tool} (mm)	F (mm/min)	ω (rpm)	t (mm)	α ($^{\circ}$)	R_f (mm)
1	PLA	5	0.2	5	300	0	0.7	55	-
2	PLA	5	0.4	5	300	0	0.7	55	-
3	PLA	5	0.6	5	300	0	0.7	55	-
4	PLA	5	0.8	5	300	0	0.7	55	-
5	PLA	5	1	5	300	0	0.7	55	-
6	PLA	5	0.2	5	300	0	0.7	65	-
7	PLA	5	0.4	5	300	0	0.7	65	-
8	PLA	5	0.6	5	300	0	0.7	65	-
9	PLA	5	0.8	5	300	0	0.7	65	-
10	PLA	5	1	5	300	0	0.7	65	-
11	PLA	5	0.2	5	300	0	0.7	75	-
12	PLA	5	0.4	5	300	0	0.7	75	-
13	PLA	5	0.6	5	300	0	0.7	75	-
14	PLA	5	0.8	5	300	0	0.7	75	-
15	PLA	5	1	5	300	0	0.7	75	-
16	PLA	5	0.2	5	300	0	0.7	-	10
17	PLA	5	0.4	5	300	0	0.7	-	10
18	PLA	5	0.6	5	300	0	0.7	-	10
19	PLA	5	0.8	5	300	0	0.7	-	10
20	PLA	5	1	5	300	0	0.7	-	10
21	PLA	5	0.2	5	300	0	0.7	-	12
22	PLA	5	0.4	5	300	0	0.7	-	12
23	PLA	5	0.6	5	300	0	0.7	-	12
24	PLA	5	0.8	5	300	0	0.7	-	12
25	PLA	5	1	5	300	0	0.7	-	12
26	PLA	5	0.2	5	300	1250	0.7	-	12

Continued.

27	PLA	5	0.6	5	300	1250	0.7	-	12
28	PLA	5	1	5	300	1250	0.7	-	12
29	PLA	5	0.2	5	300	5000	0.7	-	12
30	PLA	5	0.6	5	300	5000	0.7	-	12
31	PLA	5	1	5	300	5000	0.7	-	12
32	PLA	5	0.2	5	300	7000	0.7	-	12
33	PLA	5	0.6	5	300	7000	0.7	-	12
34	PLA	5	1	5	300	7000	0.7	-	12
35	PLA	5	0.2	5	300	0	0.7	-	14
36	PLA	5	0.4	5	300	0	0.7	-	14
37	PLA	5	0.6	5	300	0	0.7	-	14
38	PLA	5	0.8	5	300	0	0.7	-	14
39	PLA	5	1	5	300	0	0.7	-	14
40	PLA	5	0.2	5	300	0	0.7	-	16
41	PLA	5	0.4	5	300	0	0.7	-	16
42	PLA	5	0.6	5	300	0	0.7	-	16
43	PLA	5	0.8	5	300	0	0.7	-	16
44	PLA	5	1	5	300	0	0.7	-	16
45	PVC	5	0.2	5	300	0	1.5	-	12
46	PVC	5	1	5	300	0	1.5	-	12
47	PVC	5	1.8	5	300	0	1.5	-	12
48	PVC	5	0.2	5	300	1250	1.5	-	12
49	PVC	5	1	5	300	1250	1.5	-	12
50	PVC	5	1.8	5	300	1250	1.5	-	12
51	PVC	5	0.2	5	300	5000	1.5	-	12
52	PVC	5	1	5	300	5000	1.5	-	12
53	PVC	5	1.8	5	300	5000	1.5	-	12
54	PVC	5	0.2	5	300	7000	1.5	-	12
55	PVC	5	1	5	300	7000	1.5	-	12
56	PVC	5	1.8	5	300	7000	1.5	-	12

8.1.2 Results

As it is shown in table 8-1, each experiment ID was repeated 5 times. The mode of failure, which was repeated the most (at least 3 times), was reported as mode of failure for

that specific set of process parameters. The specimens, which have the most repeated failure mode, were chosen to calculate error bar and the average for the graphs which are shown in chapter 2. The average depth at fracture for cone shape/wall angle at failure for funnel shape represent the depth at fracture/wall angle at failure for cone/funnel shape. The standard deviation was calculated and used for plus and minus of the error bar.

Figure 2-3b shows that at $\Delta z = 0.6$ *mm*, Z-depth at failure is significantly lower than $\Delta z = 0.4$ and $\Delta z = 0.8$ *mm*. This odd and out of trend data point might be due to following potential errors during running the experiments:

- Setting the forming tool zero offset in Δz direction at a position lower than the blank top surface before running the experiments (Experiment ID=8).

- Low quality of the as-received sheet. The samples for each experiment ID were cut out from a sheet. Therefore, the samples were used for the experiment ID= 8, might have been cut out of a softer PLA sheet or a sheet with low surface quality like having scratches on the surface. PLA sheets were white; therefore, identifying scratches were harder for the operator.

It is also possible that the combination of the process parameters like blank sheet thickness and material, friction condition, tool diameter, incremental depth, part shape results to the aforimentioned odd data point. More repeatation of the experiment ID= 8, is needed to find out if the presented results was and exception or not.

8.2 Design of Experiments of Chapter 3

8.2.1 Experiments

An SPIF setup (Fig. 3-2a) was used for performing experiments. To set the zero offset point of the tool over the forming area in the XY plane of the CNC machine. The tool was moved along X-axis in the negative direction until it touched the inner edge of the forming area and the X value was recorded (X1). Next step was moving the tool along X-axis in the positive direction until it touched the inner edge at the opposite side of the forming area and the X value was recorded (X2). The average of the recorded X values was used to set the X offset and co-center the forming tool axis with the center of the forming area in X-axis. Similar steps were followed for offset in Y-axis. To define the zero offset along incremental depth direction (Z-axis) the forming tool was moved along Z-axis until it touched the blank at the center of the forming area.

Figure 8-2 shows the part shape with the toolpath strategy, which was used for performing experiments in chapter 3.

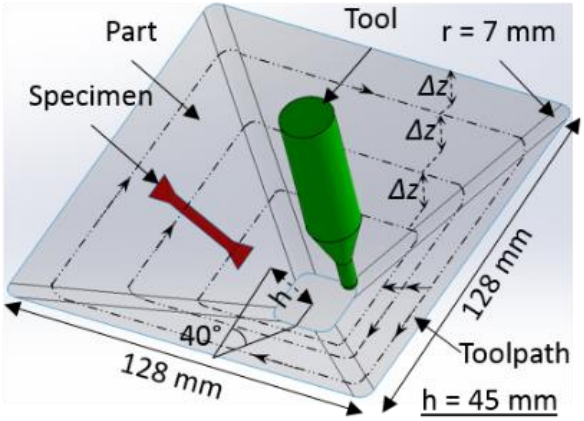

Figure 8-2: Schematic of part, specimen, tool, toolpath and incremental depth in SPIF

Table 8-2 shows the design of experiment table for experiments in chapter 2. The abbreviation of the table are as follows:

- ID: Each ID represents a set of process parameters
- Mat.: Blank sheet material which is PVC and PLA
- Rep.: Represents how many times each experiment ID has been performed
- Δz: Incremental depth in mm
- d_{tool}: Forming tool diameter in mm
- F: Feedrate in mm/min
- ω: Tool rotation speed in rpm
- t: Initial blank sheet thickness in mm
- α: Pyramid wall angle in degree

8.2.2 Results

To identify the mode of failure the operator observed the specimen during the forming process and after observing any form of failure (Tearing or Wrinkling) the tool position in Z-direction was recorded. No failure mode has been observed in the experiments of chapter 3 and all experiment IDs were formed to the end of the toolpath.

The forming time was 90-120 minutes depending on the incremental depth, therefore 3-4 parts were formed each day. The tensile specimens were cut out from the formed part's wall to perform tensile and relaxation tests. The tensile test has been performed on every formed part. The average of Young modulus, UTS, strain at fracture and yield stress were used as data point related to each incremental depth and tool rotation speed. The standard deviation of the data points was used to perform error bars in plus and minus.

Relaxation test, temperature measurement, DSC and XRD have been performed only on one specimen for each experiment ID, therefore no error bar has been shown in the graphs resulted from the aforementioned post measurements.

Table 8-2: Design of experiments

ID	Mat.	Rep (#)	Δz (mm)	d_{tool} (mm)	F (mm/min)	ω (rpm)	t (mm)	α (˚)
1	PA	5	1.4	5	300	0	1.5	40
2	PA	5	1.8	5	300	0	1.5	40
3	PA	5	2.0	5	300	0	1.5	40
4	PA	5	1.4	5	300	1000	1.5	40
5	PA	5	1.8	5	300	1000	1.5	40
6	PA	5	2.0	5	300	1000	1.5	40
7	PA	5	1.4	5	300	5000	1.5	40
8	PA	5	1.8	5	300	5000	1.5	40
9	PA	5	2.0	5	300	5000	1.5	40
10	PVC	5	1.4	5	300	0	1.5	40
11	PVC	5	1.8	5	300	0	1.5	40
12	PVC	5	2.0	5	300	0	1.5	40

Continued.								
13	PVC	5	1.4	5	300	500	1.5	40
14	PVC	5	1.8	5	300	500	1.5	40
15	PVC	5	2.0	5	300	500	1.5	40
16	PVC	5	1.4	5	300	1000	1.5	40
17	PVC	5	1.8	5	300	1000	1.5	40
18	PVC	5	2.0	5	300	1000	1.5	40

8.3 Design of Experiments of Chapter 4

8.3.1 Experiments

An SPIF setup (Fig. 3-2a) was used for performing experiments. To set the zero offset point of the tool over the forming area in the XY plane of the CNC machine. The tool was moved along X-axis in the negative direction until it touched the inner edge of the forming area and the X value was recorded (X1). Next step was moving the tool along X-axis in the positive direction until it touched the inner edge at the opposite side of the forming area and the X value was recorded (X2). The average of the recorded X values was used to set the X offset and co-center the forming tool with the center of the forming area in X-axis. Similar steps were followed for offset in Y-axis. To define the zero offset along incremental depth direction (Z-axis) the forming tool was moved along Z-axis until it touched the blank at the center of the forming area.

Figure 8-3 shows the part shape with the toolpath strategy, which was used for performing experiments in chapter 4.

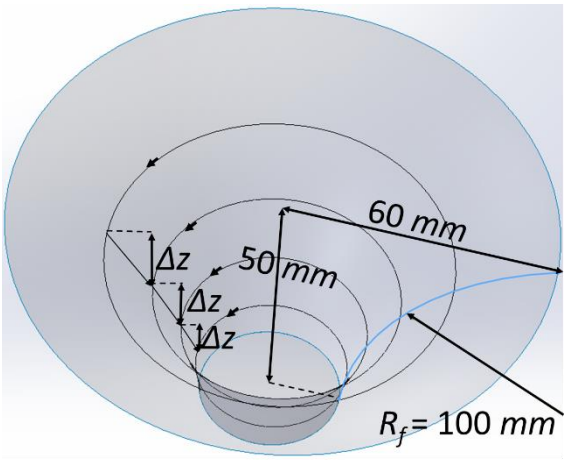

Figure 8-3: Funnel shape with schematic of the toolpath strategy

Table 8-3 shows the design of experiment table for experiments in chapter 2. The abbreviation of the table are as follows:

- ID: Each ID represents a set of process parameters
- Min Rep.: Represents the minimum times each experiment ID has been performed
- Δz: Incremental depth in mm
- d_{tool}: Forming tool diameter in mm
- F: Feedrate in mm/min
- t_{PA}: Initial Polyamide sheet thickness in mm
- t_{Al}: Initial Aluminum sheet thickness in mm

8.3.2 Results

To identify the mode of failure, the operator observed the specimen during the forming process and after observing any form of failure (Delamination, Metal Tearing or Galling) the tool position in Z-direction was recorded. The recorded tool position was used to calculate the wall angle at failure. The forming time was 20-240 minutes depending on the incremental depth and mode of failure, therefore the number of parts were formed each day varied between 2 to 6. Each experiment ID was performed 3 times and if the observed failure mode was not consistent an extra one or two parts that were formed to identify the failure mode. The specimens, which have the most repeated failure mode, were chosen to calculate error bar and average for the graphs which are shown in chapter 4. The average wall angle at failure represent the wall angle at failure. The standard deviation was calculated and used for plus and minus of the error bars.

Table 8-3: Design of experiments

ID	Min Rep (#)	Δz (mm)	d_{tool} (mm)	F (mm/min)	t_{PA} (mm)	t_{Al} (mm)
1	3	0.2	5	300	0.79	0.8
2	3	0.2	5	300	1.19	0.8
3	3	0.2	5	300	1.58	0.8
4	3	0.2	5	300	1.98	0.8
5	3	0.2	5	300	2.38	0.8
6	3	0.4	5	300	0.79	0.8
7	3	0.4	5	300	1.19	0.8
8	3	0.4	5	300	1.58	0.8
9	3	0.4	5	300	1.98	0.8
10	3	0.4	5	300	2.38	0.8

Continued.						
11	3	0.2	5	300	0.79	1.0
12	3	0.2	5	300	1.19	1.0
13	3	0.2	5	300	1.58	1.0
14	3	0.2	5	300	1.98	1.0
15	3	0.2	5	300	2.38	1.0
16	3	0.4	5	300	0.79	1.0
17	3	0.4	5	300	1.19	1.0
18	3	0.4	5	300	1.58	1.0
19	3	0.4	5	300	1.98	1.0
20	3	0.4	5	300	2.38	1.0

8.4 Design of Experiments of Chapter 5

8.4.1 Experiments

An DSIF setup at Northwestern University was used for performing experiments. Figure 8-4 shows the part shapes with the toolpath strategy, which was used for performing experiments in chapter 4.

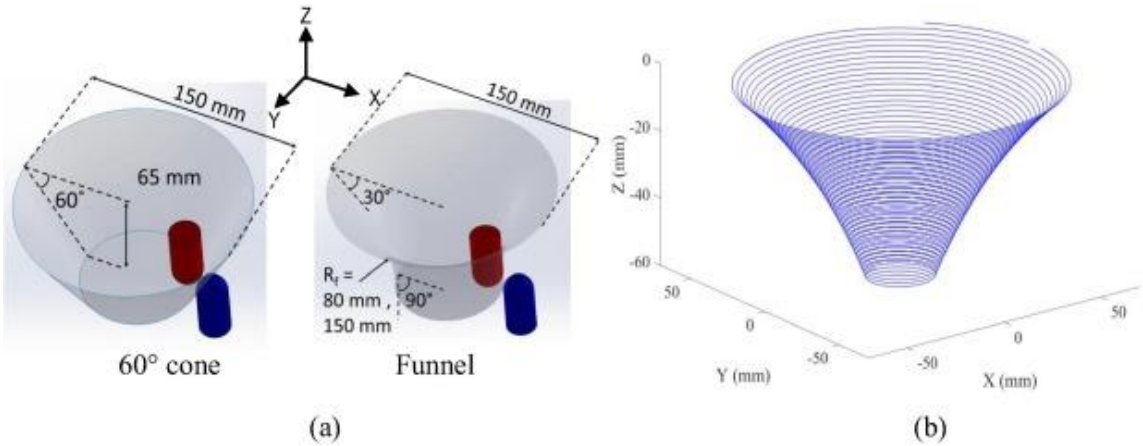

Figure 8-4: (a) Schematic of formed cone and funnel parts. (b) representative example of spiral toolpath used, shown here for a funnel shape

- ID: Each ID represents a set of process parameters

- Rep.: Represents how many times each experiment has been performed.

- Process: Represents the type of process which has been used for forming process
- Δz: Incremental depth in mm
- d_{tool}: Forming tools diameter in mm
- F: Feedrate in mm/min
- t: Initial blank sheet thickness in mm
- α: Cone shape part wall angle in degree
- R_f: Radius of curvature of funnel shape in mm

Table 8-4: Design of experiments

ID	Mat.	Process	Rep (#)	Δz (mm)	d_{tool} (mm)	F (mm/min)	t (mm)	α ($^\circ$)	R_f (mm)
1	PVC	SPIF	1	1.8	10	600	1.5	60	-
2	PVC	CDSIF	1	1.8	10	600	1.5	60	-
3	PVC	CDSIF	1	1.8	10	600	1.5	60	-
4	PVC	CDSIF	1	1.2	10	600	1.5	60	-
5	PVC	CDSIF	1	1.2	10	600	1.5	60	-
6	PVC	ADSIF	1	1.8	10	600	1.5	60	-
7	PVC	CDSIF	1	1.8	10	600	1.5	-	80
8	PVC	CDSIF	1	1.8	10	600	1.5	-	80
9	PVC	CDSIF	1	1.2	10	600	1.5	-	80
10	PVC	CDSIF	1	1.2	10	600	1.5	-	80
11	PVC	CDSIF	1	1.2	10	600	1.5	-	150

8.4.2 Results

To identify the mode of failure, the operator observed the specimen during the forming process and after observing any form of failure (Tearing or Wrinkling) the forming tool position in Z-direction was recorded. The recorded forming tool position was used to calculate the wall angle at failure for funnel shape and the depth at fracture for cone shape experiments. Each experiment has been performed only once due to the goal of research which was a preliminary investigation, therefore no error bar has been shown in the presented results in chapter 5.

9 APPENDIX B

This appendix contains extended information related to the results in chapters 2, 3 and 5.

9.1 Chain/Crystalline Lamella Orientation in Polymers

In Chapter 3, effect of SPIF on mechanical properties of PVC (amorphous polymer) and Polyamide (Semi-crystalline polymer) was shown. It has been shown [1, 2] [75, 76] [74, 75] [74, 75] [73, 74] [73, 74] [72, 73] [72, 73] that deformation of amorphous polymers at temperatures lower than the glass transition, results in retention of chain orientation in the major stress direction. Molecular dynamics simulations [3-5] have shown that plastic deformation in semicrystalline polymers occurs via reorientation of crystalline lamellae toward the major principal stress axis, and then fragmentation of largest crystalline lamellae, followed by unfolding and alignment of chains in both amorphous and crystalline portions of the polymer. Therefore the molecular mechanisms, which resulted in the observed results in chapter 3, can be summarized as follows:

- Unfolding and alignment of molecular chains in amorphous portion of polymers.
- Reorientation of crystalline lamellae and fragment of large crystalline lamellae in crystalline portion of polymers.

Figure 10-1 and 10-2 schematically show the aforementioned mechanism.

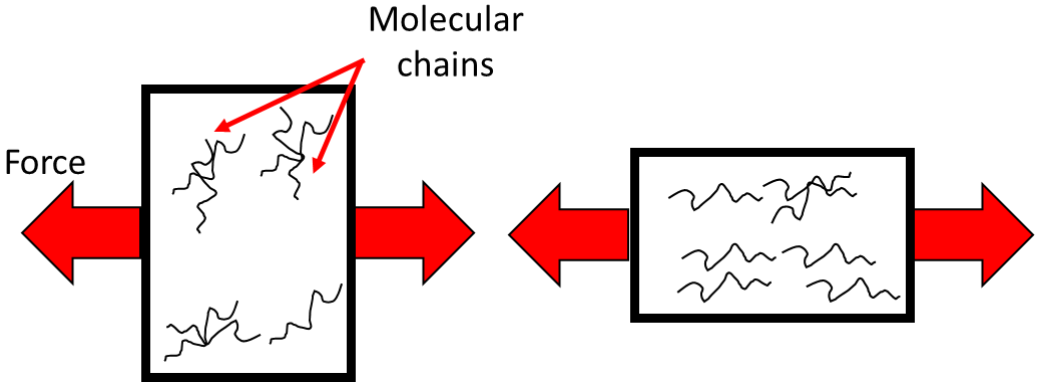

Figure 9-1: Schematic presentation of an amorphous polymer section (a) before and (b) after deformation

Figure 10-1a, shows a section of an amorphous polymer (PVC) before forming. It shows that the molecular chains are folded together and are oriented in different orientation. Figure 10-1b, shows the same section after deformation. It shows that many of the molecular chains are unfolded and many of them aligned in the direction of the force.

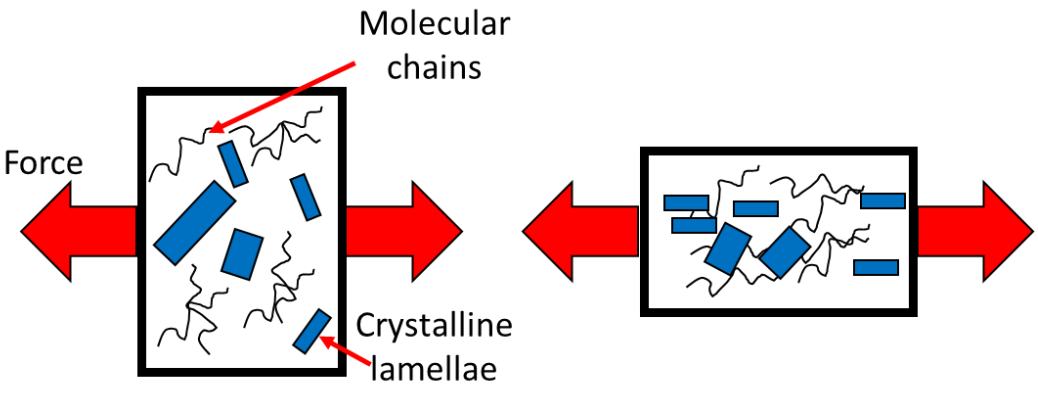

Figure 9-2: Schematic presentation of a semi-crystalline polymer section (a) before and (b) after deformation

Figure 10-2a shows a section of a semi-crystalline polymer (Polyamide) before forming. It shows that in the amorphous portion of the polymer, the molecular chains are

folded together and are oriented in different directions. In crystalline portion of the polymer, the crystalline lamellae are oriented in different directions. Figure 10-2b shows the same section after deformation. It shows that the amorphous portion of the polymer undergoes a similar molecular mechanism as amorphous polymer. Many of the molecular chains are unfolded and many of them are aligned in the direction of the major principal stress. It shows that in the semi-crystalline portion, crystalline lamellae reorient toward the major principal stress axis and large crystalline lamellae fragment to smaller crystalline lamellae.

9.2 Deformation Mechanism of SPIF

Jackson et al. [6] investigated the mechanism of single point incremental forming of metal sheet. The authors stated that the deformation mechanism in SPIF is increasing stretch strain (ε_{11}) and shear strain (γ_{13}) in the plane perpendicular to tool direction as well as shear strain (γ_{23}) in the tool direction. The results showed that shear in the tool direction (γ_{23}), which is due to friction between the tool and the sheet, has the most significant shear strain component.

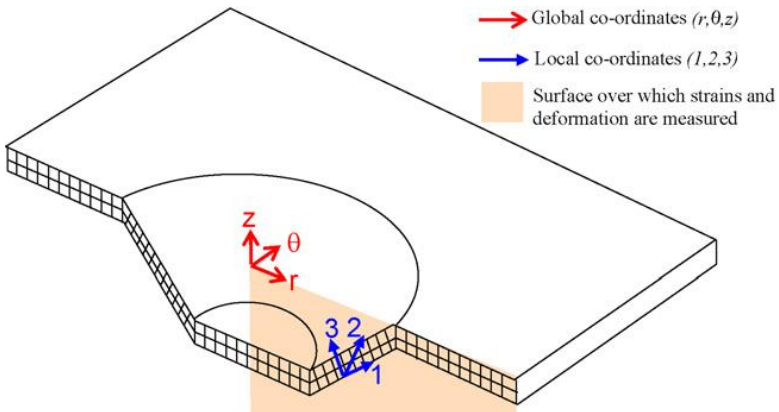

Figure 9-3: A three-dimensional representation of the global and local co-ordinate sets used to interpret strains in SPIF [20].

Past works in metal SPIF did not focused on effect of variation in incremental depth on stretch or shear strains, due to better formability of metal at small incremental depths. Therefore, an investigation on deformation mechanism of polymer incremental forming needs to be done to have a better understanding of deformation mechanism.

9.3 Failure Modes in Polymer Incremental Forming

9.3.1 Wrinkling

In Chapter 3, results showed effect of SPIF on mechanical properties of the formed polymer. The results showed that Elastic Modulus of the formed polymer is lower than the unformed polymer. In an axisymmetric part shape, which is formed with incremental forming process, the walls of the formed part are made of formed polymer (Figure 10-4). Therefore, reduction in Elastic Modulus in the formed polymer results in lower structure stiffness of the formed part. In addition, it was shown that increasing incremental depth increases the in-plan forming force (Figure 2-10) during SPIF process. Lower structural stability and higher in-plane force hypothetically results in wrinkling. However, chapter 2 shows that the wrinkling and the incremental depth at which wrinkling occurs depend on the part shape. Moreover, in polymer DSIF no wrinkling was observed (Table 5-1). Therefore, more investigation is needed to examine the proposed hypothesis and to have a better understanding of wrinkling mechanism in polymer incremental forming.

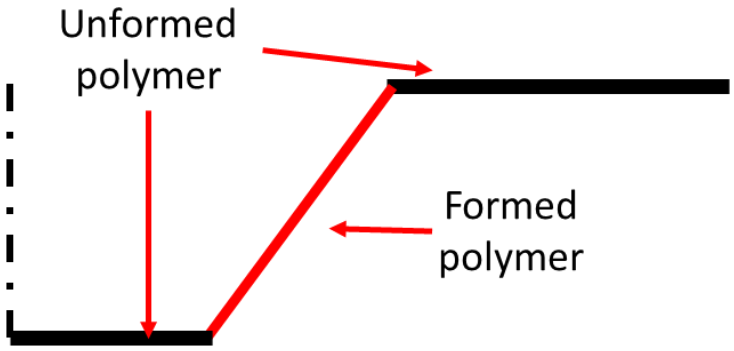

Figure 9-4: Schematic view of polymer sheet, which formed to an axisymmetric part shape with incremental forming process.

9.3.2 Tearing

In crazable glassy polymers, such as PVC, in most cases fracture starts when voids start to grow and reach the point that the fibrils (which are aligned molecular chains) break in the crazed zone. If the deformation keeps increasing, this mechanism continues until macroscopic fracture occurs [7]. Silva et al. [8] suggested to limit the formation of micro-voids in the polymer matrix by superimposing hydrostatic compression stresses during the forming process, like using a dummy sheet on the side of the polymer sheet which is not in contact with forming tool in SPIF. In DSIF process as long as the bottom tool (supporting tool) is in contact with the sheet the hydrostatic compression stress is maintained at the contact area of the top and the bottom tool with the sheet. Therefore the hydrostatic compression stress reduces the void area fraction (Figure 5-4f). After losing contact between the bottom tool and the polymer sheet, the micro-voids start to grow and the void area fraction increases (Figure 5-4f). The contact between the bottom tool and the polymer sheet in polymer DSIF (CDSIF and ADSIF) reduces crazing and resultant void growth in the polymer, resulting in greater formability as compared to SPIF.

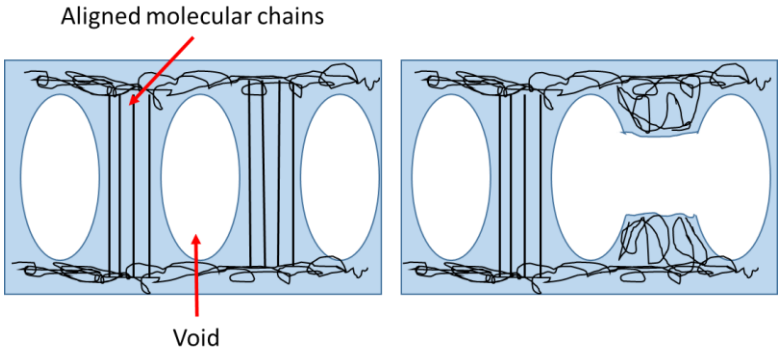

Figure 9-5: Schematic view of (a) crazing structure and (b) fibril break in crazed zone.

REFERENCES:

[1] E.M. Arruda, M.C. Boyce, Evolution of plastic anisotropy in amorphous polymers during finite straining, International Journal of Plasticity, 9 (1993) 697-720.

[2] E.M. Arruda, M.C. Boyce, R. Jayachandran, Effects of strain rate, temperature and thermomechanical coupling on the finite strain deformation of glassy polymers, Mechanics of Materials, 19 (1995) 193-212.

[3] I.-C. Yeh, J.W. Andzelm, G.C. Rutledge, Mechanical and structural characterization of semicrystalline polyethylene under tensile deformation by molecular dynamics simulations, Macromolecules, 48 (2015) 4228–4239.

[4] S. Jabbari-Farouji, J. Rottler, O. Lame, A. Makke, M. Perez, J.-L. Barrat, Plastic deformation mechanisms of semicrystalline and amorphous polymers, ACS Macro Lett, 4 (2015) 147–150.

[5] S. Jabbari-Farouji, J. Rottler, O. Lame, A. Makke, M. Perez, J.-L. Barrat, Correlation of structure and mechanical response in solid-like polymers, Journal of Physics: Condensed Matter, 27 (2015).

[6] K. Jackson, J. Allwood, The mechanics of incremental sheet forming, Journal of Materials Processing Technology, 209 (2009) 1158-1174.

[7] A.S. Argon, The Physics of Deformation and Fracture of Polymers, Cambridge University Press, 2013.

[8] M. Silva, L. Alves, P. Martins, Single point incremental forming of PVC: Experimental findings and theoretical interpretation, European journal of mechanics-A/Solids, 29 (2010) 557-566.